Theses and Dissertations   1. Thesis and Dissertation Collection, all items

1960-05-01

Investigation of a small centrifugal compressor with radial inflow diffuser

Shappell, John R.; Albee, Thomas L.

http://hdl.handle.net/10945/12489

INVESTIGATION OF A SMALL CENTRIFUGAL COMPRESSOR WITH RADIAL INFLOW DIFFUSER

JOHN R. SHAPPELL
and
THOMAS L. ALBEE, JR.

INVESTIGATION OF A SMALL CENTRIFUGAL COMPRESSOR

WITH RADIAL INFLOW DIFFUSER

by

LT. JOHN R. SHAPPELL, U.S.N.

and

LT. THOMAS L. ALBEE, JR., U.S.N.

SUBMITTED IN PARTIAL FULFILLMENT OF THE

REQUIREMENTS FOR THE DEGREE OF NAVAL ENGINEER

and

FOR THE DEGREE OF MASTER OF SCIENCE IN

NAVAL ARCHITECTURE AND MARINE ENGINEERING

at the

MASSACHUSETTS INSTITUTE OF TECHNOLOGY

May, 1960

INVESTIGATION OF A SMALL CENTRIFUGAL COMPRESSOR WITH RADIAL
INFLOW DIFFUSER by LT. JOHN R. SHAPPELL, U.S.N. and
LT. THOMAS L. ALBEE, JR., U.S.N. Submitted to the Depart-
ment of Naval Architecture and Marine Engineering on
21 May 1960 in partial fulfillment of the requirements for
the Master of Science Degree in Naval Architecture and
Marine Engineering and the Professional degree, Naval En-
gineer.

ABSTRACT

The purpose of this report is to investigate incom-
pressible flow through a radial inflow diffuser, with two
primary objectives: (1) comparison of performance with a
vaneless outflow diffuser; and (2) analysis of the flow
in the diffuser itself.

The performance of two impellers, the outflow diffuser,
and the compressor is investigated experimentally to serve
as a comparative standard. Estimations of impeller flow
conditions are made using both one-dimensional and two-
dimensional theory.

The equations of motion for fluid in an inflow diffuser
are developed, and a solution for incompressible, ir-
rotational flow is obtained by means of electrical equi-
potential lines on semi-conductor paper.

The maximum compressor efficiency with the outflow
diffuser is 50.5 percent. Maximum compressor efficiency
with an inflow diffuser of the same width as the impeller
is 43.2 percent. By increasing diffuser blade width forty
percent the maximum compressor efficiency increases to
45 percent. A forty percent increase in diffuser exit
area increases compressor efficiency to 48.5 percent. Both
changes result in improved performance at high flow rates.

Theoretical results indicate less tendency for
separation in a twelve-bladed than in a six-bladed impeller.
Tests result in a maximum compressor efficiency of 50.3
percent with a twelve-bladed impeller and outflow diffuser
For a given speed and flow rate, pressure ratio was about
ten percent higher with no significant loss of efficiency.

The solution for diffuser flow using semi-conductor
paper shows little difference between flow through the
two inflow diffusers. Experimental performance is also
similar,

It is concluded that:

(a) At low to medium flow rates, per-
formance of compressor with inflow
diffuser is similar to that with
outflow diffuser.

(b) Above medium flow rates, performance
with inflow diffuser drops very
sharply.

(c) Inflow diffuser performance at higher
flow rates is improved by widening
the blades and/or increasing exit area.

(d) Variations in reasonable blade shapes
do not greatly affect inflow diffuser
performance.

Thesis Supervisor: Kenneth R. Wadleigh

Title: Associate Professor of
                      Mechanical Engineering

ACKNOWLEDGMENT

TABLE OF CONTENTS

TABLE OF CONTENTS (con'd)

LIST OF FIGURES

vii

LIST OF FIGURES (con'd)

DEFINITION OF SYMBOLS USED

a	area, constant
B	number of blades
b	width or axial dimension
c	velocity of sound
d	diameter
g	gravitational constant
H	dimension (length)
h_w	pressure differential (in of H_2O)
J	778 lb ft/Btu
K	flow coefficient
M	Mach number
N	speed - RPM
P	pressure (in of H_2O)
p	pressure (psi)
Q	velocity relative to blade
q	flow rate (cfs)
R	gas constant
r	radius
T	temperature °R
T	dynamometer reading (in)
u	blade speed (ft/sec)
V	velocity (ft/sec)
w	flow rate, lbM/sec
x	length coordinate
y	length coordinate
α	absolute angle of flow with respect to tangent
β	blade angle with respect to tangent
γ	weight density
Δ	increment
η	efficiency or transform coordinate

θ	angular measure (radians)	
$\digamma$	transform coordinate	
ρ	mass density	$\dfrac{\text{lb sec}^2}{\text{ft}^4}$
σ	angular spacing of blades	
T	torque (lb ft)	
ϕ	flow parameter	
ψ	stream function	
Ω	speed rad/sec	
ω	speed rad/sec	

Subscripts

0	stagnation
1	impeller inlet
2	impeller tip or exit
3	diffuser exit - atmospheric
c	compressor
d	driving face
D	diffuser
i	impeller
m	motor
r	relative, radial
T	tip
t	trailing face
θ	angular

I.

INTRODUCTION

The design of radial-outflow diffusers for centrifugal com-
pressors has been the subject of considerable previous study,
and quite advanced methods are presently available for de-
sign purposes (4).

The primary advantage of attempting to diffuse flow inward
is the reduction of overall diameter with subsequent de-
creased size and weight. Outward diffusion is readily
accomplished by taking advantage of vortex motion, whereby
radial velocity decreases by continuity considerations
while tangential velocity changes inversely as the radius.

Inward diffusion attempts to violate both of these con-
ditions and instead of a free path flow, considerable
turning effect must be exerted on the fluid to obtain a
condition which is normally conducive to diffusion, viz.,
diverging mean passage area.

Literature contains little on the particular fluid
mechanics of inward diffusion. Several previous reports
were available (1,8), but the results were largely em-
pirical, with only one-dimensional analysis generally
undertaken.

The basic approach taken in this report was to study the performance of the impeller to determine conditions at diffuser inlet; to use a vaneless outflow diffuser as an arbitrary standard of diffusion with the impeller; to compare inflow diffusers with this standard; and to study the motion of fluid in an inflow diffuser.

One-dimensional analysis appears in the impeller study since it is convenient in describing the flow. It tells very little about what goes on in the impeller, however, so that a two-dimensional approach is also used.

Incompressible flow was assumed for the sake of simplicity. Compressible flow would present some additional problems in the impeller and outflow diffuser, but it would be definitely a greater complication in the inflow diffuser at this point. Air at the velocities encountered in the compressor of this study could be considered incompressible without great error.

Three-dimensional flow was not considered because axial components are small by comparison in the impellers and diffusers studied. The transition from impeller to inflow diffuser is subject to much greater three-dimensional effects, but a detailed study was not considered suitable with the apparatus used for this report.

A readily-available apparatus suitable for this inward-diffusion study was fabricated from part of an Electrolux

vacuum cleaner. Two identical impellers are normally em-
ployed, with inflow diffusers after each stage. A single
impeller absorbed about one-half horsepower from the motor.
Figures I, II, III, and IV show the general layout of the
apparatus for both vaneless outward diffusion and inward
diffusion. Much of the basic equipment was left from pre-
vious experiments conducted in 1952 and 1953 at the
Massachusetts Institute of Technology. The major changes
consisted of a new motor, an outflow diffuser, and a new
orifice flow meter.

The motor was mounted in a can and was free to rotate on
ball bearings ten degrees either side of neutral position.
A dynamometer was rigidly attached to the motor. It con-
sisted of two one-foot steel rulers mounted on opposite
sides of a one-foot sheetmetal disc. A fixed weight on
one ruler was balanced by a movable pan on the other arm
containing .311 pounds of brass weights. The rulers were
graduated in .02 inch.   Torque was read directly in inch-
pounds, with allowance for the initial position of the pan
with the motor not running.

Cooling air for the motor entered through a radial-vaned
inlet at the impeller end of the motor. The vanes mini-
mized torque due to swirl, if any, of the incoming air. The
air was sucked from the other end of the can by a second
Electrolux machine. A mercury pool was used to transmit

power from a variac to leads from the motor windings. A six-ampere fuse was included to prevent overloading.

The inlet air pipe diameter was 2.067 inch. A 1.20-inch sharp-edged orifice flow meter was installed eighteen inches from the inlet end. Static pressure taps were located up-stream and downstream to enable flow calculations based on reference (11).

A valve was included in the inlet pipe in order to throttle the flow rate to desired values. The two-inch pipe increased to a five-inch diameter chamber for eight inches in front of the impeller inlet. Inlet static and stagnation pressures were measured midway along this chamber.

The outflow diffuser was made of two fourteen-inch diameter plastic discs, .25 inch thick. One face was mounted directly to the edge of the chamber and sealed to prevent leaks. The other face was supported on three arms attached to the adjacent motor support plate. Shims were used to obtain parallelism between the diffuser faces. The initial diffuser width was .36 inch. Details of the diffuser are shown in Figure V. The inlet hole was rounded to a diameter of two inches. Both diffuser faces were undercut .06 inch to allow closer fit with the impeller. At the impeller tip the clearance was .03 inch. The second diffuser face fit over the extended motor shaft and had .05 inch of clearance with the impeller collar. Ten

.02-inch holes for pressure taps were drilled at inter-
vals radially outward along two lines 90° apart as shown
in Figure V. A kiel probe was inserted in a hole through
the upstream side, far enough from the static taps to have
no detectable effect. This probe and the first static tap
were .10 inches out from the impeller to allow flow
variations to smooth out somewhat and to prevent scraping.

A water manometer board was used for all pressure readings.
Measurements to the nearest .05 inch were readily made.

Impeller blade shapes are shown in Figure VI. Both were
five inches in diameter, with .30-inch wide blades, and
were used as received from the Electrolux Corporation.

A standard five-bladed Electrolux inflow diffuser was used
for part of the tests. Blade width was originally .30 inch,
and the arrangement is shown in Figure VII.

A seven-bladed inflow diffuser was fabricated by the
authors for comparative tests. It is more fully described
in Appendix A and is shown in Figure VIII.

Details of the can mounting for the inflow diffuser are
shown in Figure IV. This part of the apparatus was taken
directly from the Electrolux machine with only the addition
of mounting lugs.

Speeds were measured with a strobotac calibrated for each
series of runs. Temperature and barometer readings were
taken for each series.
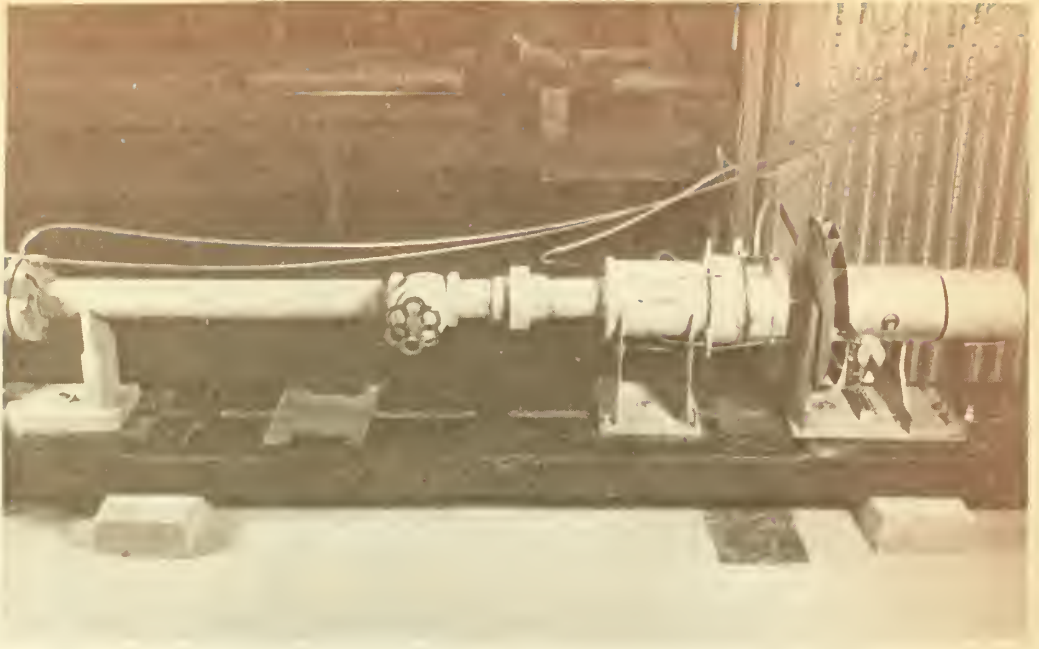
Figure I.   Apparatus with inflow diffuser
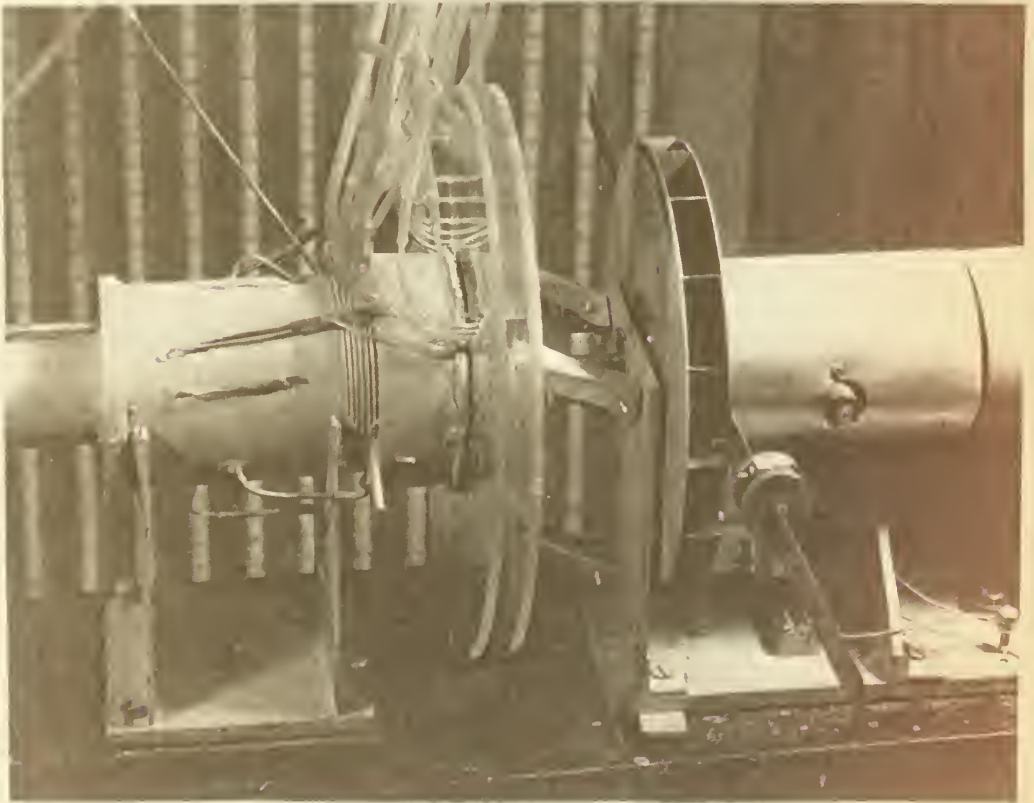
Figure II.   Installation of outflow diffuser
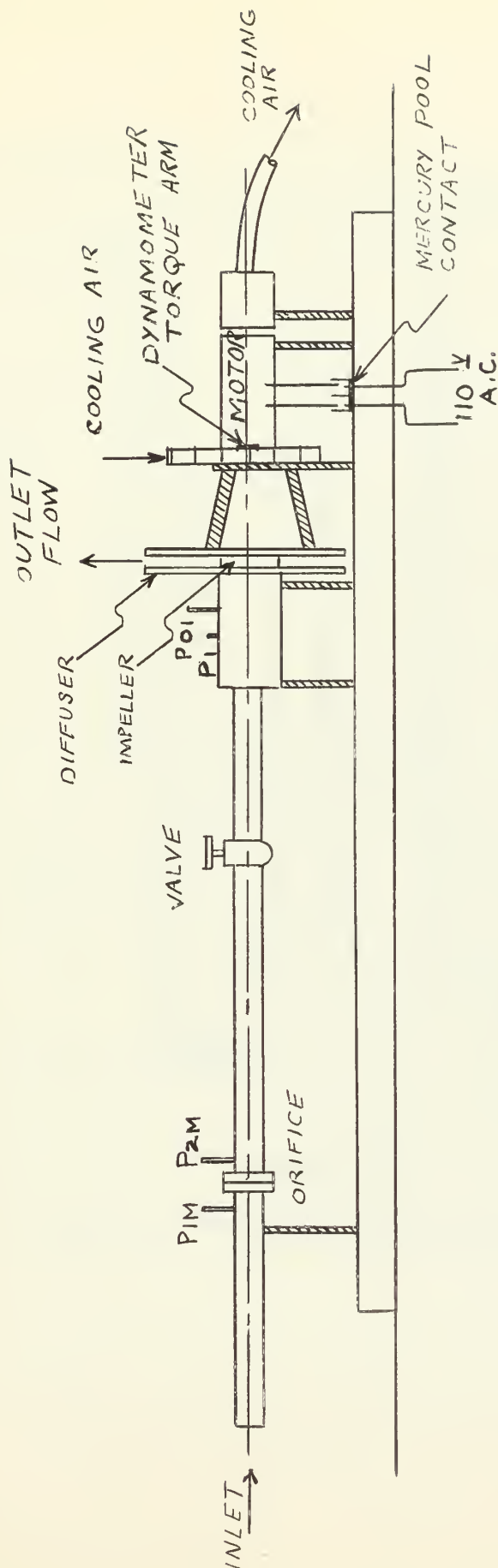
FIGURE III

Sketch of Apparatus
with Vaneless Dif-
fuser Installed.

CLAMP

INLET

CHAMBER

.138 INCH

.30 INCH

.144 INCH

IMPELLER

DIFFUSER

FLOW

SHAFT
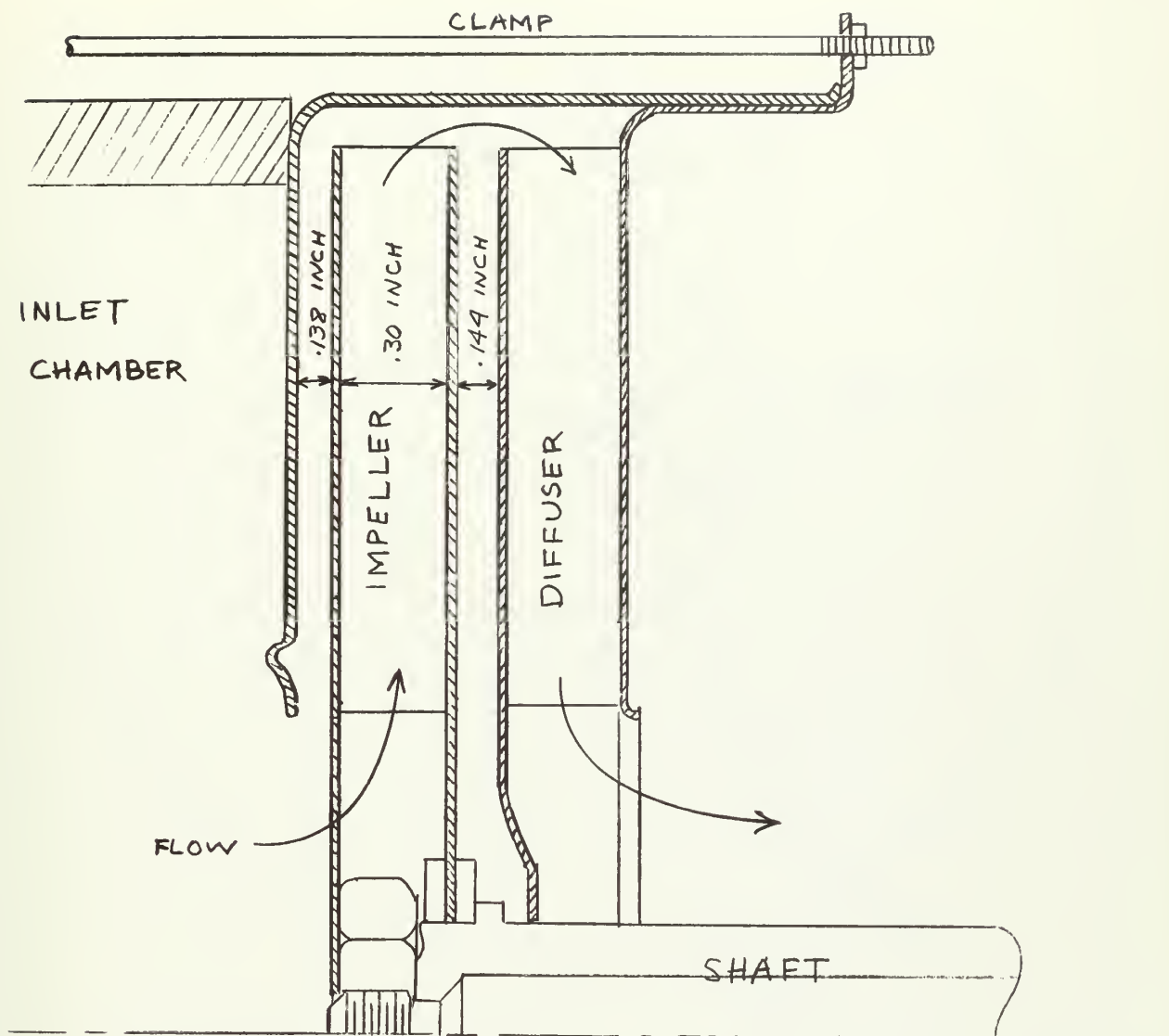
FIGURE IV

Detail of Mounting Inflow Diffusers

-8-

.02" Static Pressure Taps

Kiel Probe
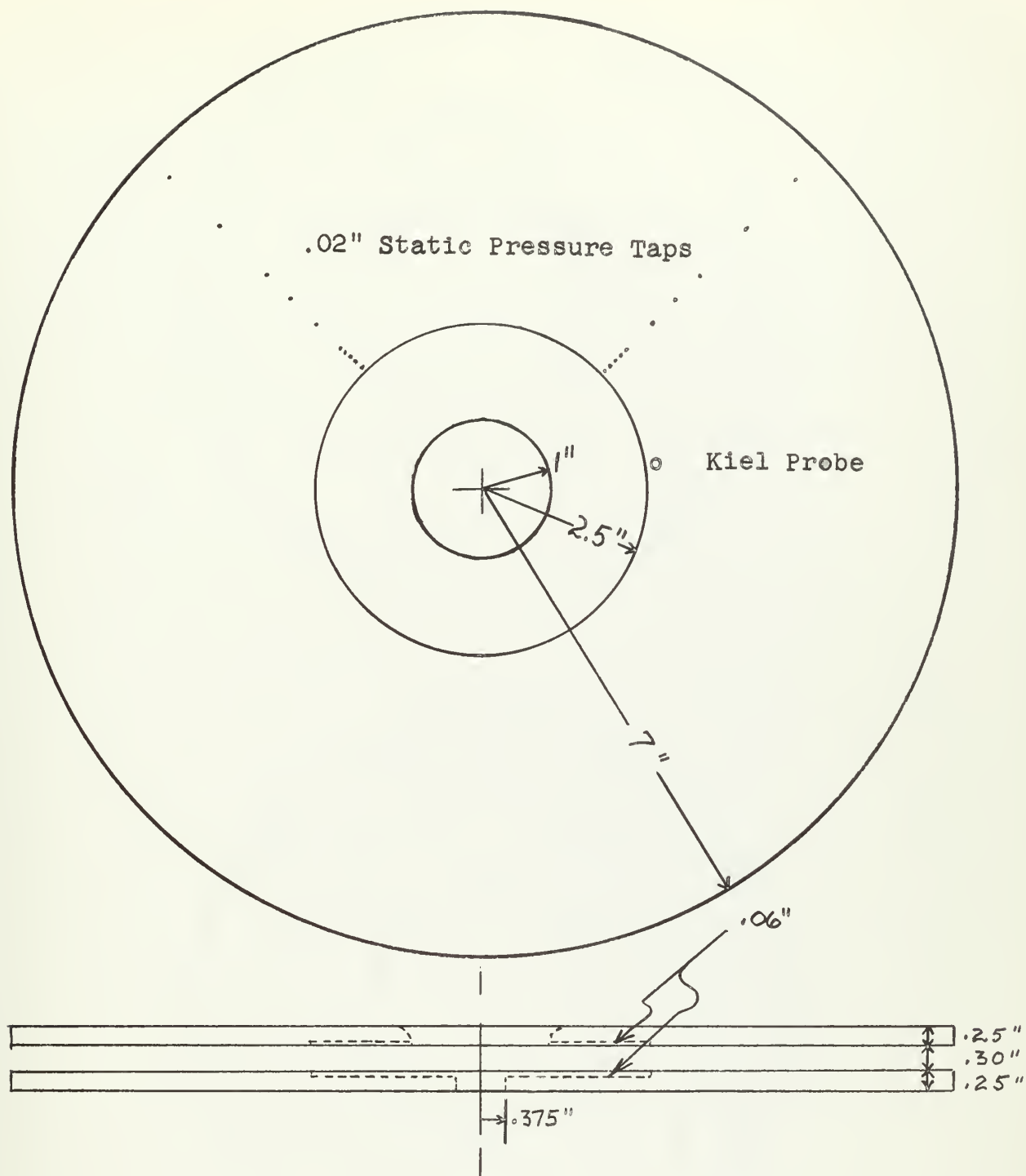
FIGURE V

Vaneless Radial Outflow Diffuser
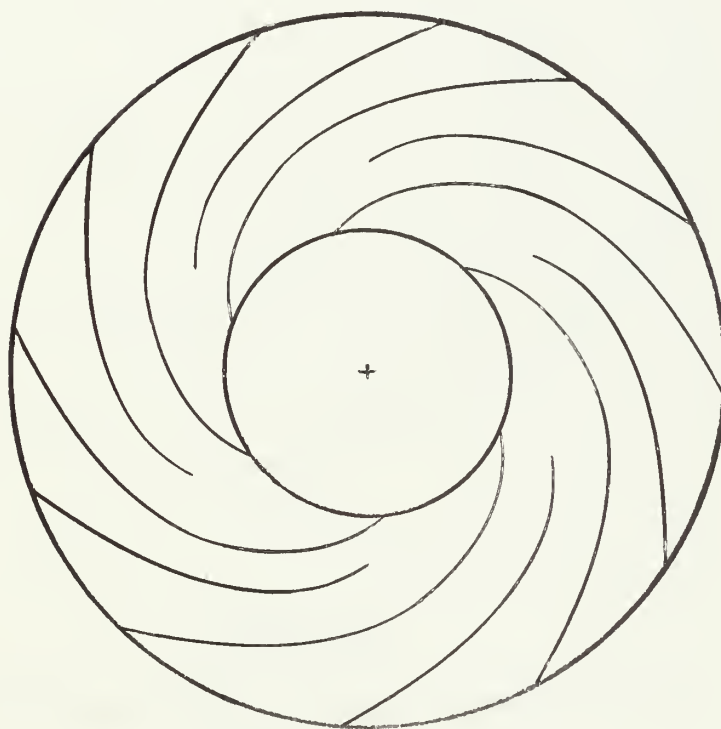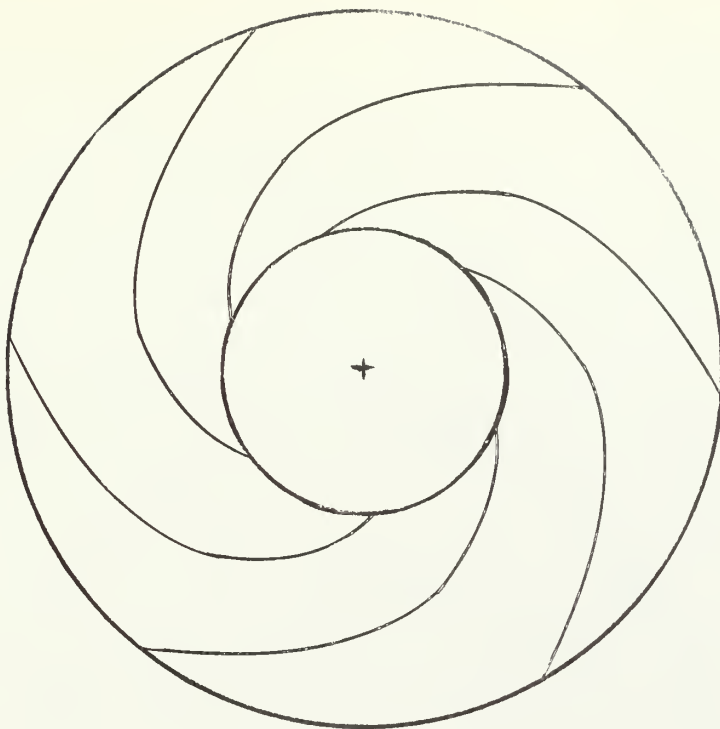
FIGURE VI

Six- and Twelve-bladed Impeller Blade Shape
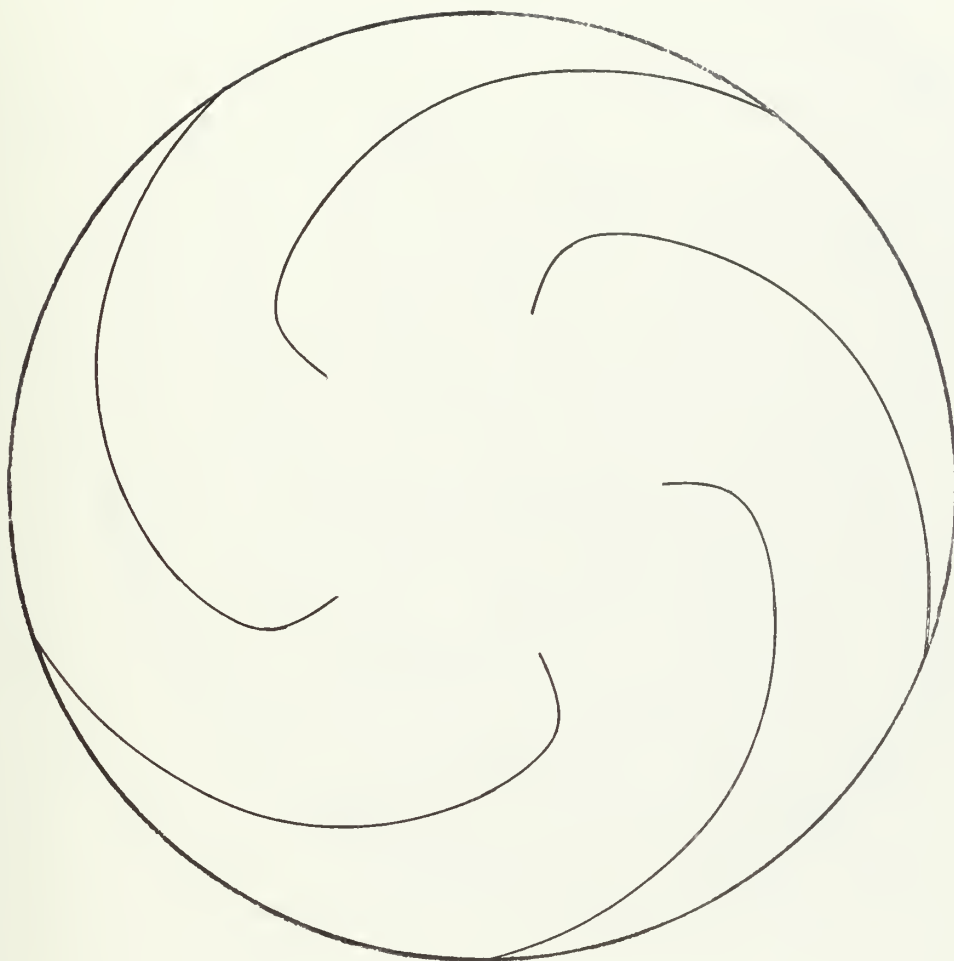
FIGURE VII

Standard Electrolux 5-Bladed Inflow Diffuser
Blade Shape

-11-
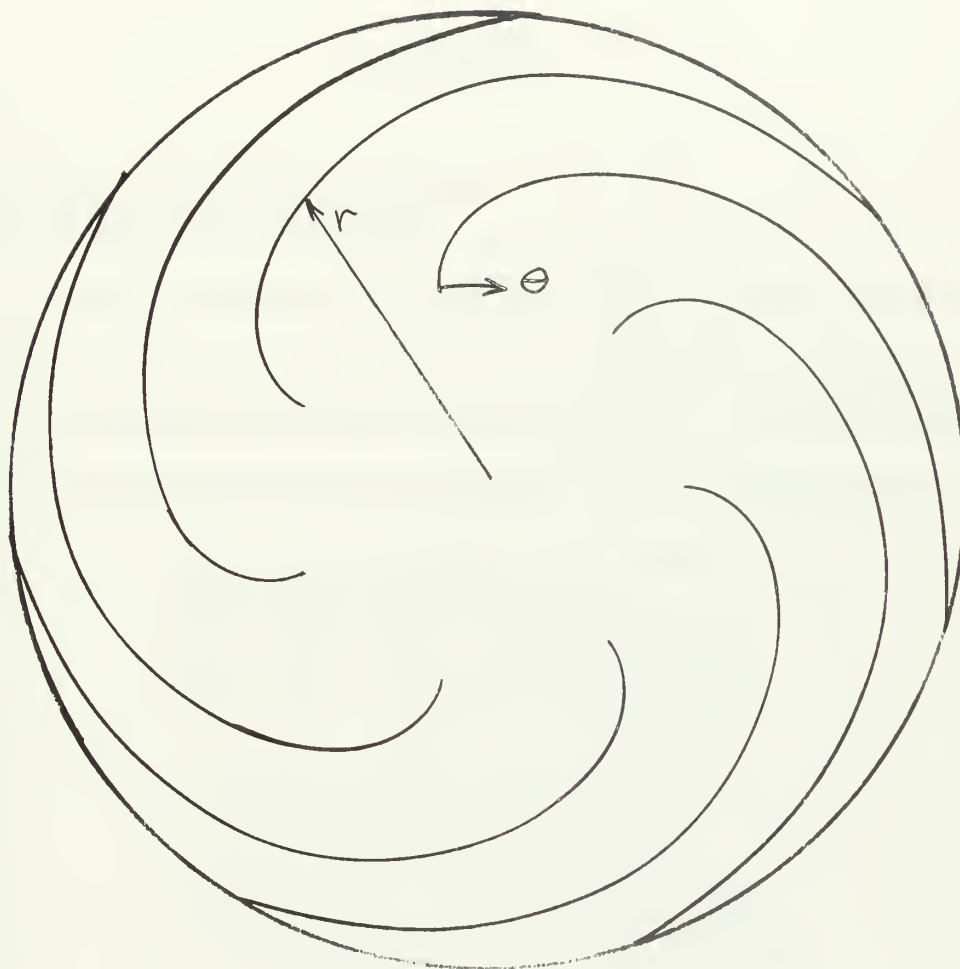
FIGURE VIII

Seven-Bladed Inflow Diffuser Blade Shape

-12-

II.

PROCEDURE

Test Procedure for Six-Bladed Impeller, Outflow Diffuser

In order to compare the inflow diffusers with the vaneless outflow diffuser, performance parameters were determined. The following quantities were measured on the test apparatus for the calculation of the values of the parameters:

(a) Flow rate through a 1.2-inch sharp-edged orifice in a 2.067-inch pipe. The pressure differential in inches of water across the orifice was measured.

(b) Static and stagnation pressure at impeller inlet and outlet. p_{O1} was measured with a kiel probe located two inches upstream from the impeller inlet and centered in the inlet chamber. p_{O2} was measured with a kiel probe located 0.1 inch from the impeller discharge and midway between the diffuser walls.

(c) Dynamometer torque. A reading in inch-pounds was made directly on the dynamometer arms by adjusting the movable weights.

(d) Impeller speed was set with the variac to the desired rotational speed as indicated by the strobotac.

(e) Diffuser outlet conditions were
taken as atmospheric. The dif-
fuser is then charged with the
loss of any velocity head re-
maining at exit.

(f) A wattmeter was used to measure
the power input to the motor on
some runs as a check on overall
performance.

(g) A yaw probe was used to measure
the direction of the flow leav-
ing the impeller.

Flow Parameters

The performance parameters which were calculated from the
measured quantities are given below. (Sample calculations
and formulae are to be found in the Appendix).

(a) $\dfrac{\omega}{P_{o1}}$

(b) $\left(\dfrac{\Delta P_o}{P_{o1}}\right)_i = \dfrac{P_{o2} - P_{o1}}{P_{o1}}$; $\left(\dfrac{\Delta P_o}{P_{o1}}\right)_c = \dfrac{P_{o3} - P_{o1}}{P_{o1}}$

(c) $\eta_i = \dfrac{g\,(\Delta P_o)_i}{T\,\omega}$

(d) $\eta_c = \dfrac{g(\Delta P_o)_c}{T\omega}$

(e) $\eta_m = const. \times \dfrac{T\,\omega}{watts}$

(f) $\eta_0 = \dfrac{P_{o3} - P_2}{P_{o2} - P_2}$

(g) β_2

Theoretical Analysis

In conjunction with the previous tests, the following theoretical investigations were made:

(a) One dimensional flow determination of pressure rise versus flow rate, β_2, and velocities at impeller discharge.

(b) Two-dimensional flow to obtain velocity distribution along the impeller blades (2).

(c) Investigation of stagnation pressure loss incurred when a flow with velocity gradient in a channel is smoothed out to uniform flow by internal shear.

Test Procedure for
Twelve-bladed Impeller

As a result of theoretical investigation of impeller flow, a twelve-bladed impeller was tested in the same manner as the six-bladed impeller.

Inflow Diffuser Tests

The experimental apparatus was altered to test the radial inflow diffusers. Flow rate, pressures, torque, and speed were measured by the same methods used for the outflow diffuser. p_{02} was measured with a kiel probe midway between the impeller and the diffuser at the center of the annular passage. Static pressure taps were located on the housing between the impeller and diffuser and at the center of the

-15-

passage. Static pressure taps were located on the housing between the impeller and diffuser (p_2) and on the diffuser disc, 0.1 inch from the outlet at the midpoint of a passage.

Both the six and the twelve-bladed impellers were used with the following diffuser configurations:

(a) Five-bladed standard Electrolux first stage inflow diffuser. (Figure VII)

(b) Seven-bladed model with blade shape of new design. (Figure VIII)

(c) Vaneless inflow device.

(d) Five-bladed inflow diffuser with blade width increased to .42 inch. (six-bladed impeller only)

(e) Five-bladed inflow diffuser with blade width increased to .42 inch and exit diameter increased to 2.15 inches. (six-bladed impeller only)

Electrical Analog of Inflow Diffusers

A two-dimensional analysis using semi-conductor paper was made on the five- and seven-bladed inflow diffusers to obtain the streamline configuration in the diffuser passage for incompressible, non-viscous fluid.

III.

RESULTS

A summary of the results is presented below. More complete results of the investigation are presented in the graphs and figures which follow.

Impeller

Experimental results show that the pressure rise through the six-bladed impeller with outflow diffuser was considerably less than that predicted by one-dimensional theory. Figures IX, X, and XI.

The twelve-bladed impeller achieved greater pressure rise throughout the operating range. Figure XII. Efficiencies were comparable to those achieved with the six-bladed impeller. Figure XIII.

Two-dimensional analysis of the six-bladed impeller showed an eddy forming well within the blade. Figure XIV. Increasing the number of blades to twelve eliminated the eddy. Figure XV. A calculation for several impellers showed a definite trend toward eddy formation as the number of blades decreased. Figure XVI.

Impeller exit flow angle was not consistently predicted by the three methods employed. In the range of interest it was

considerably lower than the design value chosen.
Figure XVII.

When testing the six-bladed impeller and outflow dif-
fuser, the outlet air flow pulsated very noticeably. With
the twelve-bladed impeller and outflow diffuser this
pulsation was almost completely eliminated.

The yaw probe, made of thin tubing, vibrated severely
at low flow rates when measuring the smaller exit angles.

Diffuser

With the six-bladed impeller the vaneless diffuser
efficiency showed a tendency to increase with the flow rate.
A distinct rise occurred over a small region at the low
flow rates, also. Figure XVIII.

Outflow diffuser performance with the twelve-bladed
impeller was comparable to that just mentioned. Efficiency
was not greatly affected by impeller speed.

The comparison of the inflow diffusers by semi-conductor
paper showed little difference in the exit conditions.
Figures XIX and XX. No extreme gradients of the stream
function were observed. Adjustment of the angle of the
equipotential line at the inlet had little effect beyond
the immediate area.

Compressor

The performance of the compressor is shown for speeds
of 17,000; 18,000; and 19,000 RPM for the following com-
binations of impellers and diffusers, with efficiency
and pressure ratio plotted versus flow rate:

> (a) Six-bladed impeller with:
>
>> Vaneless outflow diffuser;
>>
>> Five-bladed standard Electrolux
>> inflow diffuser, b = .30 inch;
>>
>> Seven-bladed inflow diffuser;
>>
>> Five-bladed inflow diffuser,
>> b = .42 inch;
>>
>> Five-bladed inflow diffuser,
>> exit diameter = 2.15 inches;
>
> (Figures XXI, XXII, XXIII, XXIV, XXV,
> and XXVI).
>
> (b) Twelve-bladed impeller with:
>
>> Vaneless outflow diffuser;
>>
>> Five-bladed standard Electrolux
>> inflow diffuser, b = .30 inch;
>>
>> Seven-bladed inflow diffuser;
>
> (Figures XXVII, XXVIII, XXIX, XXX,
> XXXI, and XXXII).

The effect of increasing the width of the vaneless diffuser
to determine the magnitude of circulation from outlet to in-
let was not great and remained reasonably constant over the
operating range. Figure XXXIII.

Results of the bladeless inflow device test are not in-
cluded because the net increase of stagnation pressure was

approximately zero with a flow rate too small to measure
accurately even at the wide-open condition.

FIGURE IX

Pressure ratio vs flow rate, 1 dimensional
theory, 6 bladed impeller, 12 bladed im-
peller, RPM constant

-21-
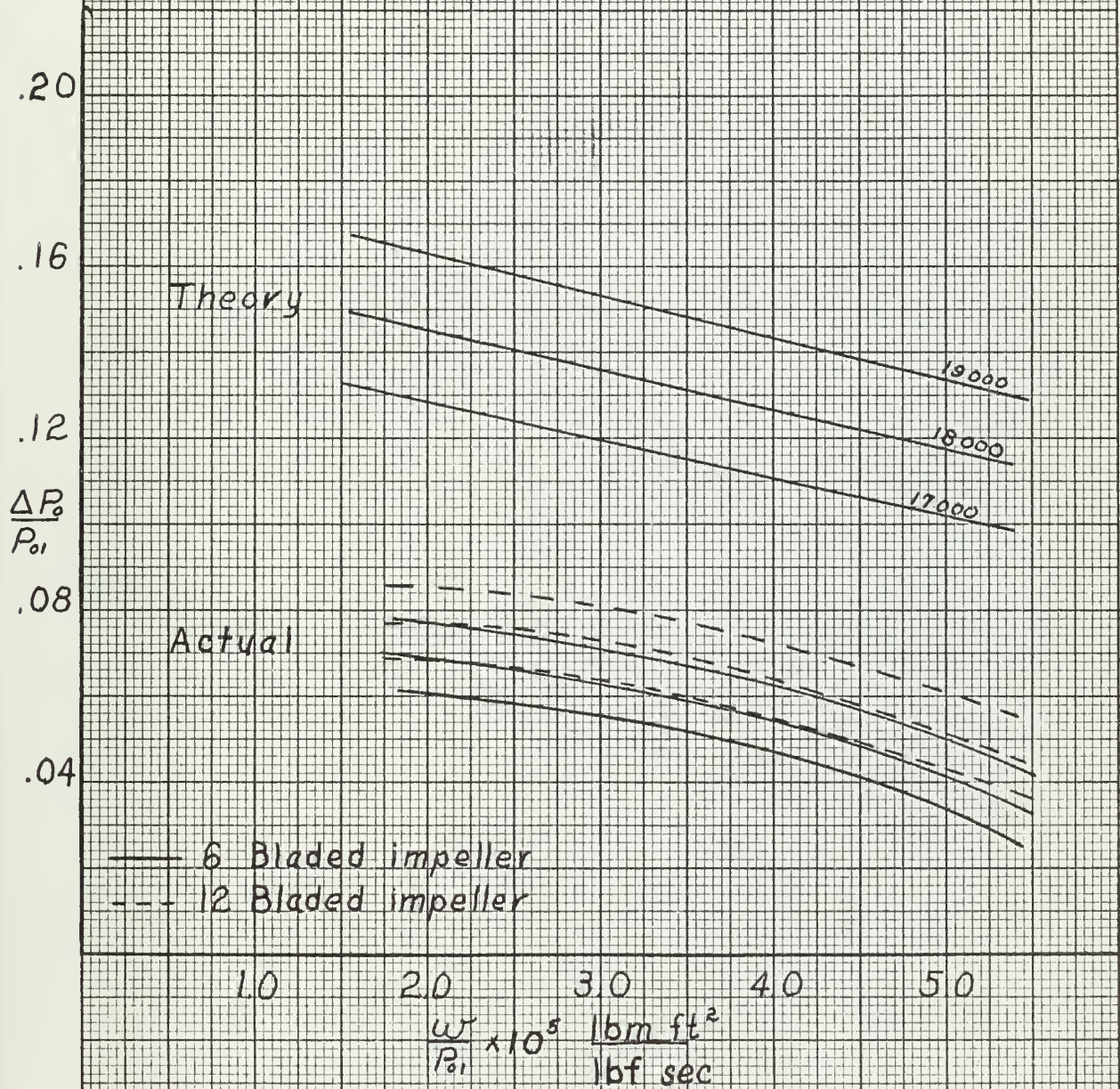
FIGURE X

Pressure ratio vs flow rate
6 bladed impeller, constant speed

20000
19000
18000
17000

$\frac{\Delta P_0}{P_{01}}$

.08
.07
.06
.05
.04
.03
.02
.01

1.0 2.0 3.0 4.0 5.0 6.0

$\frac{w}{P_{01}} \times 10^5 \frac{lbm\ ft^2}{lbf\ sec.}$
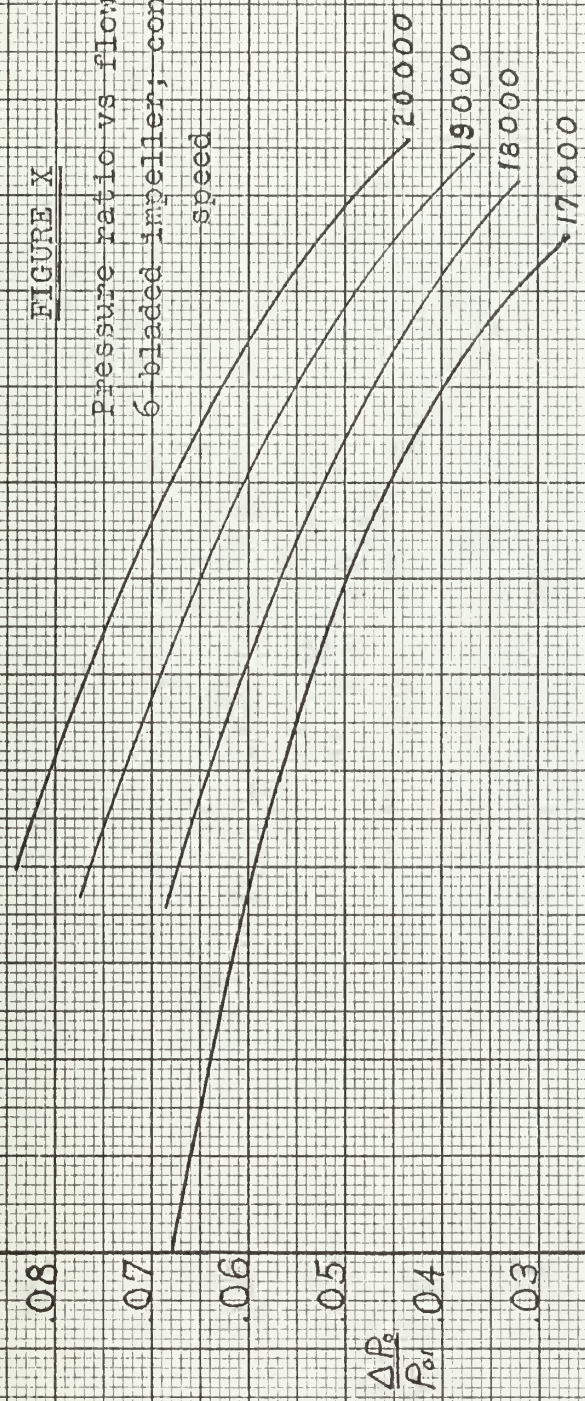
FIGURE XI

Impeller efficiency vs flow rate
6-bladed impeller, constant speed

$\dfrac{w}{P_1} \times 10^{-5} \ \dfrac{lbm \ ft^2}{lbf \ sec}$

19000
18000
17000

η_i
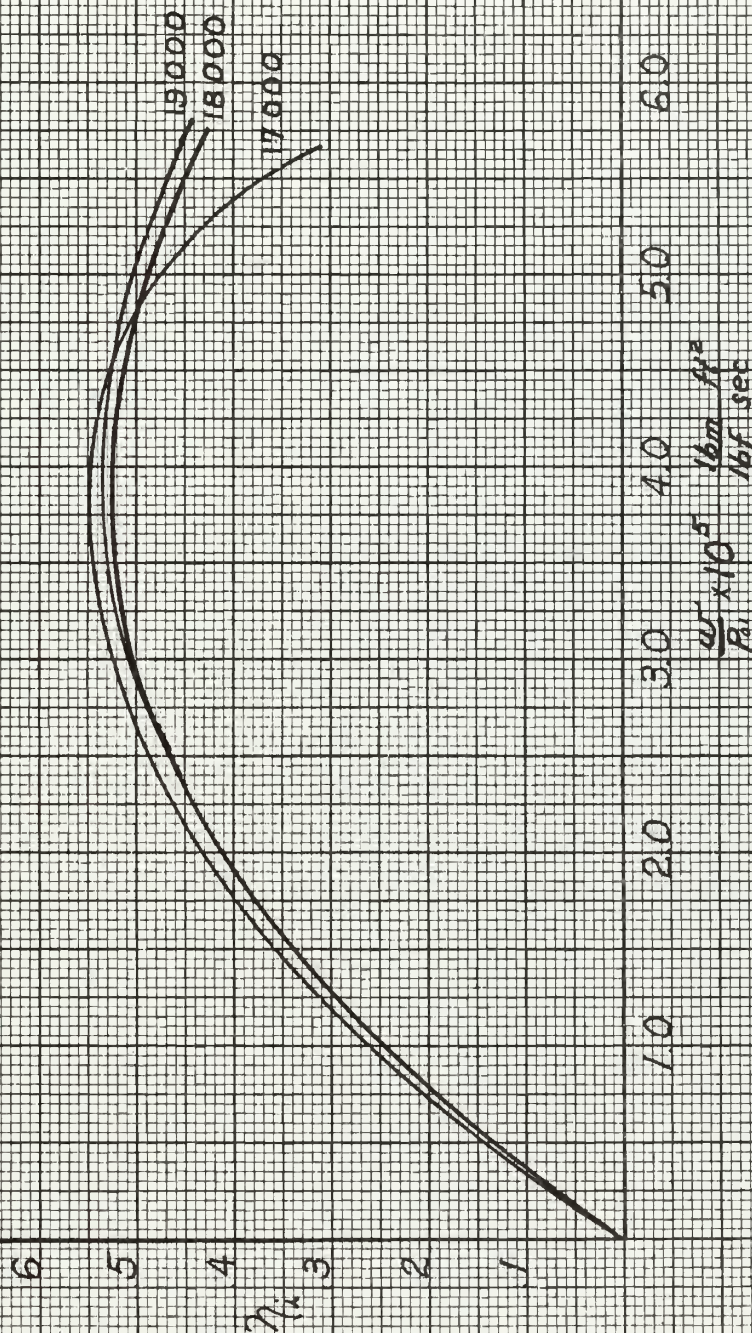
FIGURE XII

Pressure ratio vs flow rate 12-bladed impeller; constant speed.
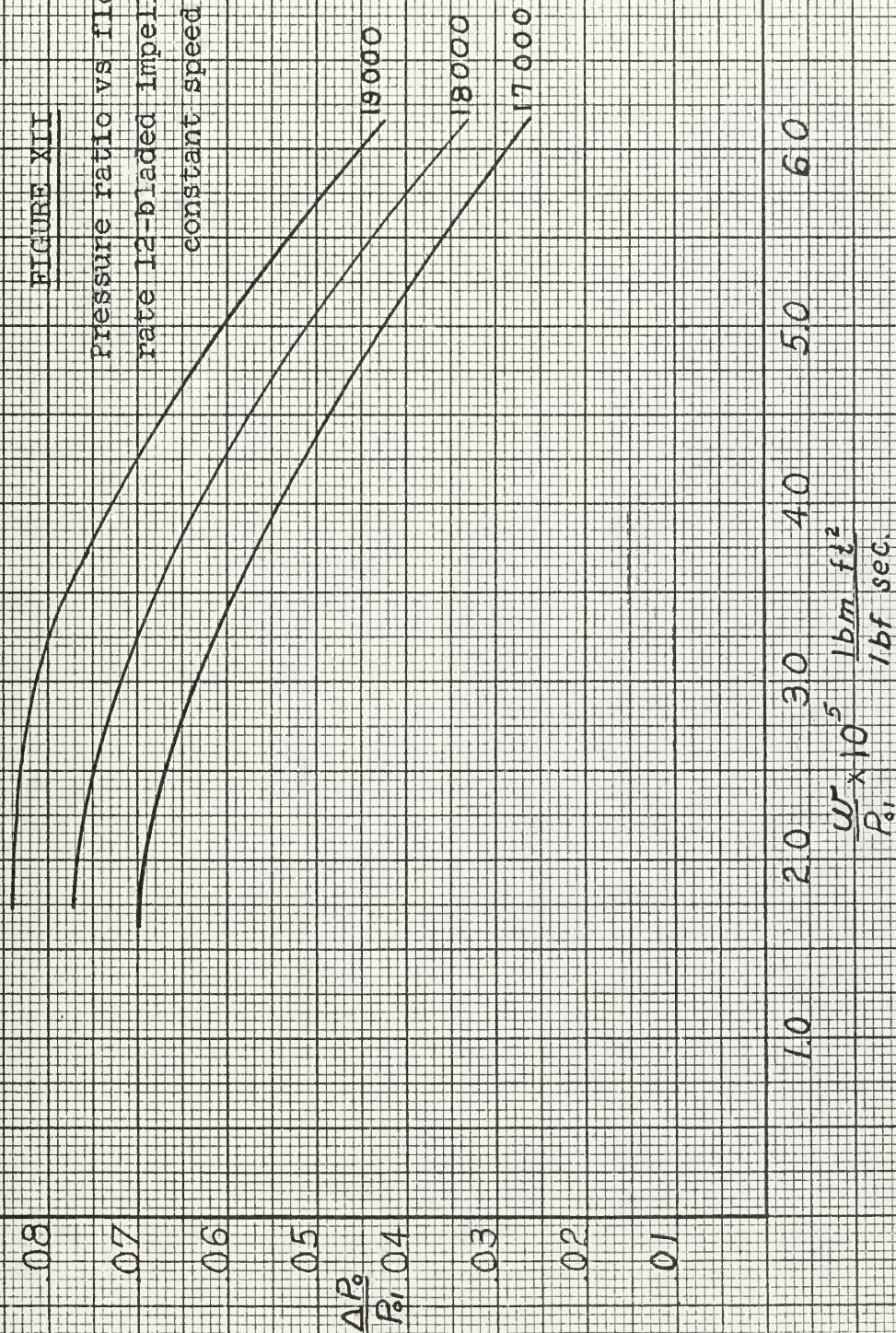
19000

18000

17000

$\dfrac{w}{P_{o_1}} \times 10^{-5} \; \dfrac{lbm \, ft^2}{lbf \, sec.}$

.08

.07

.06

.05

$\dfrac{\Delta P_o}{P_{o_1}}$ .04

.03

.02

.01

1.0   2.0   3.0   4.0   5.0   6.0

-24-

FIGURE XIII

Impeller efficiency vs flow rate 12-bladed impeller; constant speed.

η_i

17000
18000
19000

$\dfrac{wr}{p_{oi}} \times 10^{5} \dfrac{lbm\,ft^{2}}{lbf\,sec}$

-25-

Logarithmic Spiral Blade Shape

Analytical Solution of Two-dimensional Impeller Flow

Relative velocity parallel to blade indicated, ft/sec

17,000 RPM

$$w/p_{01} = 2.76 \times 10^{-5} \ \frac{\text{lbm ft}^2}{\text{sec lb}_f}$$

Six Blades
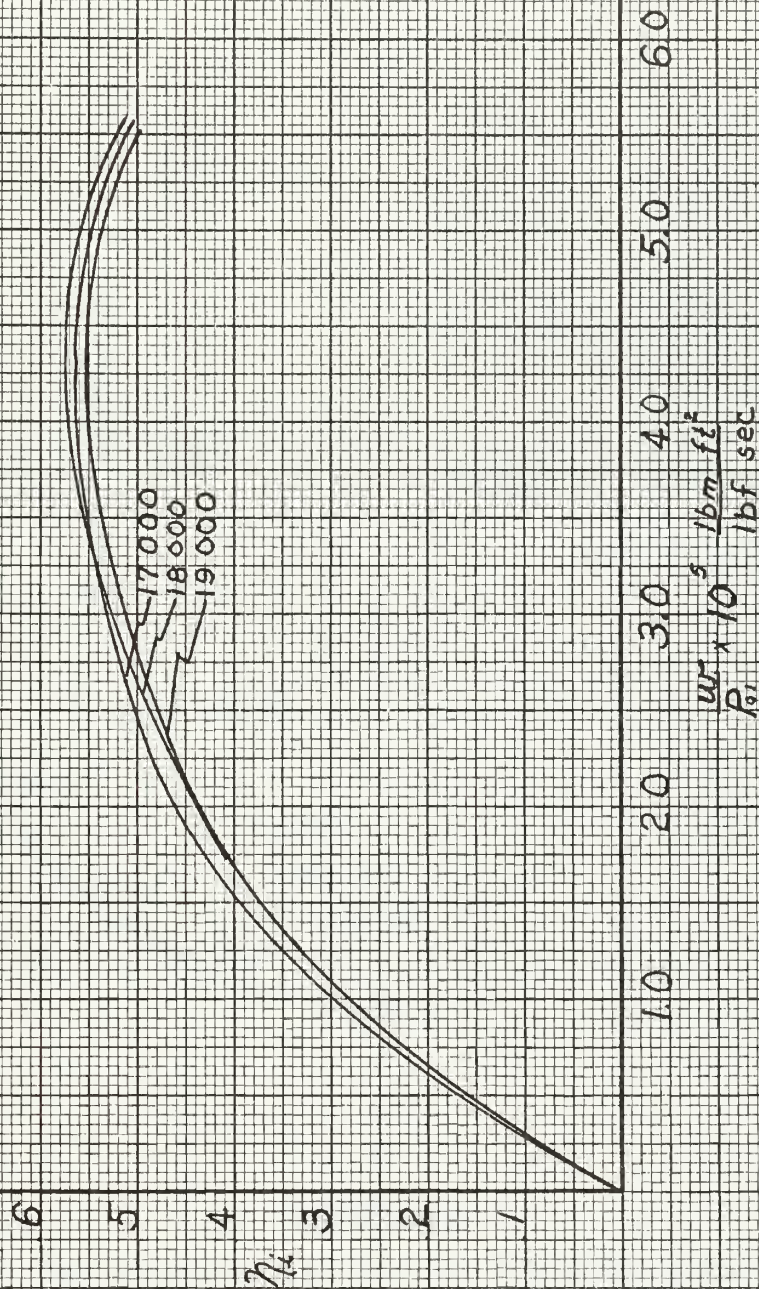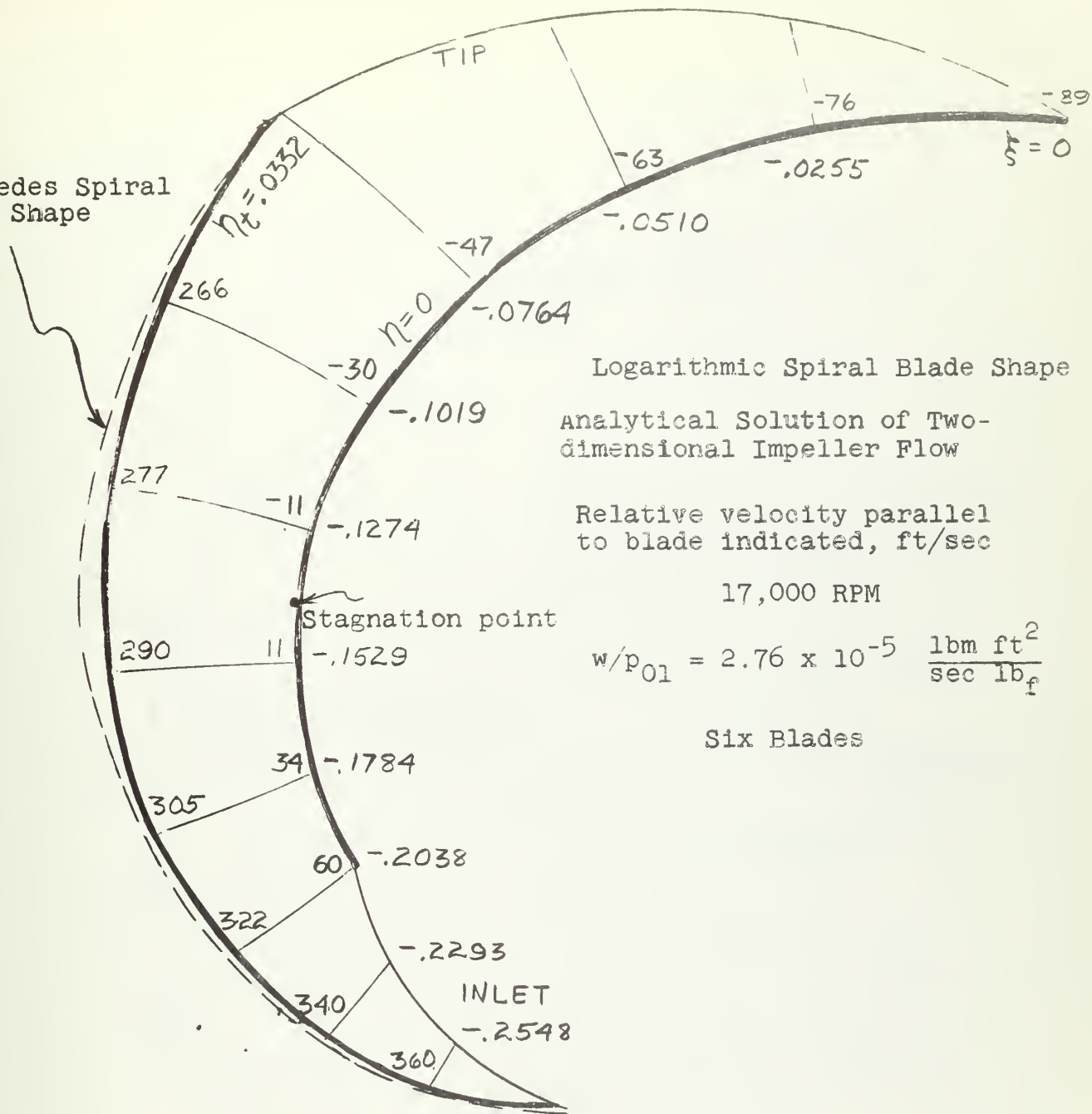
FIGURE XIV

Two-dimensional Theory 6-bladed Impeller

$\eta t = .0166$

176

TIP

27

186

39

$\eta = 0$

$\xi = 0$

$-.0255$

55

$-.0510$

$-.0764$

200

71

$-.1019$

Logarithmic Spiral Blade Shape

Analytical Solution of Two-dimensional Impeller Flow

Relative velocity parallel to blade indicated, ft/sec

17,000 RPM

$w/p_{01} = 2.76 \times 10^{-5} \ \dfrac{\text{lbm ft}^2}{\text{sec lb}_f}$

Twelve Blades

$215 \quad 89$

$-.1274$

Stagnation Point for 6-bladed Impeller.

110

231

$-.1529$

133

$-.1784$

250

158

$-.2038$

269

$-.2293$
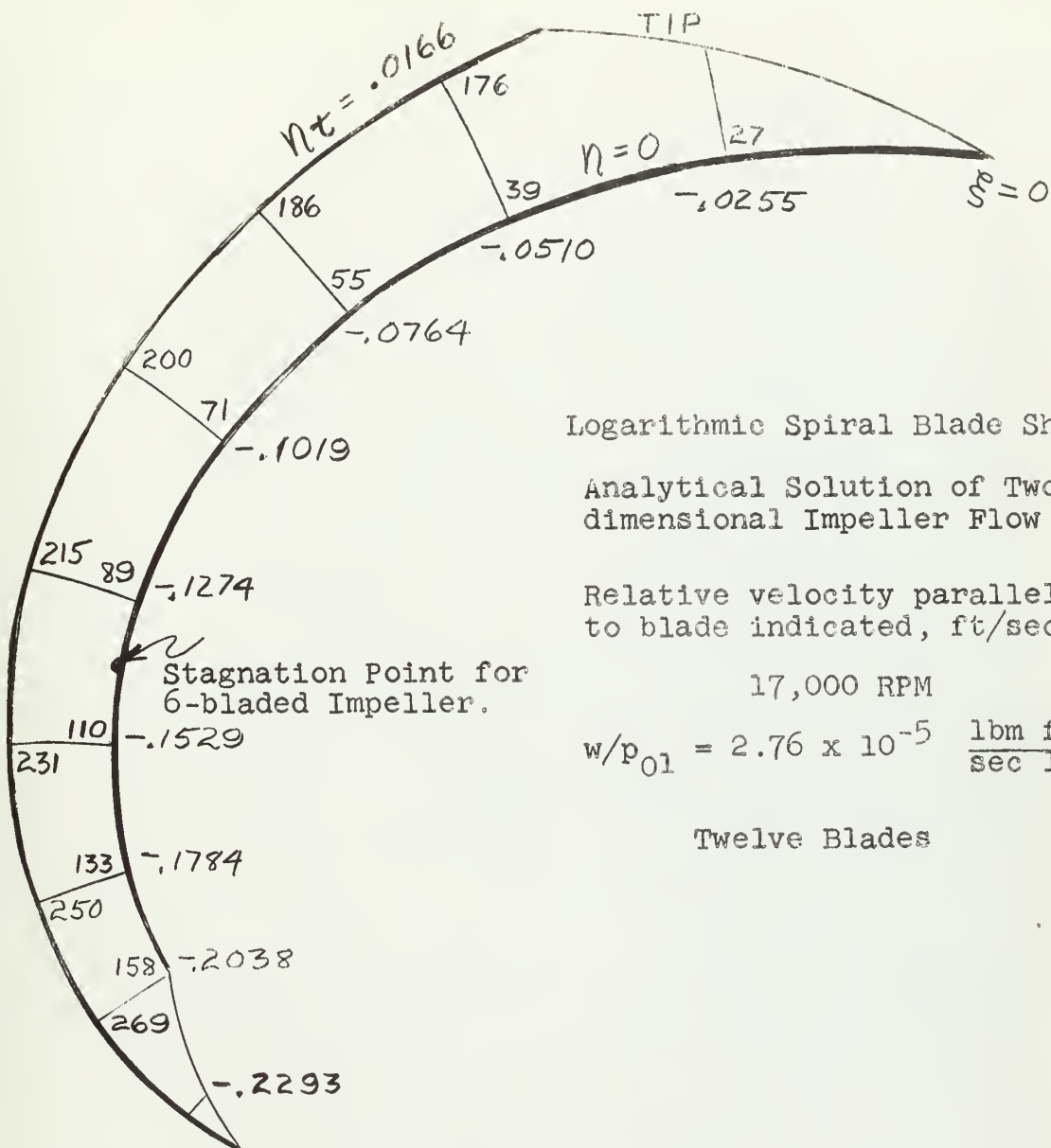
FIGURE XV

Two-dimensional Theory 12-bladed Impeller

-27-

FIGURE XVI

Number of blades vs relative velocity along
driving face; simplified theoretical solution

$\beta = -0.05096$

$\eta = 0$

N = 17,000 RPM

$\dfrac{w}{P_{01}} = 2.76 \times 10^5 \quad \dfrac{lbm\ ft^2}{lbf\ sec}$
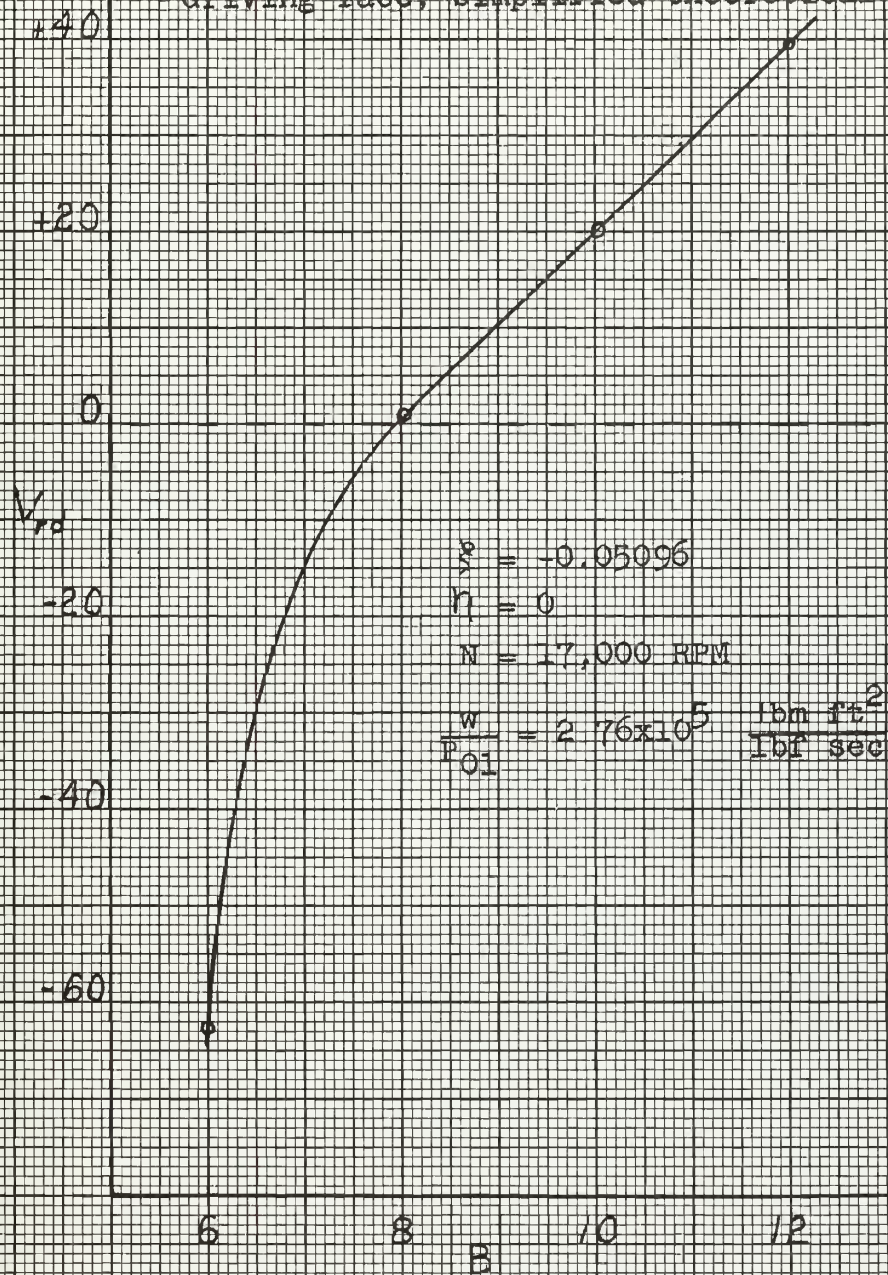
FIGURE XVII

Flow angle relative to impeller vs flow rate. 17,000 RPM

$\otimes$ DESIGN POINT
$\beta_2 = 22°$

DIRECT

SLOPE $\otimes$

MEASURED

$\beta_2°$

$\dfrac{w}{P_{01}} \times 10^5 \quad \dfrac{lbm\ ft^2}{lbf\ sec}$
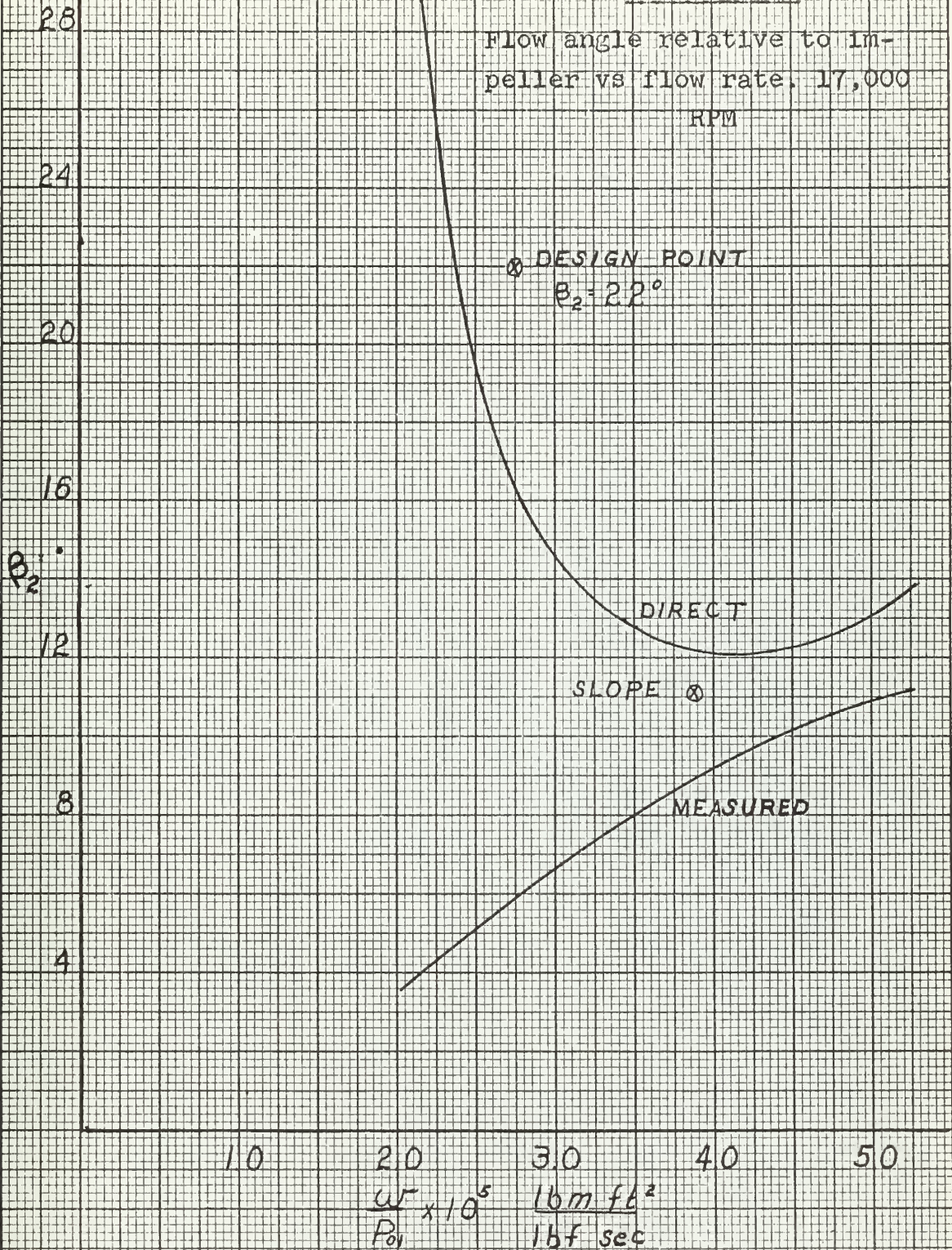
FIGURE XVIII.

Diffuser Efficiency vs Flow rate for Vaneless diffuser

$$\frac{W}{P_{01}} \times 10^{-5} \cdot \frac{lbm \cdot ft^2}{lbf \cdot sec}$$

η_D

-30-

ψ/ψ_t

0

.2

.4

.6

.8

.9

1.0
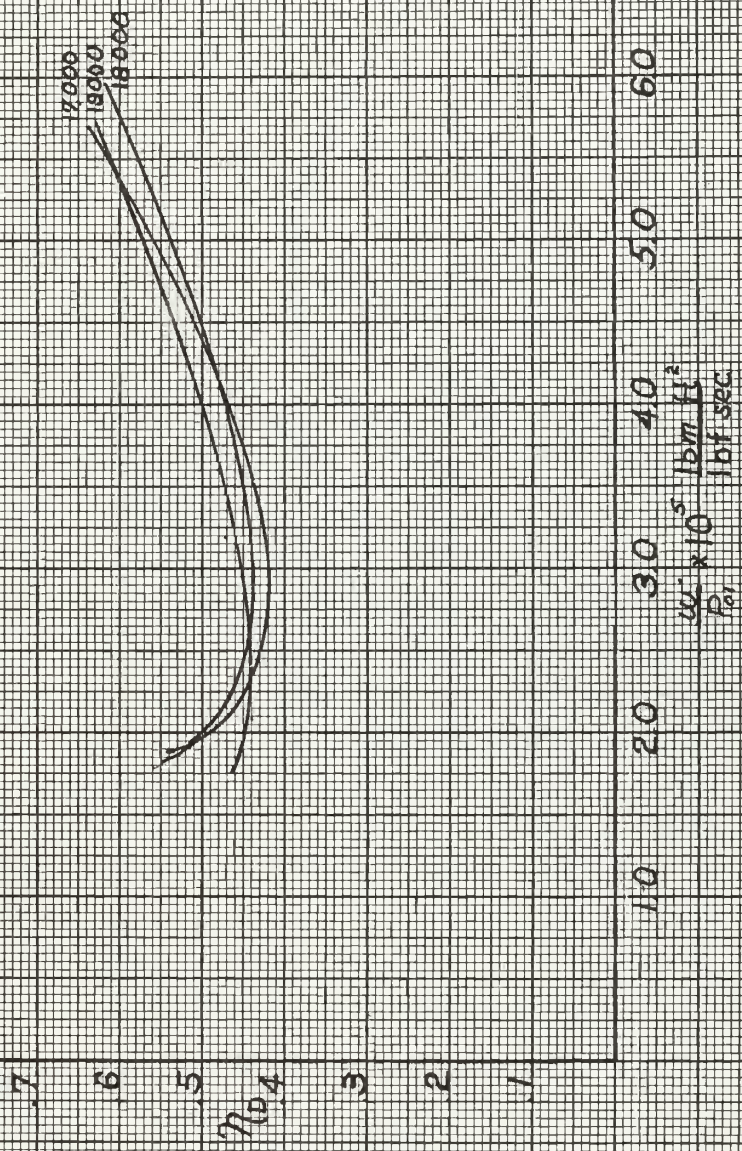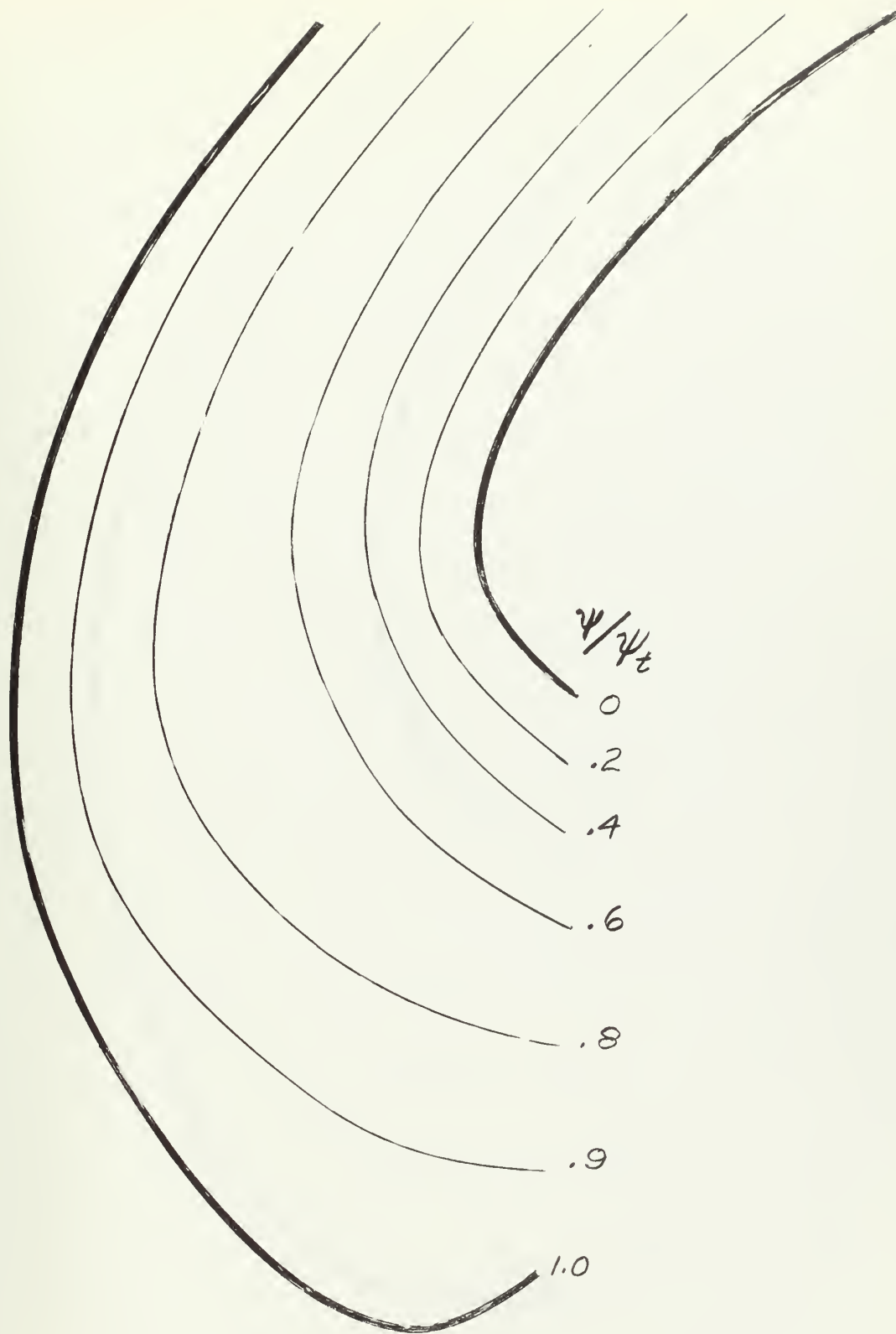
FIGURE XIX

Semi-conductor Solution for 5-Bladed
Diffuser

$$\frac{\psi}{\psi_t}$$

0
.2
.4
.6
.8
.9
1.0
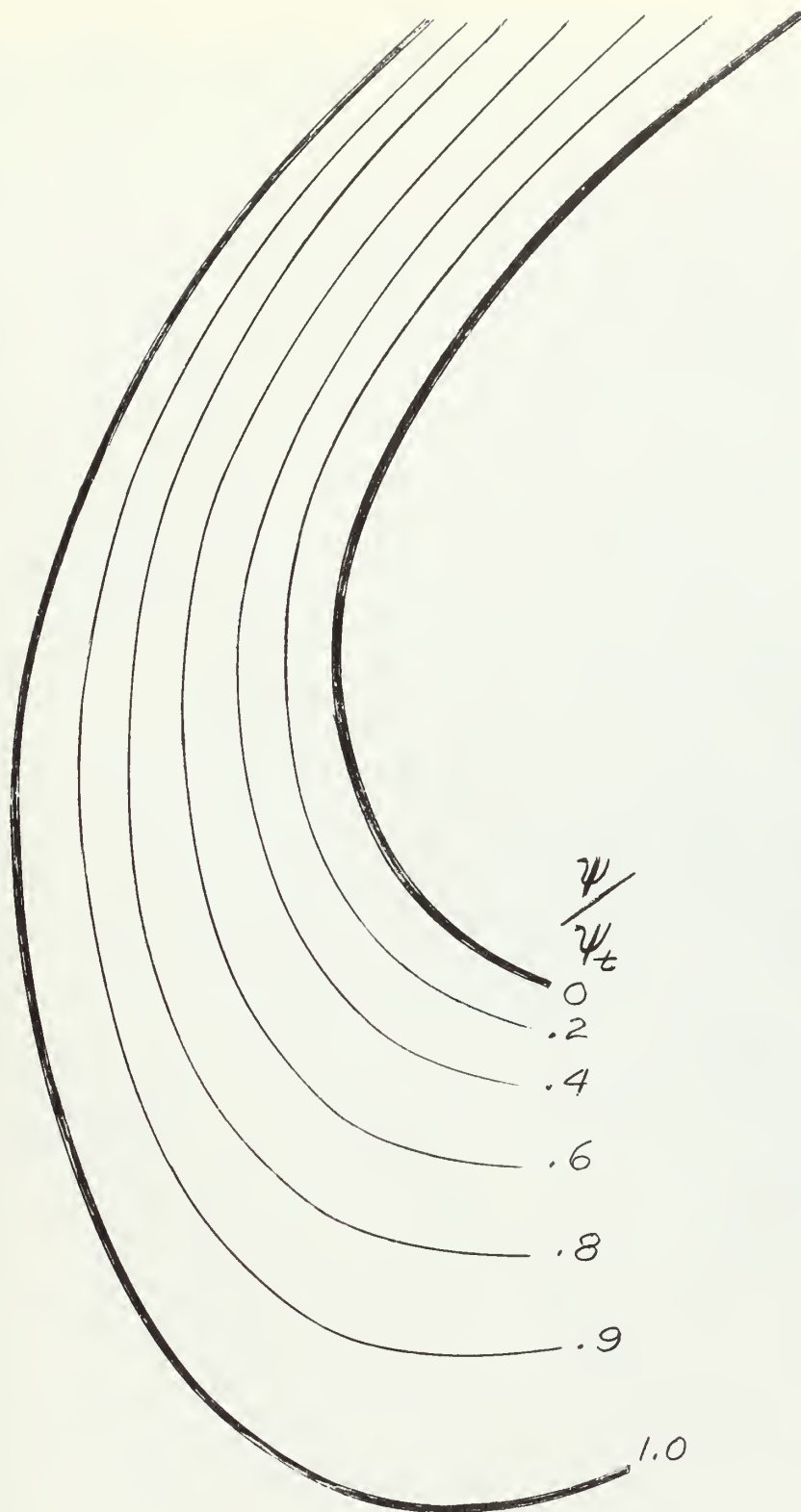
FIGURE XX

Semi-conductor Solution for 7-Bladed
Diffuser

-32-

FIGURE XXI

Compressor efficiency vs flow rate 6-bladed impeller;

17,000 RPM

a - vaneless diffuser
b - 5-bladed diffuser .3 in blades
c - 7-bladed diffuser .3 in blades
d - 5-bladed diffuser .42 in blades
e - 5-bladed diffuser .42 in blades
2.15" exit

$$\frac{\omega}{P_o} \times 10^5 \ \frac{lbm\text{-}ft^2}{lbf\text{-}sec}$$

η_c
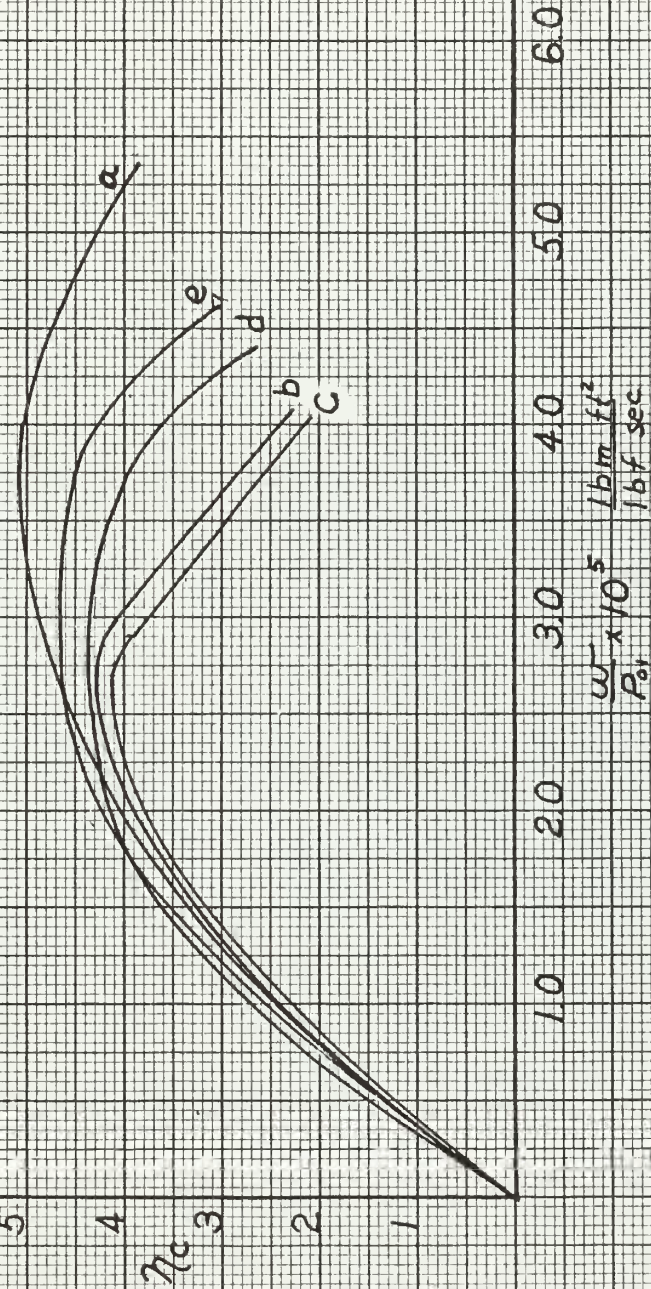
FIGURE XXII

Efficiency vs flow rate 6-bladed impeller; 18,000 RPM

a — vaneless diffuser

b — 5, 3 in blades

c — 7, 3 in blades

d — 5, .42 in blades

e — 5, .42 in blades 2.15 in exit

$\frac{\omega r}{P_{01}} \times 10^5 \; \frac{lbm \; ft^2}{lbf \; sec}$

n_c

-34-
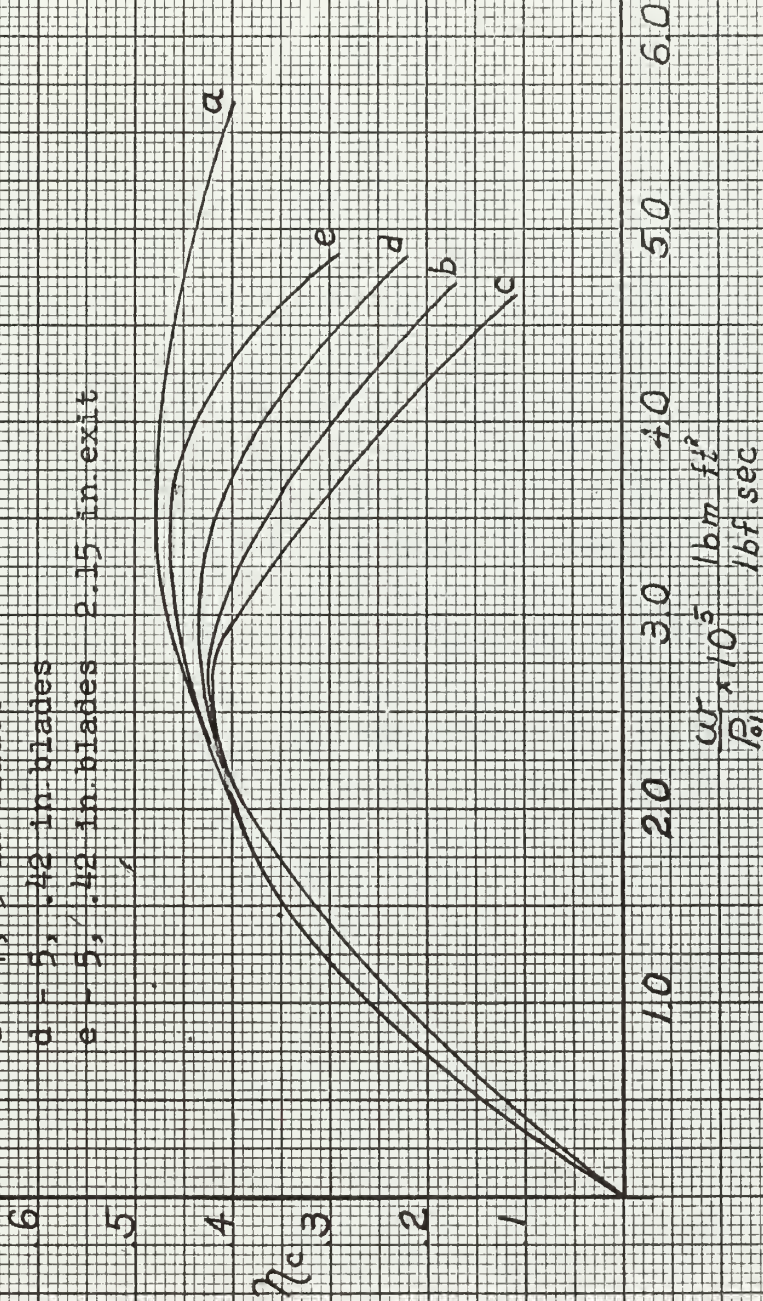
FIGURE XXIII

Efficiency vs flow rate 6-bladed impeller; 19,000 RPM

a - vaneless diffuser

b - 5, 3 in. blades

c - 7, 3 in blades

d - 5, .42 in blades

e - 5, .42 in blades 2.15 in exit

$\dfrac{w r}{P_{01}} \times 10^5 \ \dfrac{lbm \ ft^2}{lbf \ sec}$

-35-
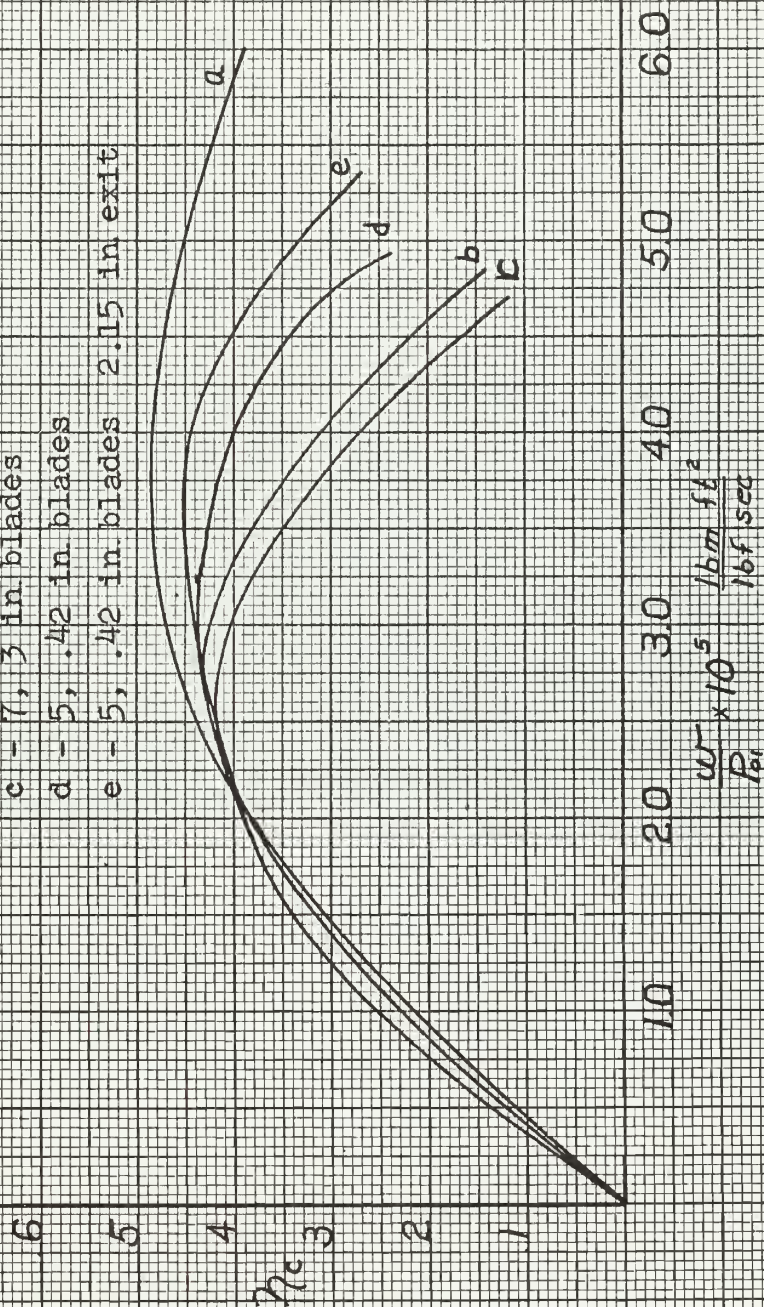
FIGURE XXIV

Pressure ratio vs flow rate 6-bladed impeller,

17,000 RPM

a - vaneless diffuser

b - 5, 3 in blades

c - 7, 3 in blades

d - 5, .42 in blades

e - 5, .42 in blades 2.15 in exit

$\frac{\Delta P_o}{P_{o1}}$

$\frac{w}{P_{o1}} \times 10^5 \frac{lbm\, ft^2}{lbf\, sec.}$
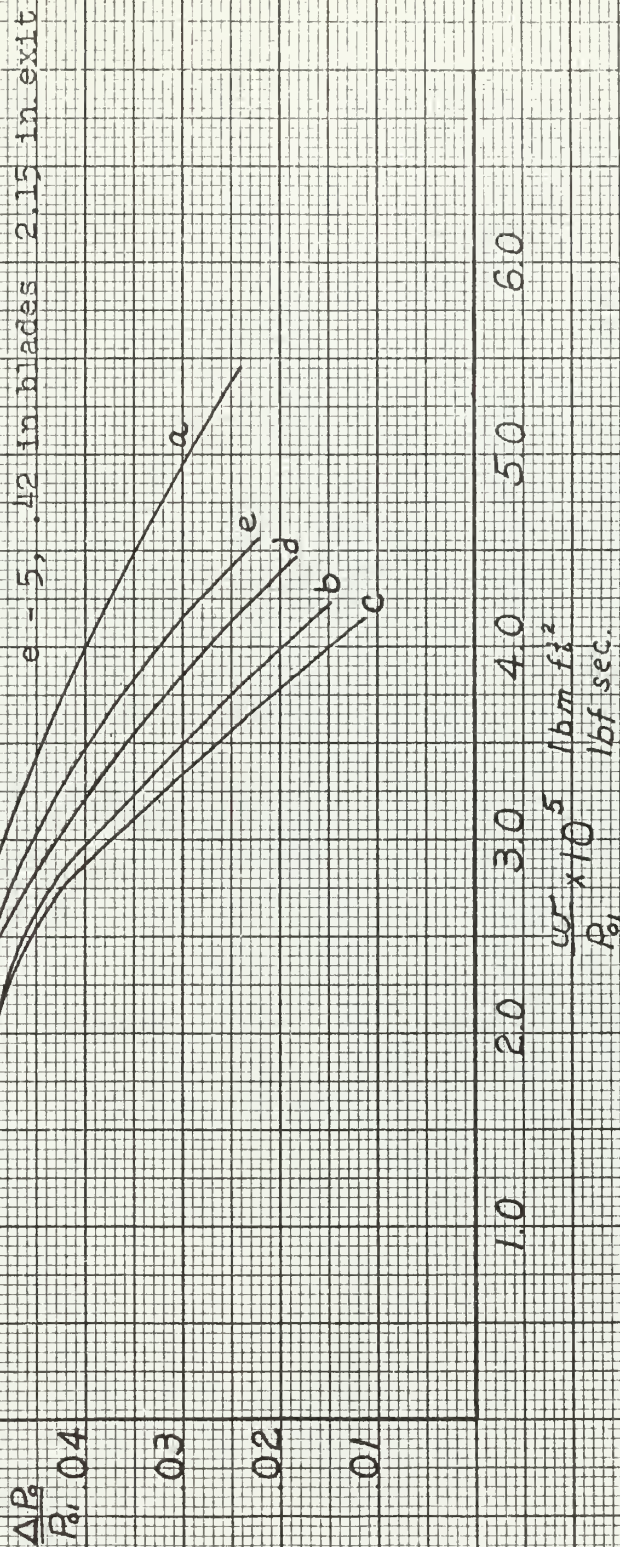
FIGURE XXV

Pressure ratio vs flow rate 6-bladed impeller, 18,000 RPM

a - vaneless diffuser
b - 5, 3 in. blades
c - 7, 3 in. blades
d - 5, .42 in. blades
e - 5, .42 in blades 2.15 in. exit

$\frac{\omega \sqrt{\tau}}{P_{o_1}} \times 10^5 \ \frac{lbm \ ft^2}{lbf \ sec}$

$\frac{\Delta P_1}{P_{o_1}}$

-37-
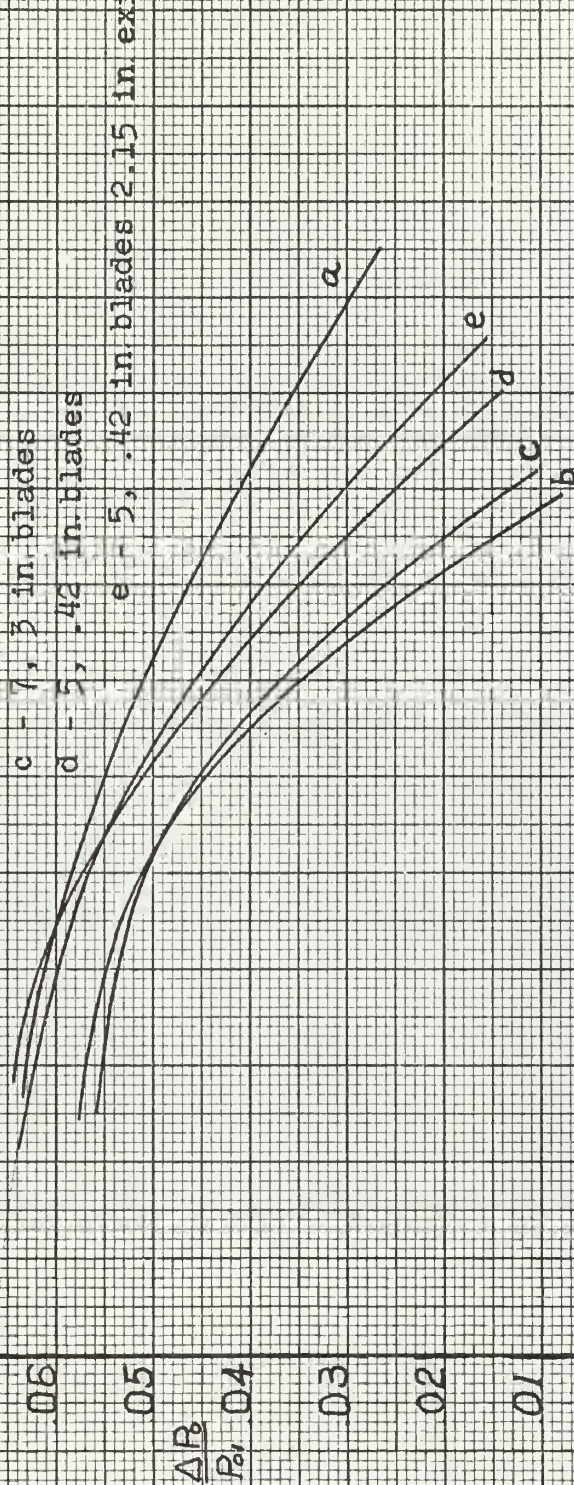
FIGURE XXVI

Pressure ratio vs flow rate 6-bladed impeller; 19,000 RPM

a – vaneless diffuser
b – 5, 3 in. blades
c – 7, 3 in. blades
d – 5, .42 in. blades
e – 5, .42 in. blades
2.15 in. exit

$\frac{\omega r}{P_{01}} \times 10^5 \quad \frac{lbm \cdot ft^2}{lbf \cdot sec}$

$\frac{\Delta P_0}{P_{01}}$
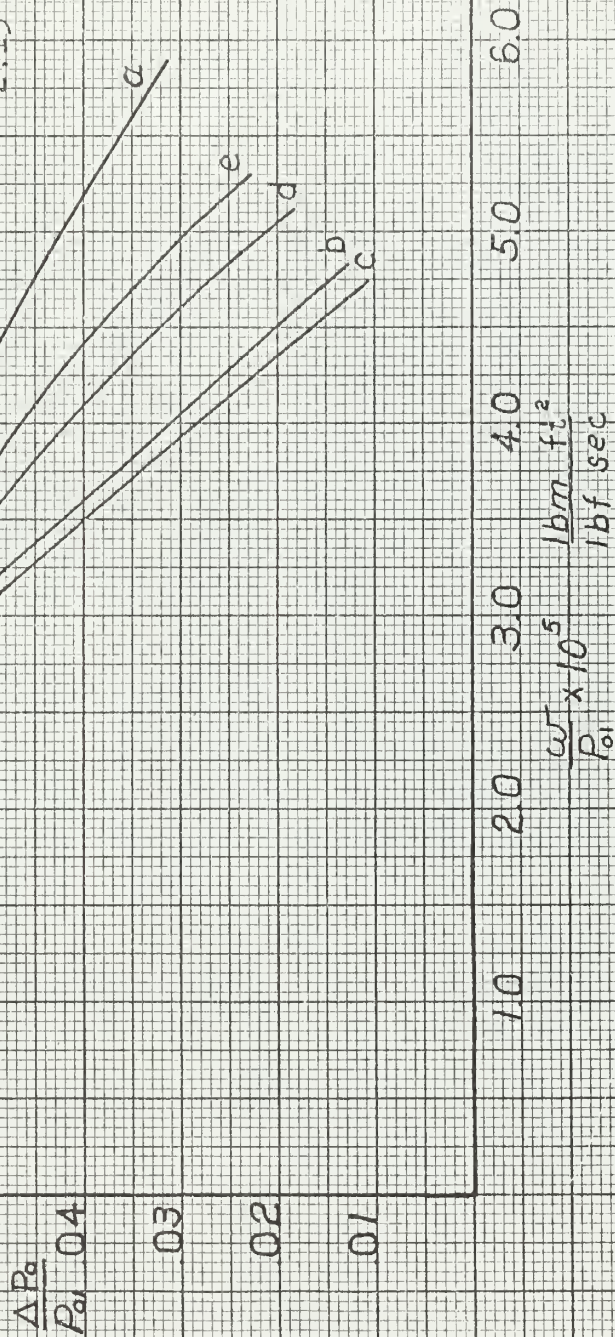
FIGURE XXVII

Efficiency vs flow rate 12-bladed impeller, 17,000 RPM

a – vaneless diffuser
b – 5 bladed diffuser, .3 in blades
c – 7 bladed diffuser, .3 in blades

$\frac{w}{p_{o_1}} \times 10^5 \quad \frac{lbm \cdot ft^2}{lbf \cdot sec}$

η_c

6 5 4 3 2 1

10   20   30   40   50   60

a
b
c

FIGURE XVIII

Efficiency vs flow rate 12-bladed impeller, 18,000 RPM

a - vaneless diffuser

b - 5 bladed diffuser, 3 in blades

c - 7 bladed diffuser, 3 in blades

$\dfrac{\omega}{P_a} \times 10^5 \ \dfrac{lbm \ ft^2}{lbf \ sec}$

η_c
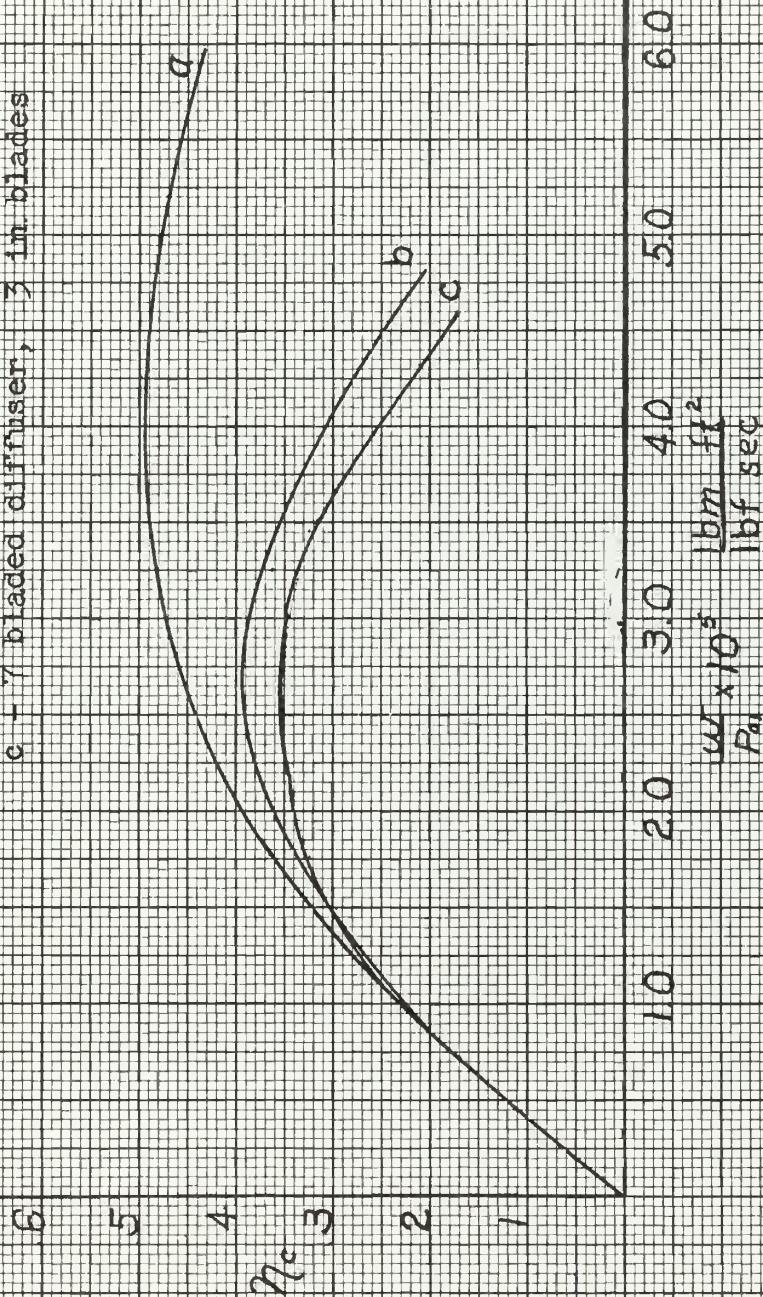
FIGURE XXIX

Efficiency vs flow rate 12 bladed impeller; 19,000 RPM

a - vaneless diffuser

b - 5 bladed diffuser, .3 in. blades

c - 7 bladed diffuser, .3 in. blades

$\frac{\omega \tau}{P_{01}} \times 10^5 \ \frac{lbm \ ft^2}{lbf \ sec}$

η_c

-41-
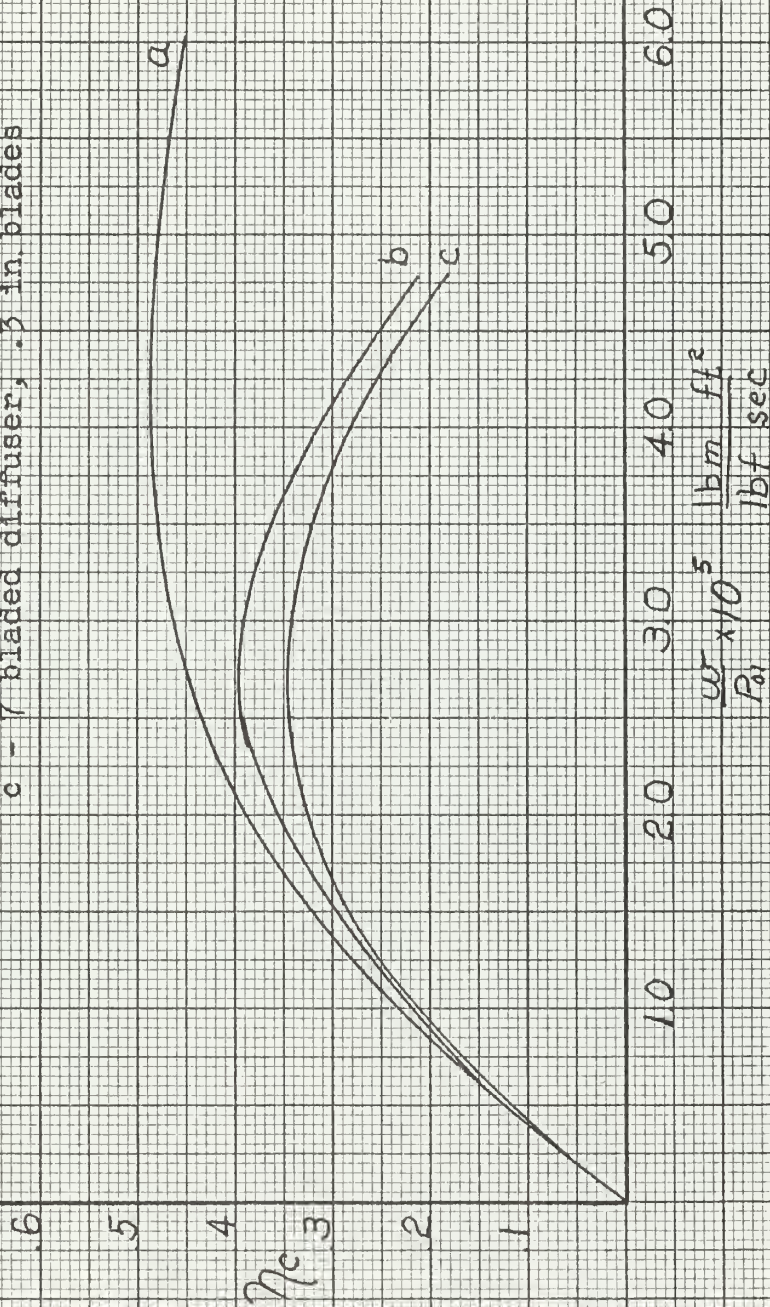
FIGURE XXX

Pressure ratio vs flow rate 12-bladed impeller; 17,000 RPM

a – vaneless diffuser
b – 5 bladed diffuser, 3 in. blades
c – 7 bladed diffuser, 3 in. blades
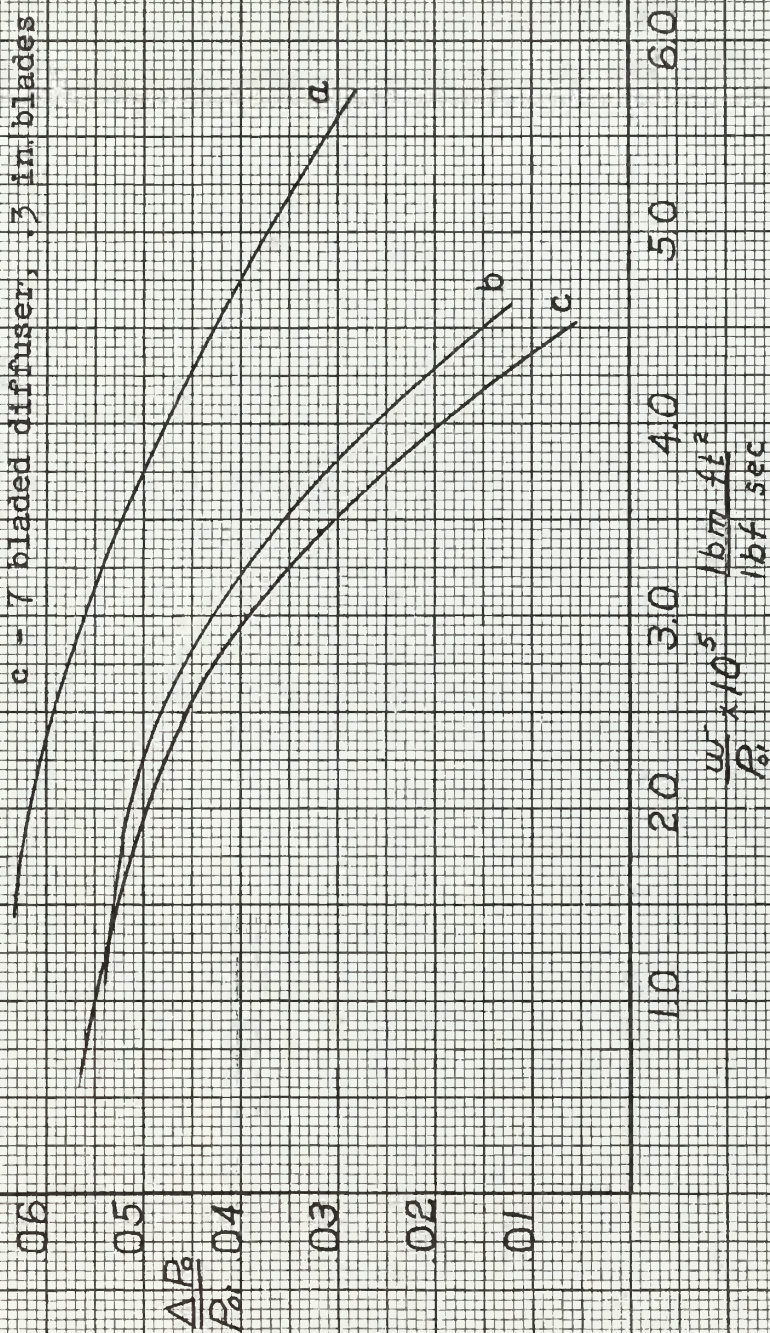
FIGURE XXXI

Pressure ratio vs flow rate 12-bladed impeller; 18,000 RPM

a - vaneless diffuser
b - 5 bladed diffuser, 3 in. blades
c - 7 bladed diffuser, 3 in. blades

$\dfrac{\Delta P_o}{P_{o'}}$

$\dfrac{w}{P_{o'}} \times 10^5 \quad \dfrac{lbm\ ft^2}{lbf\ sec}$

-43-

FIGURE XXXII

Pressure ratio vs flow rate 12-bladed impeller, 19,000 RPM

a. - vaneless diffuser
b. - 5 bladed diffuser,.3 in.blades
c. - 7 bladed diffuser,.3 in. blades

$$\frac{w}{P_{01}} \times 10^5 \quad \frac{lbm\ ft^2}{lbf\ sec}$$

-44-
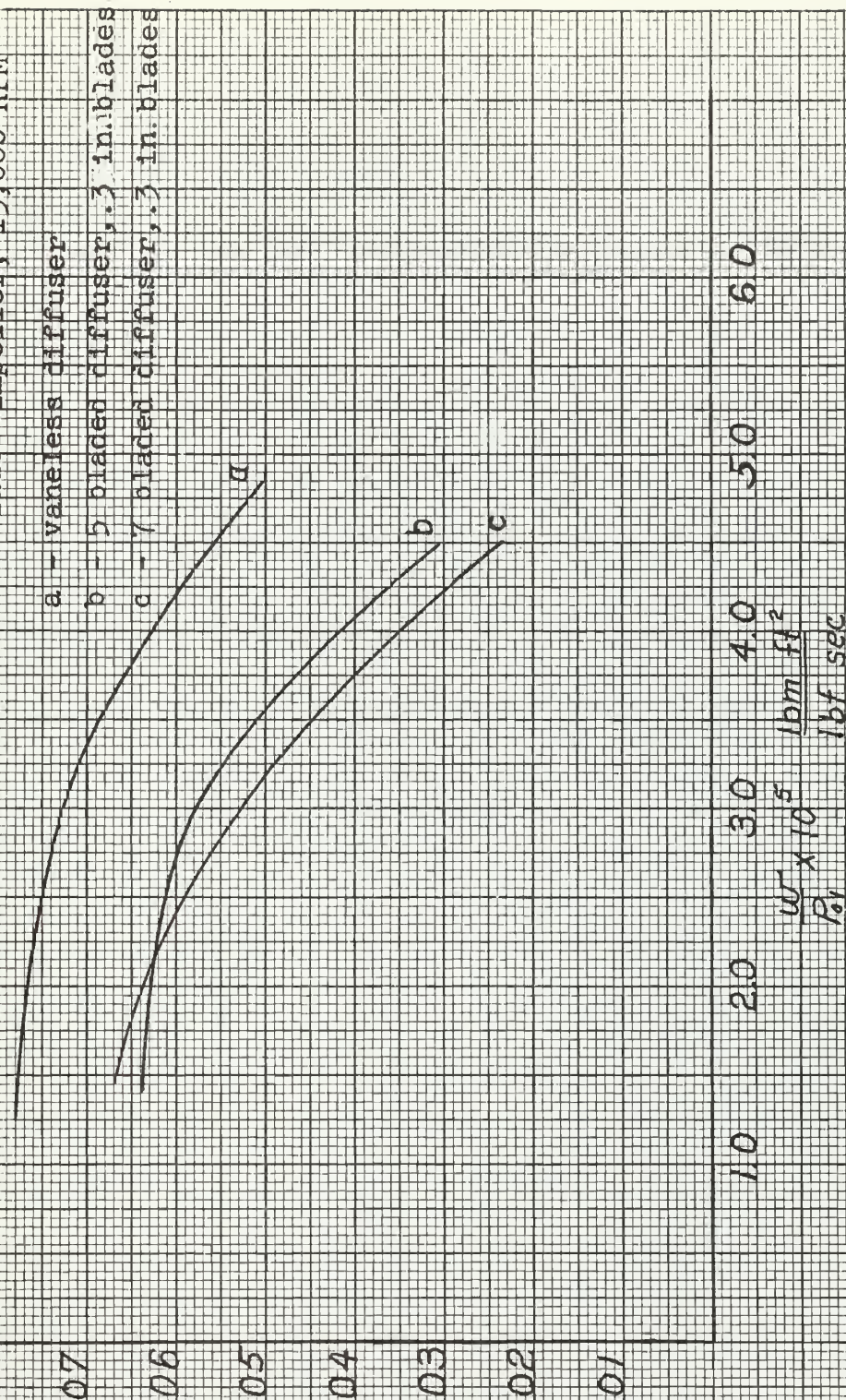
FIGURE XXXIII

Pressure ratio vs flow rate 6-bladed impeller; 17,000 RPM

Effects of varying b_D
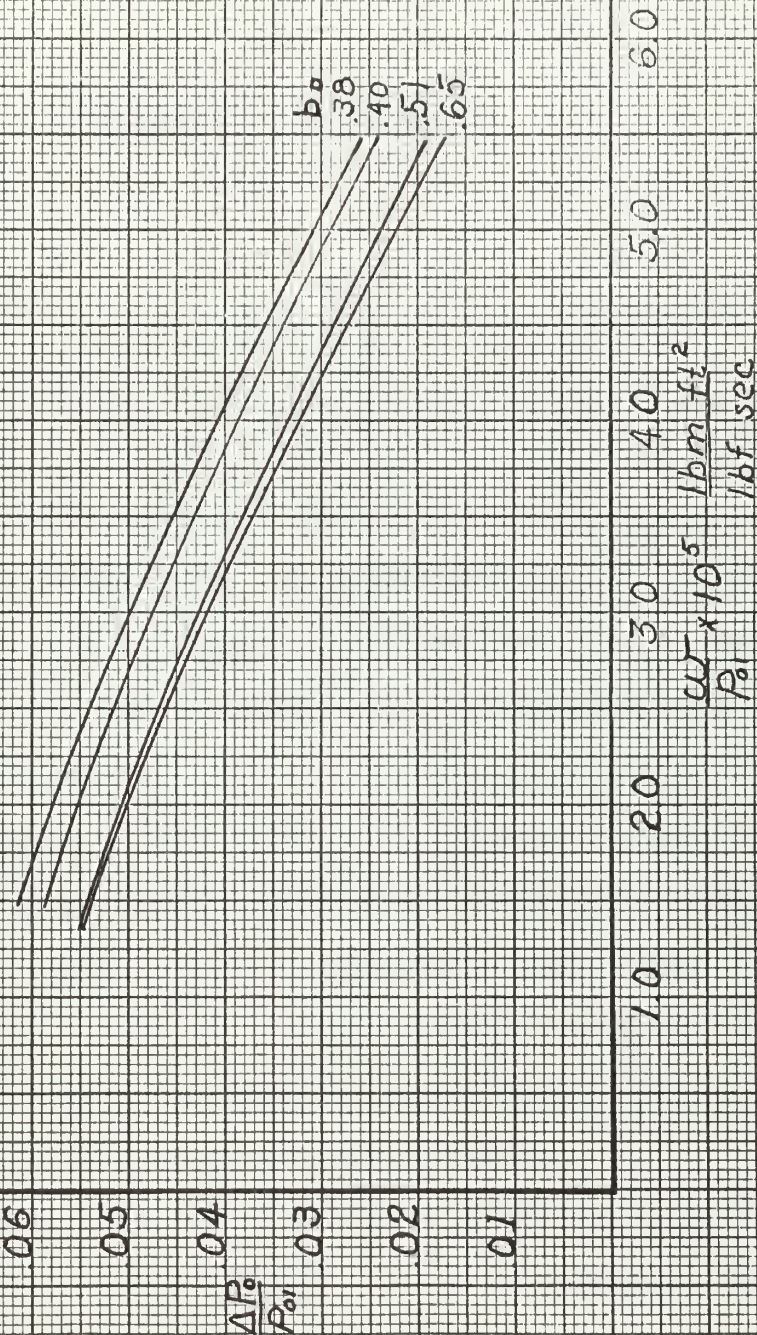
IV.

DISCUSSION OF RESULTS

Impellers

The curves of efficiency and pressure ratio for the impellers were typical for backward-curved blades. The results showed a definite advantage in pressure ratio for the twelve-bladed impeller, and the two-dimensional analysis confirmed the likelihood. The geometry of the impellers was similar, with possibly more friction loss in the twelve-bladed impeller, but no other factor indicated the improvement in performance as much as the elimination of eddies on the driving face of the blades. It was not likely that the eddies themselves were observed as pulsations in the flow, since the frequency was much less than rotational speed times the number of blades. The effect was more apt to be associated with the rotational stalls mentioned in Reference (12) at certain angles of exit flow.

The twelve-bladed impeller was considered more desirable from a performance standpoint. It is recommended that tests with twelve full blades be conducted.

Impeller Outlet Conditions

Because the flow at impeller outlet was not one-dimensional, it was difficult to predict the flow conditions accurately with such theory. Neither the flow angle nor the velocity was uniform in the radial or tangential direction. Any values chosen must be a mean. The flow pattern entering the diffuser was rotating also, such that only a mean condition could be assigned. The one-dimensional theory considered no friction losses or eddies, and hence was not adequate in evaluating flow conditions.

The exit flow angle relative to the impeller was not well defined by one-dimensional theory. Even the two-dimensional analysis was inadequate for this purpose because the solution was not complete for the whole blade, and the flow was assumed frictionless (irrotational). The Kutta condition of tangency of flow at exit could be satisfied, but that did not fix a constant angle across the passage.

The tests with variable outflow diffuser width showed little influence of increased clearance within the alignment limits of the apparatus. Circulation from impeller outlet to inlet rendered flow rate measurements quite ineffectual at large clearances.

At low flow rates the measurement of velocity became subject to the effects of windage. Even with the inlet sealed off, a velocity head was observed at impeller discharge, and

this was considered responsible for the upturn in the curve of vaneless outflow diffuser efficiency at low flow rates. Diffuser inlet conditions were taken as the measured angle of absolute velocity as determined by the yaw probe, and a velocity mean between that determined from known radial velocity (continuity) and that obtained from the difference between static and stagnation pressures at the diffuser inlet.

Outflow Diffuser Performance

The efficiency of the outflow diffuser chosen as a standard was somewhat less than expected. In Appendix D an investigation is presented which shows that friction may have accounted for appreciable loss of stagnation pressure. In addition, the decrease in efficiency at low flow rates was predicted. It has already been shown in Appendix A that reduction of a velocity gradient by internal shear also resulted in a loss of stagnation pressure. In addition, there was very likely a loss of pressure due to the rotating stalls associated with the surge stability limit of the compressor, but the magnitude was not predicted by this investigation.

It is recommended that more thorough study be made of the outflow diffuser to determine that an optimum arrangement is used as the comparative standard.

Inflow Diffuser Performance

The severe pressure gradients at the transition from impeller to diffuser rendered it impossible to fix values for determining impeller and diffuser performance with any accuracy. For this reason the performance of the two were considered only as a combination for the compressor. It was not assumed that the impeller conditions were the same as with the outflow diffuser, so that inflow diffuser performance could not be arrived at indirectly.

The semi-conductor paper analysis made no allowance for friction. The condition of constant rotation was therefore not a completely satisfactory model of the actual flow. The assumption of irrotationality was even less accurate. It was considered that there was value in the comparison of the two inflow shapes, however, if only in showing the relatively small effect of blade shape under the same flow conditions.

Evaluation of the stream function and velocities was not made, but would provide an indication of tendency toward separation. In addition, it is felt that the comparison of even more blade shapes may show features which show minimum tendency toward separation under the flow conditions encountered in these tests.

Compressor Performance

Although not considered an optimum diffuser, the curves of the vaneless diffuser were taken as the standard of performance. In the regions of small flow rate, the compressor performance with inflow diffuser was very nearly identical with that using the outflow diffuser. The transition from impeller to diffuser did not appear to cause substantial losses. At medium flow rates the sharp decline in performance of the inflow diffusers could be caused by increased losses in the transition, separation in the diffuser, or failure of the diffuser to be able to diffuse the larger mass of fluid to a low exit velocity. The five-bladed diffuser showed slightly better performance than the seven-bladed diffuser. It would be expected that the seven-bladed diffuser would have more friction losses caused by more and longer blades. The seven-bladed diffuser was also designed to operate at a slightly lower flow rate, based on inlet angle.

The substantial improvement in compressor performance achieved by widening the diffuser occurred only above the point where performance had previously dropped sharply. Since the primary effect of greater width was to diffuse axially and reduce velocities in a plane perpendicular to the centerline, this suggested that separation played a large part in the previous decline. As the blade width

increased, flow departed further from the two-dimensional model. A three-dimensional or mixed-flow diffuser would appear to offer better performance.

It is recommended that tests be made of larger-scale diffuser channels to determine both two- and three-dimensional pressure and velocity gradients. In addition, a more detailed study of the transition may permit clearer delineation between impeller and inflow diffuser performance.

The improvement in performance obtained by increasing the outlet diameter of the inflow diffuser may be attainable if there are limitations of exit pipe size or inlet to another stage. It is possible even to increase the diffuser outlet diameter to that of the impeller outlet, in which case no diffuser as such exists. If larger exit diameter were permissible, it would offer a convenient way of diffusing the flow further than otherwise possible.

It must be noted that this investigation concerned a compressor with small pressure ratio, and that the results are not expected to be valid for substantially higher pressure ratios. The effect of clearances especially is apt to be much greater at higher pressure ratios. Impeller performance will decrease if adverse pressure gradients become too severe. Experiments with compressors containing inflow diffusers should be made at higher pressure ratios to serve as a comparison with these results.

V.

CONCLUSIONS

1.

At low pressure ratios, performance of the compressor with inflow diffuser was similar to that with vaneless outflow diffuser in the region of low to medium flow rates.

2.

Above medium flow rates, the performance of the inflow apparatus decreased sharply. Separation appeared to be the primary cause. Transition losses leaving the impeller and failure to diffuse the larger mass of fluid were considered contributing factors.

3.

Increasing the width of the inflow diffuser blades substantially improved the inflow diffuser performance at higher flow rates. This was attributed to a reduction in separation along the blades caused by partial diffusion in the axial direction.

4.

Increasing the inflow diffuser outlet diameter improved performance at higher flow rates by permitting the flow to diffuse to a lower exit velocity.

5.

   With two different blade shapes, each achieving mean-
streamline divergence, the shape of the blades had little
effect on the inflow diffuser performance.

6.

   Large pressure gradients in the transition from impeller
to inflow diffuser made it impractical to separate the per-
formance of the impeller and inflow diffuser by measurement.
Combined performance as a compressor was more readily attained.

VI.

RECOMMENDATIONS

1. If an outflow diffuser is used as a comparative standard, it should be studied thoroughly to determine that it is an optimum.

2.
   More inflow diffuser blade shapes should be studied by means of semi-conductor paper. Velocity gradients should be evaluated in order that separation tendencies may be noted and minimized.

3.
   Three-dimensional analysis is indicated. Experimentally this will require a larger apparatus than that used for this report.

4.
   Larger single- or multiple-channel models of inflow diffusers would offer a means of measuring actual pressure and velocity gradients for either two- or three-dimensional diffusers.

5.
   A study of the transition from impeller to inflow diffuser should be made to insure minimum losses and to assist experi-

mentally by allowing the impeller and inflow diffuser performance to be separately defined.

6.

Tests should be made at higher pressure ratios to compare inflow and outflow diffuser performance and the effects of internal circulation.

7.

Impeller tests with twelve full blades should be made to determine if even higher pressure ratios can be achieved with this apparatus.

A P P E N D I X

APPENDIX A

Details of Procedure

For the problem under consideration, the following parameters are independent or controllable: rotational speed; geometry of the apparatus; flow rate; inlet temperature; and outlet (atmospheric) pressure.

The following quantities are dependent upon those listed above: impeller inlet pressure; pressure in the impeller and the diffuser; torque applied; velocities in the impeller and the diffuser; and the compressor, impeller, and diffuser efficiencies.

In the derivation of both one- and two-dimensional analyses it is assumed that the flow enters the impeller with no pre-swirl.

The flow parameter w/p_{01} is taken from reference (6). The complete expression is $\dfrac{w}{D^2}\dfrac{\sqrt{c_p T}}{p_{01}}$, but temperature effects were neglected because of constant environmental temperature at the apparatus. The procedure for evaluating w is that given in references (10,11). The basic flow equation is

$$\frac{w}{\gamma} = .0997 \; CFd^2 \; \frac{y \sqrt{h_w \, \gamma}}{\gamma}$$

For the specific case of a 1.2" diameter orifice in a 2.067" pipe, this equation may be written

$$q' = .528 \ K'y \sqrt{h_w} \qquad (1)$$

K' is obtained from Figure XXXIV, and a Reynolds Number of 10^5 is assumed initially for each run. In this case, K' = .6539. The weight density of air was found to vary less than one percent in all runs, and a constant value of .0736 pounds per cubic foot was used. Y is a function of h_w and p_{1m} and is plotted in Figure XXXV. q' is a trial flow rate, dependent upon an assumed Reynolds number.

The Reynolds number may be expressed by

$$R = \frac{.004244w}{D \ g\mu} \qquad (2)$$

Inserting appropriate constants, equation (2) becomes

$$R = 1.25 \times 10^5 q \qquad (3)$$

From this relationship, a new K can be found from Figure XXXIV. Finally,

$$q = \frac{K}{K'} \ q' \qquad (4)$$

To obtain w/p_{01}, the flow rate q is multiplied by a constant and divided by the inlet stagnation pressure manometer reading in inches of water:

$$\frac{w}{p_{01}} = \frac{.01415q}{p_{01}} \quad \frac{lb_m \ ft^2}{sec \ lb_f} \qquad\qquad (5)$$

As a result of many runs on different days, it was determined that q may be expressed merely as a function of h_w given by Figure XXXVI without undue loss of accuracy. This curve applies only to the orifice and inlet pipe associated with this apparatus.

The torque arm of the dynamometer was graduated in .02 inches, and it was felt that reading to the nearest .05 inch was a practical limit of accuracy. The resultant error was within one percent in the usual operating range.

Impeller and compressor efficiencies were based on flow work actually done on the fluid $(q\Delta P)$ compared to the input work to the impeller $(T\omega)$. Various thermodynamic efficiencies are defined for gases; however they are not as appropriate when working in the incompressible range. Figure XXXVII was obtained as a check on approximate motor efficiencies and power requirements.

One of the major problems involved in this study was the determination of conditions at the impeller exit, or conversely, at the diffuser inlet. A one-dimensional approach offers the simplest estimate of impeller exit velocity and pressure ratio. Considering the following sketch,

-58-

FIGURE XXXIV

Flow coefficient vs Reynolds number

orifice diameter/pipe diameter = 0.580
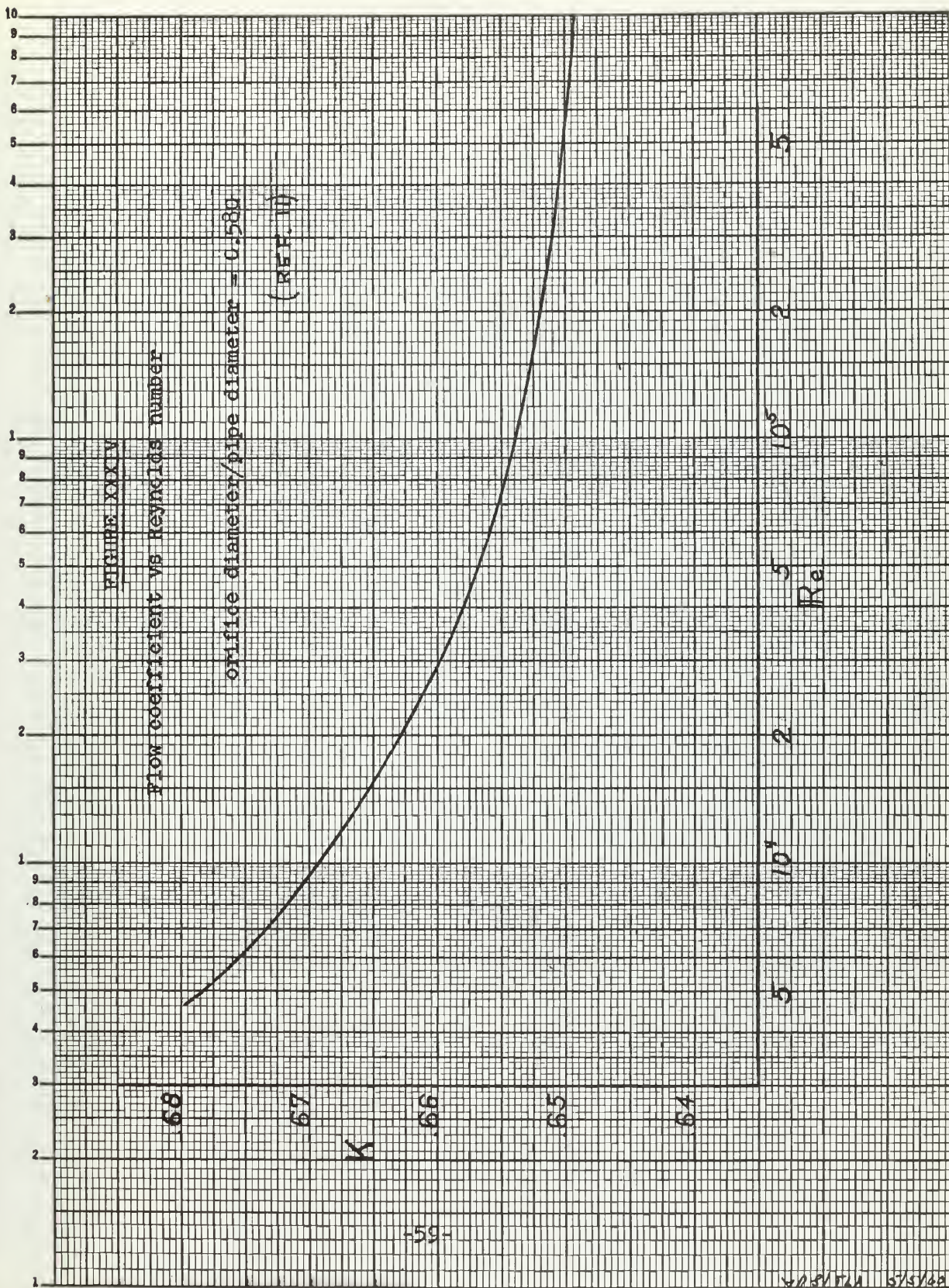
(REF. 1)

FIGURE XXXV

Flow correction coefficient

(REF. 10)

YRS TLN 6/9/60

FIGURE XXXVI

Volumetric flow rate vs pressure differential
across orifice

h_w (in of H_2O)

q (cfs)

J.P.S. 12A 5/15/40
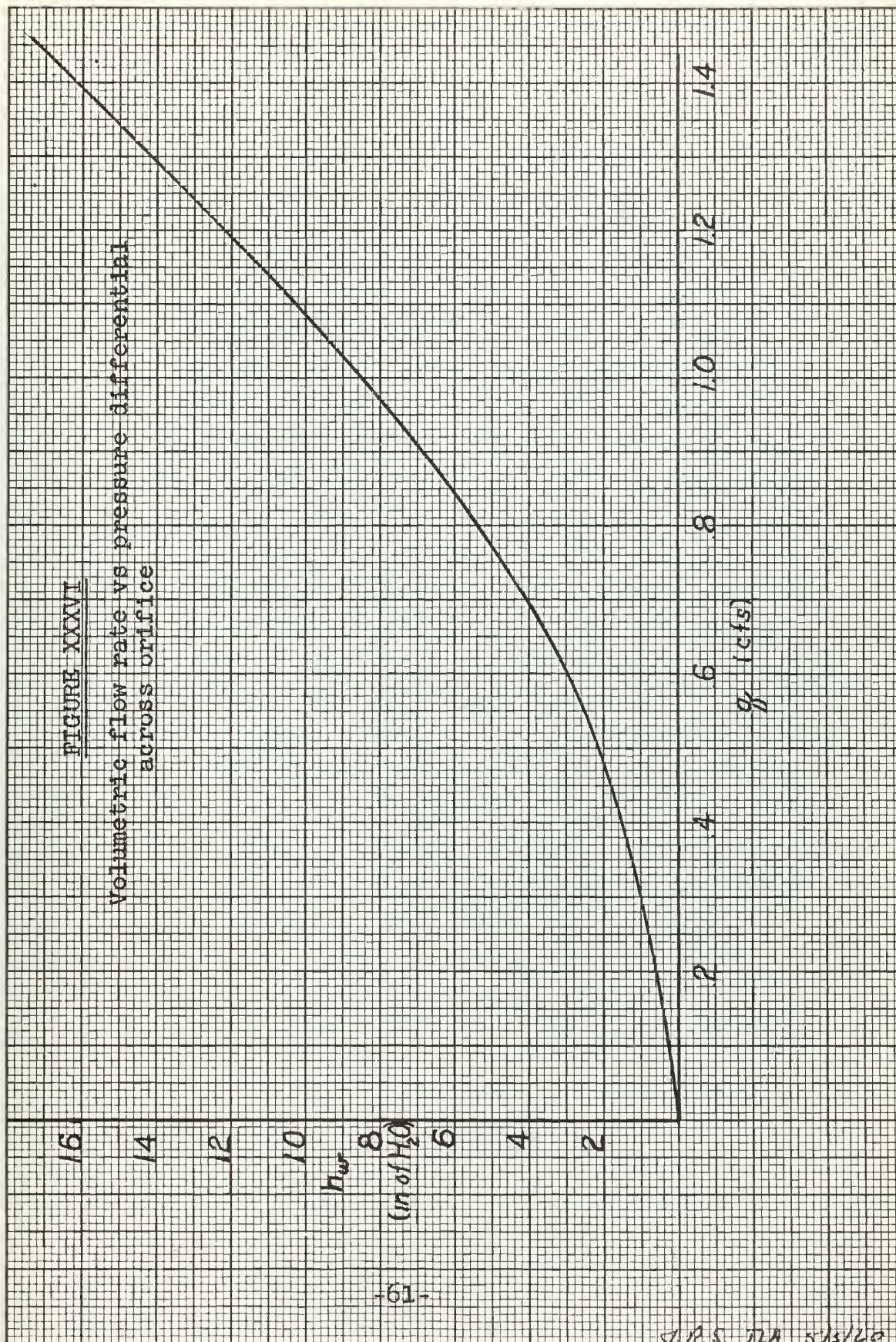
FIGURE XXXVII

Compressor power to motor and impeller
vs flow rate at constant speed

Motor

Impeller

19000
18000
17000
19000
18000
17000

HP
.8
.7
.6
.5
.4
.3
.2
.1

$\dfrac{wr}{P_{o_1}} \times 10^5 \quad \dfrac{lbm \cdot ft^2}{lbf \cdot sec}$

0   10   2.0   3.0   4.0   5.0   6.0
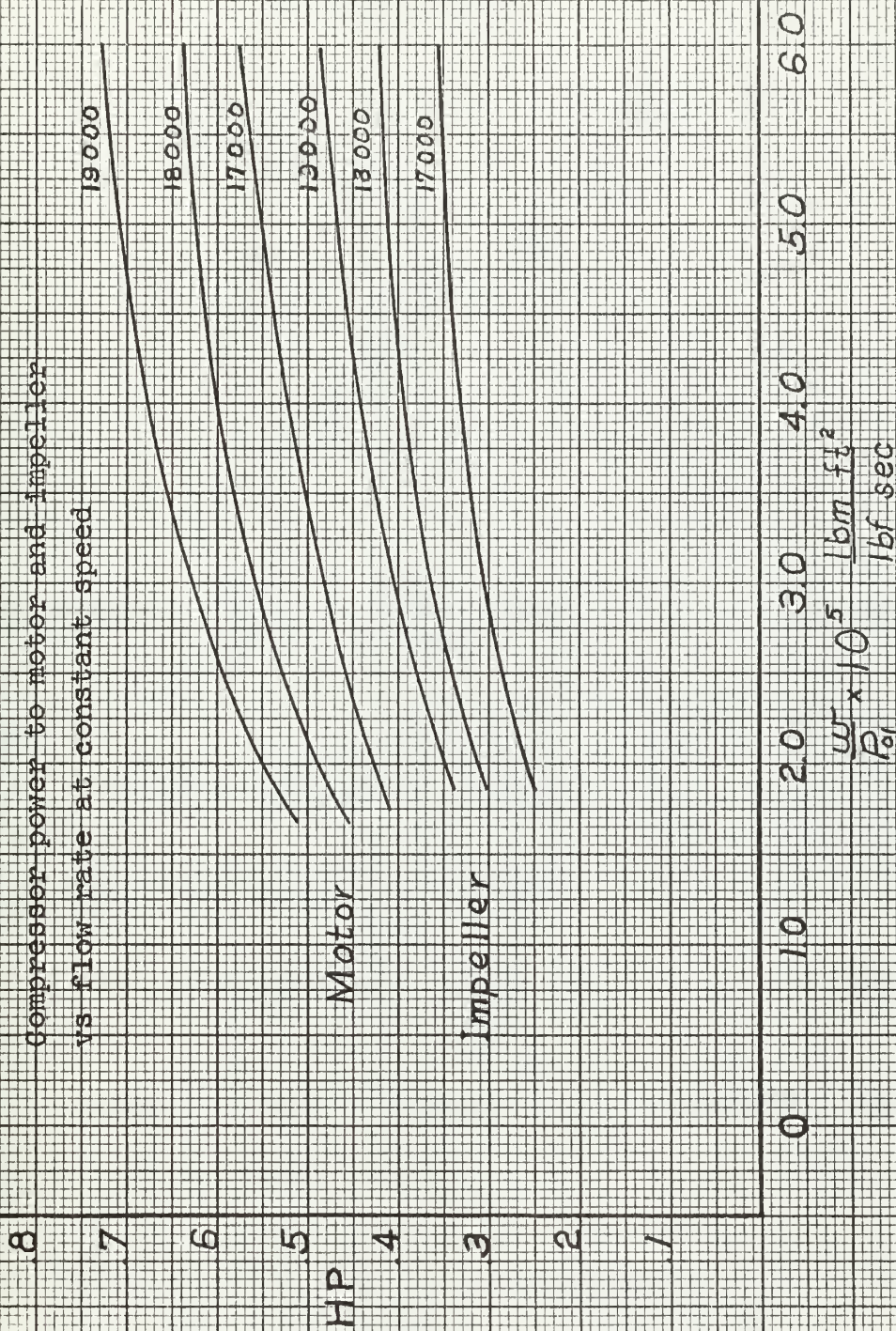
FIGURE XXXVIII
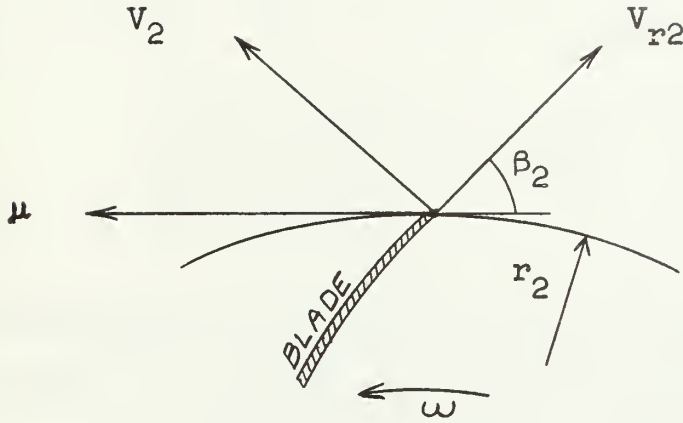
$$\text{input work} = -\frac{\mu^2}{g_o} \left(1 - \frac{V_{r2}}{\mu} \cos \beta_2\right) \tag{6}$$

where,

$$V_{r2} = \frac{w}{2\pi\, r_2\, b\, \rho\, \sin \beta_2} \tag{7}$$

Neglecting changes in height,

$$\text{output work} = \frac{\Delta\, p_o}{\rho} \tag{8}$$

For one hundred percent impeller efficiency, equations (6) and (8) combine to give

$$\frac{\Delta\, p_o}{p_{01}} = \frac{\mu^2}{g_o\, R\, T_{01}} - \frac{w}{p_{01}}\; \frac{\mu}{2\pi\, r_2\, b\, g_o\, \tan \beta_2} \tag{9}$$

The impeller which was initially studied was a standard Electrolux impeller which was run at 17,000, 18,000, 19,000 and 20,000 RPM. The principal dimensions are:

Outlet diameter of blades   4.92"
Inlet diameter of blades   2.00"
Blade width   0.30"

This impeller was designed as an Archimedes spiral, with inlet blade angle of 39° to the tangent, and outlet blade angle of 18° to the tangent. One impeller was disassembled, and the actual inlet angles were 18° to 20°. The maximum angle was approximately 27° near mid-blade. In the interest of future analysis, the actual blade was represented by a logarithmic spiral making an angle of 22° to the tangent. A comparison of actual and approximate blade shapes is shown in Figure XIV. For purposes of analysis a 22° exit angle is used throughout.

Equation (9) expresses the theoretical pressure rise which may then be compared with actual conditions. This is shown in Figure IX.

Equation (9) is also useful in roughly estimating the actual exit flow angle. By rearrangement, for actual flow according to the one-dimensional model:

$$\tan \beta_2 = \frac{\dfrac{\eta_1 \mu}{2\pi\, r_2\, b\, g_o} \dfrac{w}{p_{01}}}{\dfrac{\mu^2 \eta_1}{g_o R\, T_{01}} - \dfrac{\Delta p_o}{p_{01}}} \qquad (10)$$

Using actual values of η_1 and $\frac{\Delta p_o}{p_{01}}$ for a given w/p_{01}, a plot of effective angle β_2 can be obtained.

Furthermore, if equation (9) is differentiated with respect to w/p_{01}, at the point of maximum η_i, $(\frac{\partial \eta_i}{\partial \frac{w}{p_{01}}} = 0)$, there is obtained:

$$\tan \beta_2 = \frac{\frac{\mu^2 \eta_i}{g_o R T_{01}}}{\frac{-\partial \frac{\Delta p_o}{p_{01}}}{\partial \frac{w}{p_{01}}}} \qquad (11)$$

The result is shown later on a graph as the slope method.

Still another estimate of β_2 may be obtained by measuring the actual absolute exit flow angle α_2. From the velocity vector relationship at exit, it can be shown that

$$\tan \beta_2 = \frac{1}{\frac{2\pi r_2 b \rho \mu}{w} - \cot \alpha_2} \qquad (12)$$

A yaw probe was used to measure α_2 at impeller exit for several flow rates at 17,000 RPM, and the absolute angles were obtained. A comparison of the three methods of determining β_2, all based on a one-dimensional flow model, is shown in Figure XXVII.

A series of data was taken at 17,000 RPM to determine the effect of axial clearance on the performance of the

apparatus. It was desired to obtain an estimate of the amount of circulation from impeller outlet to inlet. The effects are shown in Figure XXXIII.

The impeller was also sealed off at inlet and run at 17,000 RPM to determine how much pressure rise could be obtained only from leakage past the impeller.

Two-Dimensional Analysis of Impeller

Since one-dimensional theory gives only a very rough picture at the impeller exit, it was considered appropriate to make a two-dimensional analysis for the purpose of estimating velocities within the six-bladed impeller. The development of this analysis is based on work in reference (2).

It is assumed that the flow is guided perfectly by the blades; hence this analysis is valid only along the blades, with no boundary layer or separation present. Limits of accuracy are discussed in reference (2) based on comparison with relaxation solutions.

The approximation of the actual impeller with a logarithmic-spiral impeller permits the transformation of polar coordinates to new orthogonal coordinates ξ and η. The following symbols are defined in reference (2).

-66-

$$\phi = \frac{w}{\rho_0 \, a_2 \, c_0}$$

$$\eta = \phi(\theta - \cot \beta \, \ln R)$$

$$c_0 = \sqrt{k \, g \, R \, T_{01}}$$

$$\xi = \phi(\ln R + \theta \cot \beta)$$

$$a_2 = B \, \sigma_2 \, r_2 \, h_2$$

$$R = \exp \left[4.425 \left(\xi + 2.48 \eta \right) \right]$$

$$M_2 = \frac{\omega \, r_2}{c_0} = \frac{\mu}{c_0}$$

$$\psi_t = \eta_t = \phi \, \sigma$$

FIGURE XXXIX
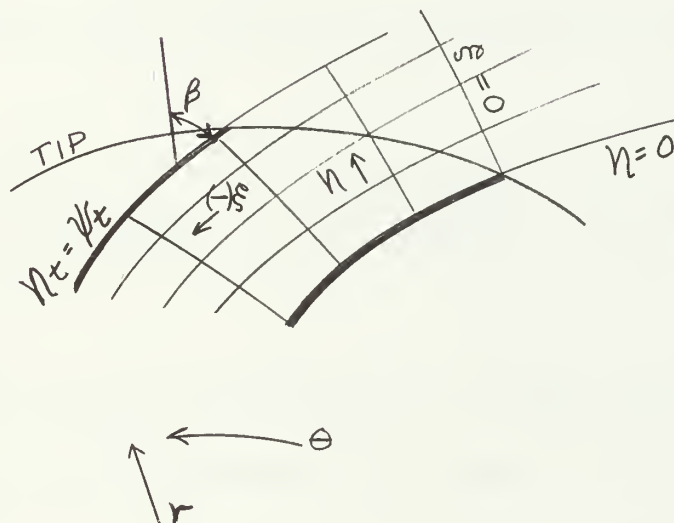
For imcompressible flow the Mach number is fictitious
and inlet conditions are used only as a reference. Ir-
rotational flow is assumed, expressed in the form

$$-2M_2 = \frac{V_\Theta}{R} + \frac{\partial V_\Theta}{\partial R} - \frac{1}{R} \frac{\partial V_r}{\partial \Theta} \tag{13}$$

where

$$Q = \text{velocity relative to blade}$$
$$V_\Theta = Q \cos\beta$$
$$V_r = Q \sin\beta$$

Substituting and transforming coordinates:

$$-2M_2 \exp\left(\frac{\xi - \eta \cot\beta}{\emptyset \cos^2\beta}\right) = Q \csc\beta - \frac{2\emptyset}{\sec\beta} \frac{\partial Q}{\partial\eta} \tag{14}$$

Integrating this expression and applying boundary conditions:

$$Q = \frac{2M_2}{\csc\beta} \exp\left[\frac{\xi}{\emptyset \cos^2\beta}\right] \sinh\left[\frac{\eta \cot\beta}{\emptyset \cos^2\beta}\right] + Q_d \exp\left[\frac{\eta \cot\beta}{\emptyset \cos^2\beta}\right] \tag{15}$$

In terms of the stream function, velocities are defined as follows, for incompressible flow in a blade of constant width:

$$V_r = \frac{1}{R} \frac{\partial \psi}{\partial \Theta}$$

$$V_\Theta = - \frac{\partial \psi}{\partial r}$$

Taking the derivative of the stream function,

$$d\psi = \frac{\partial \psi}{\partial \Theta} d\Theta + \frac{\partial \psi}{\partial r} dr$$

or

$$d\psi = r\,V_r\,d\theta - V_\theta\,dr$$

Expressing this in the transformed coordinates,

$$d\psi = \frac{Q\,R\,\sec\beta}{\phi}\,d\eta$$

and therefore

$$\psi_t = \frac{\sec\beta}{\phi}\int_0^{\eta_t} Q\,R\,d\eta \qquad (16)$$

where Q is given by Equation (15).

This function may be integrated numerically to the known value of ψ_t. It is then possible to solve for Q_d. Applying the value of η at the trailing face, it is also possible to compute Q_t. For this integration η was taken in four equal increments and ξ was taken in ten equal increments.

As shown in Section III, this theoretical study indicated the desirability of using impellers with more than six blades. An impeller with twelve blades was available from the Electrolux Corporation, although the alternate blades were shortened slightly at the inlet and thus deviated somewhat from the analytical model. This impeller was tested with the vaneless outflow diffuser using the same procedure as in the six-bladed tests.

Since the primary reason for using a vaneless outflow diffuser was to provide an indication of the maximum diffuser performance, a brief analysis was made to determine the effect of a linear tantential velocity gradient entering the diffuser. It was assumed that the exit flow was uniform as a result of internal shear forces while the fluid passed through the channel. For the simplest case, a straight two-dimensional channel was considered.

FIGURE XL
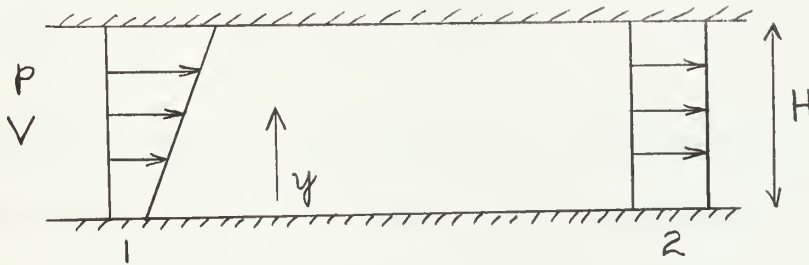
$$V_1 = V_o + c\,y \tag{17}$$

$$\overline{p_{01}} = \frac{\int_0^H \rho\, V_1 (p_1 + \frac{\rho\, V_1^2}{2})\,dy}{\int_0^H \rho\, V_1\, dy}$$

$$\overline{p_{01}} = p_1 + \rho/2\,(V_o^2 + CHV_o + \frac{C^2 H^2}{2}) \tag{18}$$

-70-

From continuity,

$$V_2 = V_o + \frac{C}{2} H \tag{19}$$

From conservation of momentum,

$$p_1 H - p_2 H = \rho V_2^2 H - \rho \int_o^H V_1^2 \, dy \tag{20}$$

Combining (17), (18), (19), and (20),

$$\overline{p_{01}} - p_{02} = \frac{1}{12}(\rho/2 \; c^2 \; H^2) \tag{21}$$

Applying the same procedure to a diverging channel, the stagnation pressure loss cannot be expressed in simple terms. For the case where the channel height doubles, it can be shown that

$$\overline{p_{01}} + \frac{1}{4} \rho V_o^2 + \frac{1}{4} \rho V_o CH + \frac{\rho \; c^2 \; H^2}{48} = 2 \; p_{02} \tag{22}$$

Assuming $\overline{p_{01}} > p_{02}$, (22) becomes

$$\overline{p_{01}} > \frac{1}{4} \rho V_o^2 + \frac{1}{4} \rho V_o CH + \rho \frac{c^2 H^2}{48} \tag{23}$$

But, from Equation (18),

$$\overline{p_{01}} = p_1 + \rho/2 \; V_o^2 + \rho/2 \; V_o CH + \rho \frac{c^2 H^2}{4} \tag{24}$$

Since p_1 is zero or positive, Equation (24) is term by term greater than Equation (23), and the assumption of a stagnation pressure loss is correct for this case. It is not expected that there be a quantitative comparison with the diffuser flow in question.

Inflow Diffuser Study

The investigation of the inflow diffusers was not begun. A five-bladed diffuser of standard Electrolux design was available for testing. In addition, a seven-bladed diffuser of new design was tested. The new diffuser satisfied the conditions that the blades be purely radial at exit and that the area normal to a mean streamline increase along the streamline. It was possible to express analytically the new blade shape by

$$r = r_2 + a \sqrt{\theta} \tag{25}$$

where r_2 is the inner blade radius, and θ was measured from the inner end of the blade. The shapes of these diffusers are shown in Figures VII and VIII.

Figure IV shows a sketch of the mounting of the inflow diffusers. Essentially the same apparatus was used as in the previous tests. Clearances were somewhat greater because of the can design, as shown in Figure IV. Stagnation and static pressures were measured midway between impeller

and diffuser. It is to be expected that there is a strong axial and radial pressure gradient in this bend, so any location is somewhat arbitrary in measuring impeller output. Results of tests using both diffusers with both six- and twelve-bladed impellers are shown in Section III.

A vaneless inflow "diffuser" was tested under the same conditions as the bladed diffusers. This device was more properly a vortex chamber, and performance was so poor that the entire output of the impeller appeared as loss in the diffuser. The results of these tests are not quantitatively considered any further.

Thus far only experimental procedure has been discussed for the inflow diffusers. In conjunction with these tests, the equations of motion were developed for the flow to assist in understanding the nature of the flow in the diffuser passages.

For incompressible, two-dimensional flow consider the following element of fluid:

FIGURE XLI

-73-
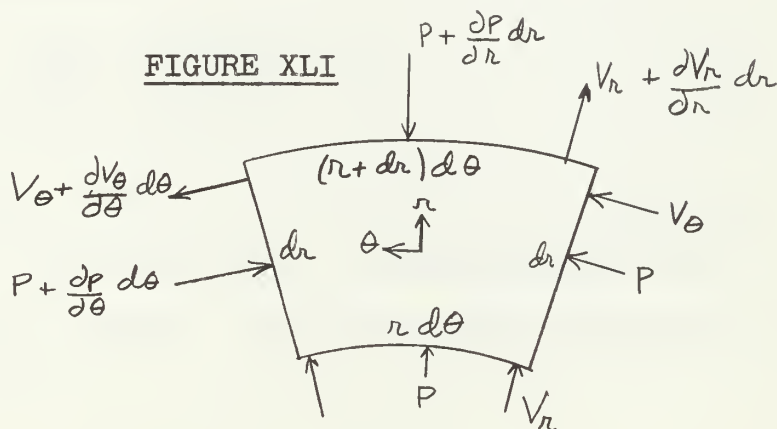
The equation of continuity is expressed by

$$V_r + r \frac{\partial V_r}{\partial r} + \frac{\partial V_\theta}{\partial \theta} = 0 \qquad (27)$$

Considering moment of momentum,

$$Pr\ dr - (P + \frac{\partial P}{\partial \theta}d\theta)r dr = \int \left[\frac{\partial}{\partial r}(r^2 V_\theta V_r d\theta)dr + \frac{\partial}{\partial \theta} (r\ V_\theta^2 dr)d\theta \right]$$

$$(28)$$

Taking derivatives and combining the above equations,

$$- \frac{1}{\rho} \frac{\partial P}{\partial \theta} = V_\theta \frac{\partial V_\theta}{\partial \theta} + r\ V_r \frac{\partial V_\theta}{\partial r} + V_\theta\ V_r \qquad (29)$$

Considering the change of momentum in the radial direction,

$$Pd\ d\theta + P\ dr\ d\theta - (P + \frac{\partial p}{\partial r}dr)(r + dr)d\theta =$$

$$\int \left[\frac{\partial}{\partial r}(r\ V_r^2\ d\theta)dr + \frac{\partial}{\partial \theta}(V_\theta\ V_r\ dr)d\theta - V_\theta^2\ d\theta\ dr \right] \qquad (30)$$

From which is obtained,

$$- \frac{1}{\rho} \frac{\partial P}{\partial r} = V_r \frac{\partial V_r}{\partial r} + \frac{V_\theta}{r} \frac{\partial V_r}{\partial \theta} - \frac{V_\theta^2}{r} \qquad (31)$$

Equations (29) and (31) are the Navier-Stokes equations for non-viscous, two dimensional, incompressible flow in a polar coordinate system. By taking cross derivatives it can be shown that:

$$(V_r \frac{\partial}{\partial r} + \frac{V_\theta}{r} \frac{\partial}{\partial \theta})(\frac{\partial V_\theta}{\partial r} + \frac{V_\theta}{r} - \frac{1}{r} \frac{\partial V_r}{\partial \theta}) = 0 \qquad (32)$$

The second term is the rotation of the fluid. Hence, if irrotational flow is assumed at the entrance to the diffuser, the flow will be irrotational throughout. Expressed in terms of the stream function, irrotationality may be written

$$r^2 \frac{\partial^2 \psi}{\partial r^2} + r \frac{\partial \psi}{\partial r} + \frac{\partial^2 \psi}{\partial \theta^2} = 0 \qquad (33)$$

This is Laplace's equation in polar coordinates, also applicable to an electrical potential in two dimensions.

The blade shapes of both the five and seven-bladed diffusers were drawn triple-scale with conducting paint on semi-conductor paper. A rectified seven-volt direct current supply was led in parallel to each of seven (or five) helipot voltage dividers adjusted in one-volt increments. Each voltage was led to one blade and a point inside and outside of that blade, the arrangement being symmetrical. Between the high and low-potential blades a slit was made along an assumed equipotential line which was very close to the result later obtained. By adjusting the positions of the inner and outer contacts for all blades simultaneously the equipotential lines were made tangent to the blade tips. A probe was used to read voltages between the blades, and the results are shown in Figures XIX and XX. The streamlines correspond to equipotential lines.

The final experimental phase concerned alterations
in the standard five-bladed inflow diffuser to determine
the effect on overall compressor performance. In lieu of
the standard .30-inch width, the axial dimension was in-
creased forty percent by installing .42-inch blades. Tests
with a six-bladed impeller were run using the same pro-
cedure as before. Results for three speeds are shown in
Figures XXI to XXVI.

The exit diameter of the five-bladed inflow diffuser
with .42-inch blades was increased from 1.81 inches to
2.15 inches, an area increase of forty percent. Tests were
again run with the six-bladed impeller, and the results are
also shown in Figures XXI and XXVI.

APPENDIX B

Summary of Data and Calculations

TABLE 1

Summary of Data and Calculation

h_w	θ	P_{01}	$(\Delta P_0)_i$	$(\Delta P_0)_c$	T	$\left(\frac{\Delta P_0}{P_{01}}\right)_i$	η_i	$\frac{\omega_i}{P_{01}} \times 10^5$	$\left(\frac{\Delta P_0}{P_{01}}\right)_c$	η_c	$N \times 10^{-3}$
17.45	1.412	391	12.30	10.95	.1088	.0315	.465	5.11	.028	.420	17
13.70	1.297	389	14.70	12.85	.1075	.0398	.516	4.72	.0331	.460	
9.80	1.072	386	17.20	15.50	.0985	.0445	.548	3.93	.0402	.503	
6.30	0.860	384	20.25	17.90	.0959	.0528	.531	3.18	.0467	.478	
2.60	0.555	381	22.65	20.50	.0829	.0595	.443	2.07	.0539	.407	
0.0	0.0	378	25.80	23.10	.0401	.0682	0	0	.0610	0	
19.45	1.490	389	13.60	12.15	.1206	.0350	.462	5.41	.0312	.420	18
16.20	1.371	387	16.05	14.05	.1192	.0415	.508	5.01	.0363	.452	
12.00	1.180	385	18.15	16.05	.1140	.0470	.516	4.34	.0416	.465	
8.20	0.979	382	21.60	19.15	.1102	.0565	.526	3.62	.0500	.475	
4.55	0.733	380	24.45	21.70	.1037	.0645	.476	2.73	.0570	.429	
2.30	0.526	378	25.70	23.25	.0906	.0680	.406	1.97	.0615	.373	
21.15	1.560	388	15.20	13.45	.1336	.0392	.461	5.67	.0346	.416	19
17.50	1.422	386	17.15	15.20	.1309	.0444	.487	5.20	.0393	.440	
13.70	1.294	384	19.65	17.20	.1290	.0511	.517	4.76	.0418	.461	
9.80	1.072	381	23.15	20.55	.1207	.0607	.537	4.04	.0540	.185	
6.10	0.846	379	26.30	22.95	.1128	.0695	.515	3.16	.0606	.157	
2.40	0.536	376	28.50	25.65	.0972	.0760	.410	2.02	.0683	.375	

Six Blade Impeller
Vaneless Diffuser

TABLE 2

Summary of Data and Calculation

h_w	δ	P_{01}	$(\Delta P_0)_i$	$(\Delta P_0)_c$	T	$\left(\frac{\Delta P_0}{P_{01}}\right)_i$	η_i	$\frac{w}{P_{01}} \times 10^5$	$\left(\frac{\Delta P_0}{P_{01}}\right)_c$	η_c	$N \times 10^{-3}$
19.45	1.490	389	14.3	12.7	.1208	.0377	.515	5.42	.0326	.458	17
11.30	1.150	384	19.7	17.3	.1170	.0525	.565	4.23	.0450	.496	
5.70	.820	380	24.2	21.7	.1090	.0636	.531	3.05	.0570	.476	
1.90	.470	378	26.1	23.5	.0816	.0690	.439	1.75	.0620	.395	
19.45	1.490	386	17.2	15.4	.1370	.0445	.515	5.45	.0398	.461	18
11.30	1.150	382	22.9	20.2	.1282	.0600	.565	4.26	.0530	.499	
5.70	.820	378	27.2	24.4	.1170	.0721	.525	3.07	.0646	.471	
1.90	.470	376	28.9	26.0	.0920	.0770	.406	1.77	.0692	.365	
19.45	1.490	—	—	—	—	—	—	—	—	—	19
11.30	1.150	379	25.8	22.6	.1390	.0680	.557	4.30	.0595	.488	
5.70	.820	375	30.2	27.1	.1260	.0805	.512	3.09	.0723	.459	
1.90	.470	373	32.1	28.7	.0973	.0839	.405	1.78	.0770	.362	

Twelve Blade Impeller

Vaneless Diffuser

TABLE 3

Summary of Data

hw	δ	P_{01}	$(\Delta P_0)_c$	T	$\left(\dfrac{\Delta P_0}{P_{01}}\right)_c$	η_c	$\dfrac{w}{P_{01}} \times 10^5$	b_0
14.9	1.325	391	9.6	.1025	.0246	.362	4.79	.65
9.4	1.060	388	12.9	.0934	.0332	.429	3.87	
5.5	.812	385	15.6	.0880	.0405	.420	2.98	
2.6	.562	382	19.1	.0790	.0500	.396	2.08	↓
14.9	1.325	391	9.9	.1010	.0253	.379	4.79	.51
9.4	1.060	388	13.4	.0960	.0346	.433	3.87	
5.5	.812	384	16.5	.0855	.0430	.457	2.98	
2.6	.562	382	19.1	.0790	.0500	.397	2.08	↓
14.9	1.325	390	11.3	.1050	.0290	.416	4.80	.40
9.4	1.060	386	15.0	.0945	.0388	.491	3.88	
5.5	.812	383	18.3	.0880	.0478	.493	3.00	
2.6	.562	380	20.8	.0765	.0548	.446	2.09	
14.9	1.325	389	11.6	.1050	.0298	.428	4.81	.38
9.4	1.060	386	15.1	.0907	.0392	.505	3.88	
5.5	.812	383	17.8	.0855	.0465	.493	3.00	
2.6	.562	381	20.4	.0725	.0537	.462	2.09	↓

N = 17,000 RPM

Vaneless Diffuser

Effect of b_0 Variation

Six Blade Impeller

TABLE 4

Summary of Data

$\frac{W}{P_{01}} \times 10^5$	η_c	$\left(\frac{\Delta P_0}{P_{01}}\right)_c$	$\frac{W}{P_{01}} \times 10^5$	η_c	$\left(\frac{\Delta P_0}{P_{01}}\right)_c$	$\frac{W}{P_{01}} \times 10^5$	η_c	$\left(\frac{\Delta P_0}{P_{01}}\right)_c$
17,000 RPM			18,000 RPM			19,000 RPM		
4.34	.281	.021	4.58	.278	.0231	4.80	.282	.0256
4.00	.405	.0268	4.23	.334	.0298	4.54	.338	.0319
3.68	.408	.0329	3.89	.384	.0368	4.20	.384	.0393
3.54	.411	.0372	3.54	.413	.0421	3.78	.412	.0455
3.07	.426	.0419	3.12	.433	.0482	3.51	.428	.0503
2.85	.431	.0445	2.67	.443	.0540	3.18	.435	.0545
2.39	.438	.0500	2.36	.479	.0597	2.76	.435	.0604
1.72	.386	.0547	0.98	.264	.0641	2.18	.410	.0662
0.80	.244	.0583				1.14	.290	.0710
4.53	.328	.0226	4.77	.320	.0251	5.05	.323	.0280
4.16	.394	.0269	4.28	.408	.0348	4.68	.382	.0352
3.81	.453	.0361	3.90	.448	.0419	4.20	.435	.0450
3.37	.464	.0413	3.36	.450	.0479	3.75	.439	.0505
2.94	.456	.0458	2.96	.451	.0519	3.33	.485	.0555
2.34	.448	.0506	2.29	.421	.0582	2.85	.440	.0601
1.50	.374	.0555	1.45	.350	.0625	2.24	.408	.0652
						1.10	.270	.0700

Six Blade Impeller
Five Blade Diffuser
Top: .42" Blade 181" D
Bottom: .42" Blade 215" D

TABLE 5

Summary of Data

h_w	g	P_{01}	$(\Delta P_0)_c$	T	$\left(\frac{\Delta P_0}{P_{01}}\right)_c$	$\frac{w}{P_{01}} \times 10^5$	η_c	$N \times 10^{-5}$
11.0	1.15	398	7.0	.1050	.0176	4.09	.224	17
6.5	.888	392	13.2	.0945	.0337	3.21	.362	
4.75	.760	388	17.0	.0880	.0438	2.77	.429	
1.35	.408	386	19.4	.0713	.0504	1.50	.325	
11.0	1.15	396	9.4	.109	.0238	4.12	.273	18
6.5	.888	389	15.8	.105	.0405	3.23	.368	
4.75	.760	385	19.5	.096	.0507	2.79	.425	
1.35	.408	384	21.1	.0765	.0550	1.51	.310	
12.4	1.21	395	9.7	.1205	.0246	4.33	.257	19
6.5	.888	387	18.2	.1040	.0470	3.25	.405	
4.75	.760	383	21.8	.1000	.0570	2.81	.432	
1.35	.408	381	23.9	.0803	.0628	1.52	.331	
9.8	1.09	397	7.5	.100	.0189	3.89	.239	17
6.5	.888	392	12.6	.0972	.0321	3.20	.336	
4.75	.760	388	16.5	.0895	.0425	2.76	.410	
1.35	.408	385	19.6	.0765	.0510	1.50	.305	
11.0	1.15	397	7.9	.1140	.0199	4.11	.219	18
6.5	.888	390	15.0	.1075	.0384	3.22	.340	
4.75	.760	386	19.2	.0960	.0498	2.78	.418	
1.35	.408	383	21.7	.0778	.0566	1.51	.313	
12.4	1.21	397	8.4	.1244	.0212	4.32	.214	19
6.5	.888	388	17.4	.1168	.0450	3.24	.346	
4.75	.760	383	21.5	.1038	.0560	2.80	.411	
1.35	.408	380	24.6	.0830	.0647	1.52	.316	

6 x 5   6 x 7
Impeller-Diffuser Combination

-81-

TABLE 6
Summary of Data

h_w	g	P_{o1}	$(\Delta P_o)_c$	T	$\left(\frac{\Delta P_o}{P_{o1}}\right)_c$	$\frac{w}{P_{o1}} \times 10^5$	η_c	$N \times 10^{-3}$
12.4	1.21	397	7.9	.1297	.0199	4.31	.215	17
6.5	.888	389	15.6	.1165	.0401	3.23	.347	
4.75	.760	386	18.5	.1115	.0478	2.78	.368	
1.35	.408	385	20.0	.0790	.0520	1.50	.302	↓
12.4	1.21	394	10.5	.1310	.0266	4.34	.267	18
6.5	.888	387	18.3	.1230	.0473	3.24	.361	
4.75	.760	385	20.3	.1075	.0528	2.79	.395	
1.35	.408	383	22.4	.0843	.0585	1.51	.299	↓
—	—	—	—	—	—	—	.—	19
6.5	.888	384	21.1	.1297	.0550	3.27	.377	
4.75	.760	382	23.2	.1130	.0608	2.88	.407	
1.35	.408	381	24.1	.0870	.0634	1.52	.295	↓
10.25	1.096	392	8.05	.118	.0206	3.95	.218	17
7.5	.940	388	12.4	.113	.0320	3.44	.301	
5.6	.815	385	15.2	.1063	.0395	3.00	.340	
3.75	.670	382	17.5	.0960	.0458	2.48	.357	
1.85	.470	381	19.4	.0817	.0510	1.75	.326	
0.40	.175	379	21.4	.0622	.0565	.652	.175	↓
12.2	1.195	392	8.3	.1297	.0212	4.32	.210	18
10.25	1.096	389	10.65	.1270	.0274	3.98	.253	
7.5	.940	385	15.4	.1230	.0400	3.46	.324	
5.6	.815	382	17.6	.115	.0460	3.02	.343	
3.75	.670	380	19.9	.104	.0524	2.50	.352	
1.85	.470	378	21.7	.087	.0574	1.76	.322	↓
12.2	1.195	389	10.7	.139	.0275	4.35	.240	19
7.5	.940	382	17.6	.134	.0460	3.48	.322	
5.6	.815	380	20.2	.126	.0532	3.04	.341	
3.75	.670	378	22.2	.114	.0589	2.51	.340	
1.85	.470	376	24.4	.096	.0650	1.77	.312	↓

12-blade Impeller
5 and 7 blade Diffuser

C.   SAMPLE CALCULATIONS

A.   Flow rate and efficiencies. (Run 1, Table 7(a))

P_{1M} = 14.5 psi h_w = 17.45 in of H_2O

ω = 1780 rod/sec $(\Delta P_o)_i$ = 12.3 in of H_2O

T_o = 4.55 in $(\Delta P_o)_c$ = 10.95 in of H_2O

W   = 0.311 lbs P_{01} = 390.6 in of H_2O

                              T = 8.75 in

from Equation (1):

$$q' = 0.528 \ K'Y \sqrt{hw} \ ,$$

where K' is taken from Figure XXXIV for an assumed R of 10^5.

    Y is taken from Figure XXXV.

Substituting this value of q' into Equation (3):

$$R = 1.25 \times 10^5 \times 1.422 = 1.78 \times 10^5 .$$

From this value of R a corrected value of K is determined
from Figure XXXIV and Equation (4) yields,

$$q = \frac{.6522}{.6539} \times 1.422 = 1.420$$

w/P_{01} is then determined from Equation (5),

$$w/P_{01} = \frac{.01415 \times 1.42}{390.6} = 5.11 \times 10^{-5} \ \frac{lbm \ ft^2}{lbf \ sec}$$

-83-

The torque to the impeller is:

$$T = \frac{T-T_o}{12} \times .311 = 0.1088 \text{ ft.lb.}$$

and the impeller efficiency is,

$$\eta_i = \frac{5.2 \times 1.42 \times 12.3}{1780 \times .1088} = 0.465$$

The compressor efficiency is,

$$\eta_c = \frac{5.2 \times 1.42 \times 10.95}{1780 \times .1088} = 0.413$$

B.   One dimensional theory assuming 100% efficiency.
For 17,000 RPM and the impeller geometry used Equation (9)
reduces to:

$$\frac{\Delta P_o}{P_{01}} = .146 - 870 \frac{w}{P_{01}}$$

so that the pressure ratio becomes a linear function of the
flow rate.

$$\frac{w}{P_{01}} = 0 \qquad\qquad \frac{\Delta P_o}{P_{01}} = .146$$

$$\frac{w}{P_{01}} = 5.0 \times 10^{-5} \qquad\qquad \frac{\Delta P_o}{P_{01}} = .1025$$

C. Determination of β_2

1. For 17,000 RPM and the impeller geometry used Equation (10) reduces to the form:

$$\tan \beta_2 = \frac{F \, \eta_1 \, w/P_{01}}{K \, \eta_1 - \frac{\Delta P_o}{P_{01}}}$$

where   F 351

K .146

From Figures X and XI for $\frac{w}{P_{01}}$ of 5.11×10^{-5}

$$\eta_1 = .465 \qquad\qquad \frac{\Delta P_o}{P_{01}} = .0315$$

and,

$$\tan \beta_2 = \frac{351 \times .465 \times 5.11 \times 10^{-5}}{.146 \times .465 - .0315} = 0.230$$

$$\beta_2 = 13.3°$$

2. Slope method.

Using Equation (11) and Figures X and XI,

for $\dfrac{\partial (\eta_1)}{\partial (w/P_{01})} = 0 \qquad\qquad \dfrac{w}{P_{01}} = 3.9 \times 10^{-5} \quad \eta_1 = .56$

and

$$\frac{\partial \left(\frac{\Delta P_o}{P_{01}}\right)}{\partial (w/P_{01})} = -1000$$

then

$$\tan \beta_2 = \frac{.351 \times .56}{1000} = .196$$

$$\beta_2 = 11.1°$$

3. Measured value of β_2 (Run 2 of table 10)

$$\alpha_2 = 15°$$

$$h_w = 13.85 \text{ in } H_2O$$

$$P_{1M} = 14.8 \text{ psi}$$

$$N = 17,000 \text{ RPM}$$

From Figure XXXVI,

$$q = 1.29 \text{ cfs}$$

$$w = \gamma q = 1.29 \times .0736 = .0948 \text{ \#/sec}$$

Substituting the values into Equation (12)

$$\tan \beta_2 = \frac{1}{\frac{.864}{.0948} - \cot \alpha_2} = 0.1865$$

$$\beta_2 = 10.6"$$

D. Two dimensional theory.

In order to determine the velocity pattern in an impeller passage, Equations (15) and (16) were solved for specific conditions.

$$N = 17{,}000 \text{ RPM} \qquad\qquad r_2 = 2.46 \text{ in}$$

$$w = .0332 \text{ lb/sec} \qquad\qquad b = 0.3 \text{ in}$$

$$T_{01} = 535 \text{ °R} \qquad\qquad B = 6$$

Evaluation of constants:

$$C_o = \sqrt{2kgRT_{01}} = 1130 \text{ ft/sec}$$

$$M_2 = \frac{u}{C_o} = \frac{365}{1130} = .323$$

$$a_2 = 13 \ \sigma_2 \ r_2 h_2 = 0.0222 \text{ ft}^2$$

$$\varphi = \frac{w}{\rho \, a_2 C_o} = 0.0317$$

$$\beta = 22° \qquad\qquad \eta_d = 0$$

$$\sigma = 1.048 \text{ rad} \qquad\qquad \eta_t = \varphi \sigma = .0332$$

Substituting these values into Equation (15) reduces it to
the form:

$$Q = 0.697 e^{.226 \, \digamma} \sinh(11 \, \eta) + Q_d e^{-11 \eta}$$

We also have the equation,

$$R = \exp \left[4.425 \left(\digamma + 2.48 \eta \right) \right]$$

Equation (16) was then integrated by finite differences
along a constant $\digamma$ line. For four equal increments of η and
other constants of the system, Equation (16) reduces to the
form

$$.339 = \sum_{n=1}^{4} R_n \, Q_n$$

and for the tip where ξ is 0:

n	η	$e^{-11\eta}$	$\sinh 11\eta$	$e^{.226\xi}$	Q
1	.00415	.9554	.0455	1.0	$.0317 + .9554Q_d$
2	.01245	.8723	.1368	1.0	$.0952 + .8723Q_d$
3	.02075	.7964	.2298	1.0	$.1600 + .7964Q_d$
4	.02905	.7270	.3240	1.0	$.2255 + .7270Q_d$

n	R	RQ
1	1.046	$.0332 + 1.0\,Q_d$
2	1.145	$.1090 + 1.0\,Q_d$
3	1.254	$.2010 + 1.0\,Q_d$
4	1.372	$.3098 + 1.0\,Q_d$

$$\sum = .6530 + 4.0\,Q_d = .339$$

$$Q_d = -.0785$$

$$V_{rd} = C_o Q_d = -88.6 \text{ ft/sec}$$

For the trailing face, η is .0332 and is constant, which reduces Equation (15) to:

$$Q_t = .259\, e^{.226\xi} + .6945\, Q_d$$

and for the case in solution

-88-

$$Q_t = .259 = .6945 \times .0785 = .205.$$

$$V_{rt} = .205 \times 1130 = 232 \text{ ft/sec}$$

The complete results of these calculations are shown for six and twelve bladed impellers in Figures XIV and XV.

D. SUPPLEMENTARY DISCUSSION

Vaneless outflow diffuser performance

As stated in Section IV, it was considered that the performance of the vaneless outflow diffuser was not as good as expected. Particularly, from the data taken, it appeared that the flow might be overdiffused, resulting in excessive friction losses causing a decrease of recoverable head.

Accordingly, the following analysis of a vaneless outflow diffuser was made to determine the magnitude of friction effects. A theoretical explanation of the decreased diffuser efficiency at lower flow rates was also sought.

Assuming symmetrical flow through the diffuser and incompressible flow, consider the following element of fluid:

FIGURE XLII

$V = V$

$V_r = V \sin \theta$

$V_\phi = V \cos \theta$

$V_r + \frac{\partial V_r}{\partial r} dr$

$P + \frac{\partial P}{\partial r} dr$

$(r + dr) d\phi$

P

dr

V_ϕ

$r \, d\phi$

P

V_r

-90-
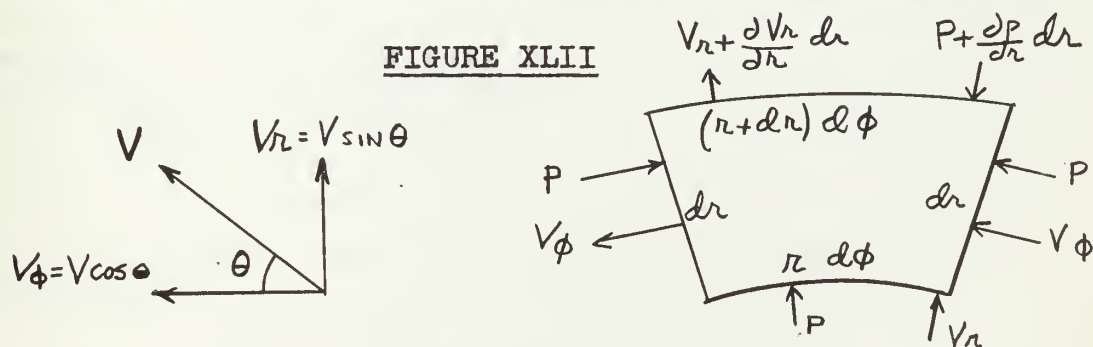
Let the wall friction factor be f and define the shear stress by

$$\tau = f \rho \frac{V^2}{2}$$

Considering moment of momentum,

$$-r^2 f \rho V^2 \, dr \, d\phi = \rho \frac{\partial}{\partial r}(V^2 \sin\theta\cos\theta r^2 d\phi)dr \tag{34}$$

From continuity, for symmetrical flow,

$$\frac{d}{dr}(r \, V \, \sin\theta) = 0$$

or

$$r \, V \, \sin\theta = \text{constant} = C \tag{35}$$

Therefore, from (34),

$$-r^2 f \, V^2 \, \cos\theta = r \, V \, \sin\theta \frac{d}{dr}(V \cos \theta)$$

and

$$- f r \frac{V \cos \theta}{\sin \theta} = \frac{d}{dr}(V \cos \theta)$$

But

$$\cos \theta = \sqrt{1-\sin^2\theta} = \sqrt{\frac{r^2 V^2 - c^2}{r^2 V^2}} \tag{36}$$

so that

$$- \frac{f}{c} \, dr = \frac{d(\sqrt{r^2 V^2 - c^2})}{rV(\sqrt{r^2 V^2 - c^2})}$$

Taking the derivative of the right-hand side,

$$d(\sqrt{r^2 V^2 - c^2}) = \frac{r \, V \, d(r \, V)}{\sqrt{r^2 V^2 - c^2}}$$

Therefore,

$$-\int_{r_1}^{r} \frac{f}{c}\, dr = \int_{r_1 V_1}^{rV} \frac{d\ r\ V}{r^2 V^2 - c^2}$$

Integrating from inlet radius to any radius,

$$2f(r-r_1) = \ln \frac{C+rV}{C-rV} - \ln \frac{C+r_1 V_1}{C-r_1 V_1}$$

Substituting (36),

$$e^{2f(r-r_1)} = \frac{(1+\sin\theta)(1-\sin\theta_1)}{(1+\sin\theta_1)(1-\sin\theta)}$$

and

$$\sin\theta = \frac{\dfrac{1+\sin\theta_1}{1-\sin\theta_1}\ e^{2f(r-r_1)} - 1}{\dfrac{1+\sin\theta_1}{1-\sin\theta_1}\ e^{2f(r-r_1)} + 1} \qquad (37)$$

When f= 0, the angle of flow is constant, from (37), and the flow is irrotational. Let

$$\frac{1+\sin\theta_1}{1-\sin\theta_1} \equiv K$$

Then

$$\sin\theta = \frac{K\ e^{2f(r-r_1)} - 1}{K\ e^{2f(r-r_1)} + 1} \qquad (38)$$

Next, considering radial momentum,

$$-r\frac{dp}{dr} - r f \rho\, V^2 \sin\theta = \rho\left[2r\,V_r \frac{dV_r}{dr} + V_r^2 - V_\emptyset^2 \right]$$

Applying continuity, this becomes,

$$-r \frac{dp}{dr} = rf \rho V^2 \sin\theta + \rho r_1 V_1 \sin\theta \frac{dV_r}{dr} - \rho V^2 \cos^2\theta \qquad (39)$$

Where

$$\frac{d}{dr}(V_r) = \frac{d}{dr}\left(\frac{r_1 V_1 \sin\theta_1}{r}\right)$$

$$= -r_1 \frac{V_1 \sin\theta_1}{r^2} \quad .$$

Since

$$r_1^2 V_1^2 \sin^2\theta_1 = r^2 V^2 \sin^2\theta_1 ,$$

Equation (39) becomes:

$$-\frac{dp}{dr} = \frac{\rho V_1^2 r_1^2 \sin^2\theta_1}{2} \left[\frac{2f}{r^2\sin\theta} - \frac{2}{r^3} - \frac{2\cos^2\theta}{r^3\sin^2\theta}\right]$$

Making use of (36), we obtain finally

$$-\frac{dp}{dr} = \frac{\rho V_1^2 r_1^2 \sin^2\theta_1}{2} \left[\frac{2f}{r^2\sin\theta} - \frac{2}{r^3\sin^2\theta}\right] \qquad (40)$$

For the case when $f = 0$, $(\theta = \theta_1)$, this may be integrated directly to give

$$p - p_1 = \frac{\rho V_1^2}{2}\left(1 - \frac{r_1^2}{r^2}\right)$$

And, as $r \rightarrow \infty$

$$P_{01} = P_1 + \frac{\rho V_1^2}{2}$$

-93-

When friction is included, $\frac{dp}{dr}$ is not readily integrated as a function of r alone:

$$- \frac{dp}{dr} = \rho \frac{V_1^2 \, r_1^2 \, \sin^2 \theta_1}{2} \left[\frac{2fr(K^2 \, e^{4f(r-r_1)} -1) -2(Ke^{2f(r-r_1)} +1)^2}{r^3(K \, e^{2f(r-r_1)} -1)^2} \right]$$

(41)

For this reason, graphical integration was utilized to obtain p as a function of r in the diffuser. Computing a hydraulic radius,

$$\frac{\text{flow area}}{\text{wetted perimeter}} = \frac{b}{2}$$

and Reynold's number is approximately, for V = 150 ft/sec,

$$\frac{V \, b}{2 \, \nu} \approx 10^4$$

Values of f of .007 and .05 were arbitrarily chosen.

Nearly constant static pressure near the diffuser outlet did not necessarily mean the friction effect was small, since a loss of stagnation pressure was surely present. An expression was derived for this loss:

$$P_o = P + \frac{\rho V^2}{2}$$

and

$$- \frac{dp_o}{dr} = - \frac{dp}{dr} - \rho V \frac{dV}{dr}$$

(42)

-94-

But

$$\frac{dV}{dr} = \frac{c}{r} \ \frac{d(\csc\theta)}{dr} - \frac{c}{r^2\sin\theta}$$

and, from (38)

$$\frac{d(\csc\theta)}{dr} = - \frac{4fKe^{2f(r-r_1)}}{(Ke^{2g(r-r_1)}-1)^2}$$

Therefore,

$$\rho V \frac{dV}{dr} = - \frac{4\rho c^2 fKe^{2f(r-r_1)}}{r^2\sin\theta(Ke^{2(r-r_1)}-1)^2} - \frac{\rho c^2}{r^3\sin^2\theta}$$

and, from (42)

$$-\frac{dp_o}{dr} = \frac{\rho r_1^2 V_1^2 \sin^2\theta_1}{2} \left[\frac{2f}{r^2\sin\theta} + \frac{8fKe^{2f(r-r_1)}}{r^2\sin\theta(Ke^{2f(r-r_1)}-1)^2} \right]$$

From (36)

$$\cos^2\theta = \frac{8Ke^{2f(r-r_1)}}{(Ke^{2f(r-r_1)}+1)^2} \tag{43}$$

or

$$8Ke^{2f(r-r_1)} = (Ke^{2f(r-r_1)}+1)^2 \cos^2\theta \tag{44}$$

Combining (43) and (44),

$$-\frac{dp_o}{dr} = \frac{\rho r_1^2 V_1^2 \sin^2\theta}{2} \left[\frac{2f}{r^2\sin\theta} \right] \left[1 + \frac{\cos^2\theta}{\sin^2\theta} \right]$$

From which is obtained,

$$-\frac{dp_o}{dr} = \frac{\rho \, r_1^2 V_1^2 \sin^2\theta_1}{2} \left[\frac{2f}{r^2 \sin^3\theta} \right] \tag{45}$$

For the case when there is no friction, $\frac{dp_o}{dr} = 0$.

Equations (40) and (45) were numerically integrated to give pressure in inches of water as a function of radius. Inlet conditions were determined from measured diffuser inlet angles and velocities based on the difference between static and stagnation pressure at diffuser inlet. Two cases were examined:

Flow rate, $\frac{w}{P_{01}} \times 10^5$	3.2	4.7
θ_1, degrees	11	15
V_1, ft/sec	150	140
r_1, inches	2.5	2.5
ρ_1, slugs/ft^3	.00229	.00229

The results are shown for measured pressures, frictionless static pressures, and pressures with friction factors of .007 and .05. See Figures XLIII, XLIV, and XLV. In addition, the loss of stagnation pressure is shown for the higher flow rate with f = .05. Figure XLVI shows the variation of θ for the two cases.

A summary of the diffusers shows:

Flow rate, $\dfrac{w}{p_{01}} \times 10^{-5}$	3.2	4.7
η_D, measured	.53	.64
η_D, $f = 0$	.86	.86
η_D, $f = .007$	.82	.83
η_D, $f = .05$	.55	.62

The value of $f = .05$ was slightly high, but indicated good agreement of this development with the actual flow. As the friction factor decreases at very high Reynold's numbers, the effect of friction becomes considerably smaller.

It appears that friction effects were quite signifi-cant, but not near the diffuser outlet. The flow was not significantly over-diffused.

FIGURE XLIIII

Curves of $\frac{dp}{dr}$ for Graphical Integration

$$P(r) = \int_{r'}^{r} \frac{dp}{dr} \Delta r$$

$\theta, 15°; f=.05$
$\theta, 15°; f=.007$
$\theta, 11°; f=.05$
$\theta, 11°; f=.007$

radius (in.)

$\frac{dP}{dr}$

(in. of H₂O)

FIGURE XLIV

Pressure vs Radius, Outflow Diffuser. Theoretical and Measured Results

$\theta_1 = 11^\circ$ $V_1 = 150$ ft/sec

$w/p_{01} = 3.2 \times 10^{-5} \dfrac{lbm \cdot ft^2}{sec \cdot lb_f}$

$f = 0$
$f = .007$
$f = .05$
measured

P_a

$P \cdot P_2$

radius (in)

FIGURE XLV

Pressure vs Radius, Outflow Diffuser Theoretical
and Measured Results

$\theta_1 = 15°$ $V_1 = 140$ ft/sec

$w/\rho_{01} = 4.7 \times 10^{-5} \dfrac{lbm\ ft^2}{sec\ lb_f}$
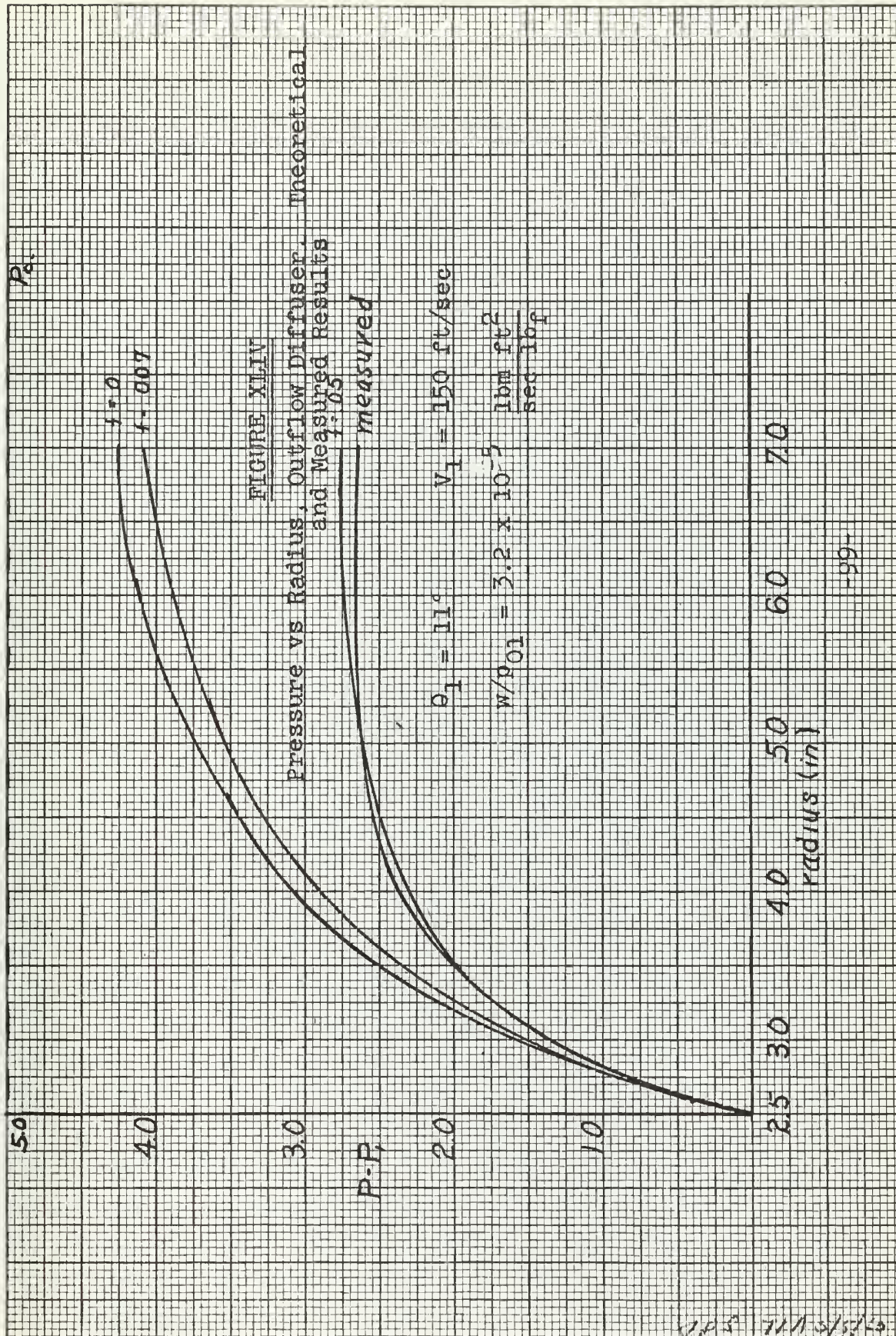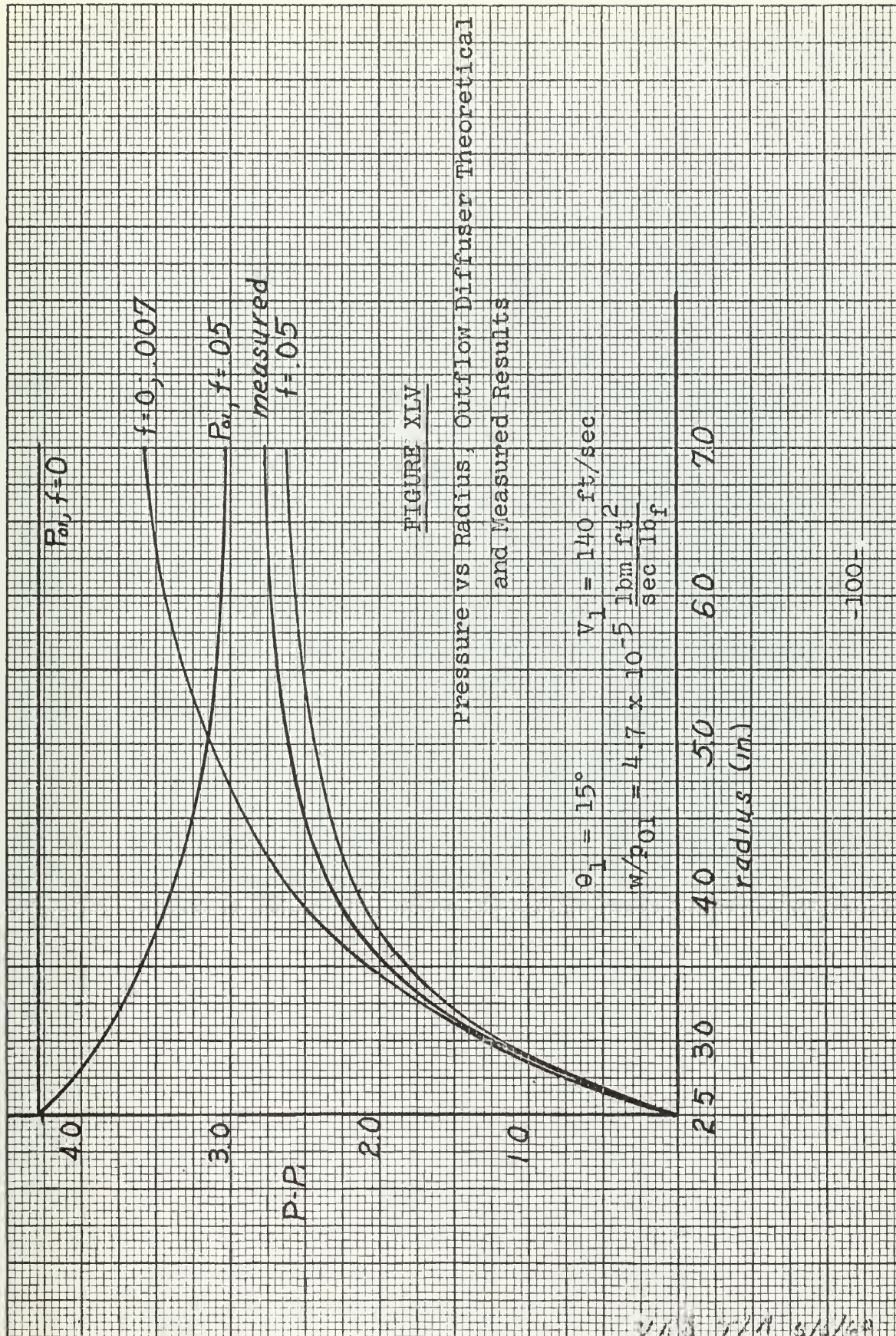
FIGURE XLVI

Variation of θ with Radius in Outflow
Diffuser

Theoretical Solution
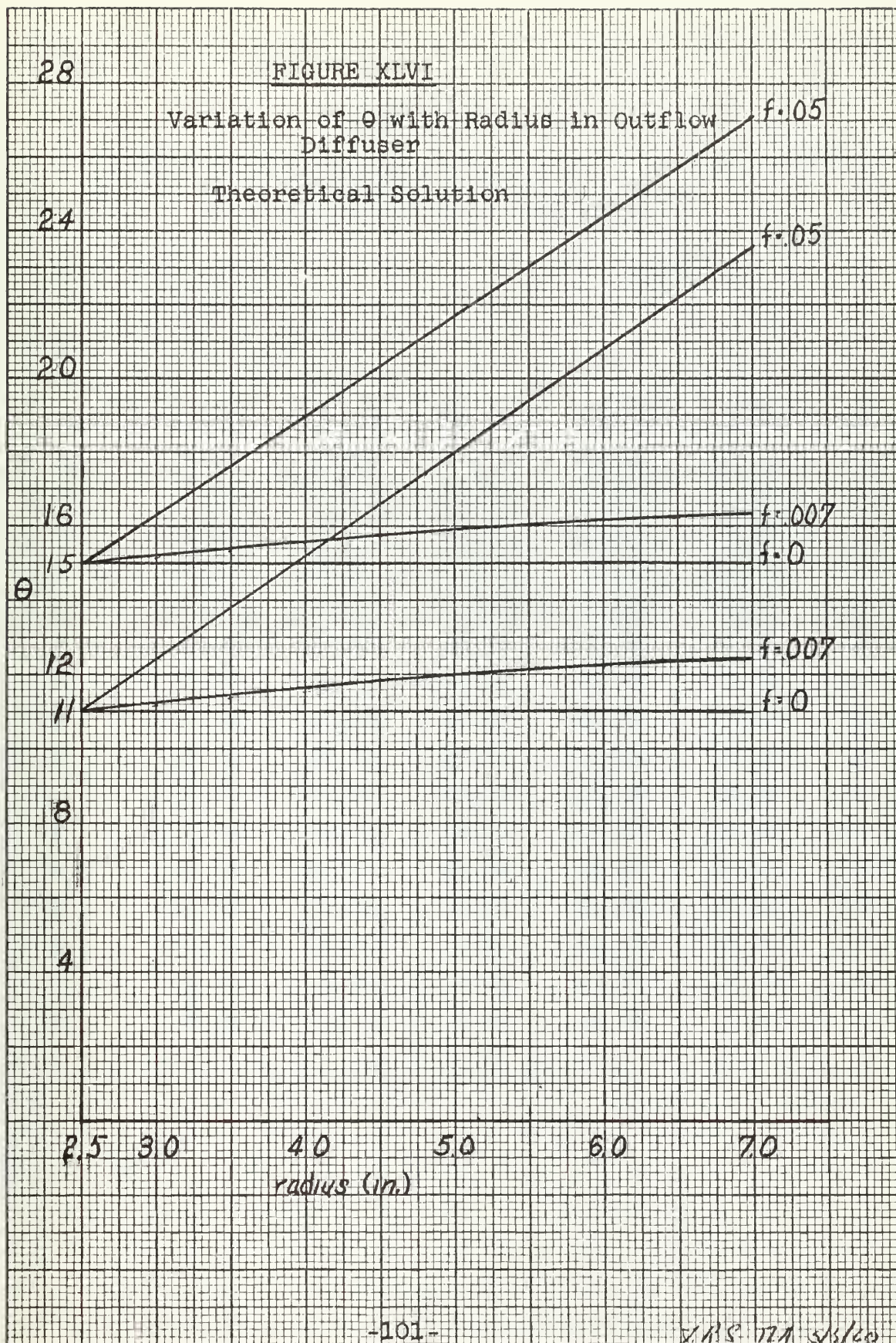
TABLE 7(a)

Data for Six-bladed Impeller and Vaneless Outflow
Difference. (29 Dec 1959)

T_o = 4.55 inches   17,000 RPM

Temp. 535°R

P_a = 29.53 inches Hg

1M	13.50	13.20	12.90	12.70	12.50	12.35
2M	30.90	26.90	22.70	19.00	15.10	12.35
O2	11.00	10.50	10.65	10.00	10.20	9.60
O1	23.30	25.20	27.85	30.25	32.85	35.40
1	25.80	27.50	30.00	33.05	35.60	37.90
a	12.35	12.35	12.35	12.35	12.35	12.35
A	15.00	14.80	15.00	14.70	14.25	14.80
B	14.70	14.35	14.50	14.15	13.65	13.90
C	14.60	14.30	14.45	14.10	13.60	13.65
D	14.50	14.25	14.20	13.90	13.35	13.35
E	14.30	14.00	14.00	13.70	13.20	13.20
F	14.15	13.65	13.80	13.40	13.00	12.95
G	13.60	13.10	13.30	12.90	12.65	12.65
H	13.10	12.60	12.85	12.60	12.55	12.50
I	12.70	12.50	12.50	12.40	12.40	12.40
J	12.45	12.35	12.35	12.35	12.40	12.35
T	8.75	8.70	8.45	8.25	7.75	6.10

TABLE 7(b)

Data for Six-bladed Impeller and Vaneless Outflow
Difference. (29 Dec 1959)

T_o = 4.55 inches   18,000 RPM

Temp. 535° R

P_a = 29.53 inches Hg

1M	13.50	12.90	13.05	12.80	12.60	12.50
2M	32.95	29.10	25.00	21.00	17.15	14.80
02	10.90	10.35	10.25	9.90	9.50	9.90
01	24.50	26.40	28.40	31.50	34.05	35.60
1	24.45	28.95	30.90	34.20	36.90	38.85
a	12.35	12.35	12.35	12.35	12.35	12.35
A	15.20	15.05	15.00	14.90	14.55	14.95
B	14.90	14.55	14.45	14.40	13.95	14.20
C	14.75	14.50	14.40	14.35	13.85	14.00
D	14.70	14.40	14.20	14.15	13.55	13.75
E	14.45	14.20	14.00	13.85	13.35	13.00
F	14.20	13.80	13.60	13.60	13.05	13.20
G	13.65	13.30	13.20	13.10	12.70	12.80
H	13.10	12.80	12.75	12.65	12.50	12.60
I	12.70	12.45	12.50	12.45	12.40	12.45
J	12.40	12.35	12.35	12.35	12.35	12.35
T	9.20	9.15	8.95	8.80	8.55	8.05

TABLE 7(c)

Data for Six-bladed Impeller and Vaneless Outflow Difference. (29 Dec 1959)

T_O = 4.55 inches

19,000 RPM

Temp. 535° R

P_a = 29.53 inches Hg

1M	13.65	13.45	13.20	12.90	12.70	12.40
2M	34.80	30.95	26.90	22.70	18.80	14.80
02	10.50	10.40	9.90	9.65	9.00	9.50
01	25.70	27.55	29.55	32.80	35.30	38.00
1	28.55	30.40	32.30	35.70	38.50	41.65
a	12.35	12.35	12.35	12.35	12.35	12.35
A	15.40	15.20	15.25	15.10	14.05	15.40
B	15.20	14.80	14.60	14.70	14.40	14.50
C	15.00	14.70	14.50	14.60	14.30	14.35
D	14.95	14.50	14.30	14.35	13.95	13.95
E	14.70	14.30	14.10	14.05	13.70	13.60
F	14.45	14.10	13.75	13.80	13.25	13.40
G	13.80	13.40	13.20	13.30	12.75	12.90
H	13.20	12.90	12.70	12.70	12.50	12.65
I	12.80	12.50	12.40	12.45	12.40	12.50
J	12.40	12.35	12.35	12.35	12.35	12.35
T	9.70	9.60	9.45	9.20	8.90	8.30

TABLE 8

Data for 12-bladed Impeller with Vaneless Outflow Diffuser
(31 Mar 1960)

T_o = 4.55
Temp. 535°R
P_a = 29.57 inches Hg

	17,000 RPM			8(a)
1M	13.15	12.70	12.30	12.10
2M	32.60	24.00	18.00	14.00
02	10.40	9.60	9.50	9.40
01	24.70	29.30	33.70	35.50
1	26.70	30.80	35.30	37.10
a	12.00	12.00	12.00	12.00
A	14.70	14.40	14.80	14.20
T	9.25	9.10	8.80	7.75

18,000 RPM				8(b)
1M	13.15	12.70	12.30	12.10
2M	32.60	24.00	18.00	14.00
02	10.20	9.30	9.20	9.10
01	27.40	32.20	36.40	38.00
1	29.40	33.80	38.20	39.70
a	12.00	12.00	12.00	12.00
A	15.00	14.80	15.00	14.40
T	9.90	9.55	9.10	8.15

19,000 RPM			8(c)
1M	12.70	12.30	12.10
2M	24.00	18.00	14.00
02	8.80	8.90	8.60
01	34.60	39.10	40.70
1	36.50	41.00	42.60
a	12.00	12.00	12.00
A	15.20	15.10	14.50
T	9.95	9.45	8.35

TABLE 9

Effect of Variation of Vaneless Outflow Diffuser Width. Six-bladed Impeller. (4 Apr 1960)

P_a = 29.49 inches Hg   17,000 RPM

T_o = 4.70

Temp 537°R

			b_D .65 in		9(a)
1M	13.10	12.70	12.50	12.30
2M	28.00	22.10	18.00	14.90
02	11.20	11.20	10.80	10.70
01	21.80	25.10	27.80	31.30
a	12.20	12.20	12.20	12.20
A	14.50	14.70	13.50	14.00
T	8.65	8.30	8.10	7.75

			b_D .51 in		9(b)
1M	13.10	12.70	12.50	12.30
2M	28.00	22.10	18.00	14.90
02	11.40	11.00	10.50	10.30
01	23.80	27.10	28.60	31.20
a	12.10	12.10	12.10	12.10
A	14.90	14.50	14.10	14.10
T	8.60	8.40	8.00	7.75

b_D .40 in   9(c)

1M	13..0	12.70	12.50	12.30
2M	28.00	22.10	18.00	14.90
02	11.10	10.70	10.30	10.50
01	23.40	27.10	30.40	32.90
a	12.10	12.10	12.10	12.10
A	14.60	14.60	14.60	14.60
T	8.75	8.35	8.10	7.65

b_D .36 in   9(d)

1M	13.10	12.70	12.50	12.30
2M	28.00	22.10	18.00	14.90
02	10.90	10.70	10.20	10.20
01	23.70	27.20	29.90	32.50
a	12.10	12.10	12.10	12.10
A	14.75	14.70	14.10	13.90
T	8.75	8.20	8.00	7.50

TABLE 10

Measured Outflow Diffuser Inlet Angles. Six-bladed Impeller. (5 Feb 1960)

P_a = 29.90 inches Hg

Temp. 537°R.

1M	13.30	13.10	12.80	12.50	12.40
2M	31.00	26.95	22.80	18.00	15.20
α_2	20	15	13	11	10
a	12.30	12.30	12.30	12.30	12.30

TABLE 11

Data for 6-bladed Impeller with 5-bladed Diffuser
(12 Apr 1960)

P_a = 29.81

T_o = 4.55

Temp. 537°R

	17,000 RPM			11(a)
1M	12.80	12.50	12.25	12.15
2M	23.80	19.00	16.00	13.50
01	19.10	25.30	29.10	31.50
a	12.10	12.10	12.10	12.10
T	8.60	8.20	7.95	7.30

18,000 RPM				11(b)
1M	12.80	12.50	12.25	12.15
2M	23.80	19.00	16.00	13.50
01	21.50	27.90	31.60	33.20
a	12.10	12.10	12.10	12.10
T	8.75	8.60	8.25	7.50

19,000 RPM				11(c)
1M	12.90	12.50	12.25	12.15
2M	25.30	19.00	16.00	13.50
01	21.80	30.30	33.90	36.00
a	12.10	12.10	12.10	12.10
T	9.20	8.95	8.40	7.65

TABLE 12

Data for 6-bladed Impeller, 7-bladed Diffuser
(12 Apr 1960)

P_a = 29.81

T_o = 4.55

Temp. 537°R

		17,000 RPM		12(a)
1M	12.70	12.50	12.25	12.15
2M	22.50	19.00	16.00	13.50
01	19.60	24.70	28.60	31.70
a	12.10	12.10	12.10	12.10
T	8.40	8.30	8.00	7.50

18,000 RPM				12(b)
1M	12.80	12.50	12.25	12.15
2M	23.80	19.00	16.00	13.50
01	20.00	27.10	31.30	33.80
a	12.10	12.10	12.10	12.10
T	8.95	8.70	8.25	7.55

19,000 RPM				12(c)
1M	12.80	12.50	12.25	12.12
2M	25.30	19.00	16.00	13.50
01	20.50	29.50	33.60	36.70
a	12.10	12.10	12.10	12.10
T	9.35	9.05	8.55	7.75

TABLE 13

Six-bladed Impeller, 5-bladed Diffuser .42 in
Blade Width. (20 Apr 1960)

T_o = 4.55
Temp. 535°R
P_a = 30.31 inches Hg

	17,000 RPM					
1M	10.95	10.80	10.60	10.50	10.30	10.05
2M	23.55	21.60	18.20	16.65	13.80	10.70
01	18.50	21.20	24.80	26.60	29.65	32.75
a	10.00	10.00	10.00	10.00	10.00	10.00
T	8.65	8.65	8.40	8.30	7.90	6.85

	18,000 RPM					
1M	10.95	10.90	10.60	10.50	10.20	10.10
2M	25.10	22.90	18.80	16.80	12.50	10.90
01	19.35	21.95	26.70	29.00	33.30	34.90
a	10.00	10.00	10.00	10.00	10.00	10.00
T	9.20	9.10	8.80	8.60	7.90	7.25

	19,000 RPM					
1M	11.05	10.95	10.70	10.60	10.35	10.10
2M	26.55	24.55	20.00	18.55	15.00	11.10
01	20.30	22.75	28.00	29.75	33.55	37.35
a	10.00	10.00	10.00	10.00	10.00	10.00
T	9.60	9.50	9.20	9.10	8.70	7.50

TABLE 14

Six-bladed Impeller, 5-bladed Diffuser With
.42 inch Blades and 2.15 inch Exit Diameter.
(20 Apr 1960)

T_o = 4.55
Temp. 535°R
P_a = 30.31 inches Hg

				17,000 RPM		
1M	10.95	10.80	10.70	10.55	10.30	10.15
2M	24.70	22.35	20.30	18.00	13.65	11.65
01	19.15	21.80	24.40	26.40	29.90	31.70
a	10.00	10.00	10.00	10.00	10.00	10.00
T	8.60	8.50	8.40	8.40	7.80	7.25

18,000 RPM						
1M	11.00	10.85	10.70	10.55	10.25	10.15
2M	26.25	22.90	20.60	17.90	13.40	11.55
01	20.10	23.90	26.60	28.90	32.70	34.30
a	10.00	10.00	10.00	10.00	10.00	10.00
T	9.10	8.90	8.85	8.70	8.15	7.50

19,000 RPM						
1M	11.10	10.95	10.80	10.70	10.40	10.25
2M	28.10	25.35	22.15	19.75	15.45	13.20
01	21.25	24.15	27.85	29.80	33.45	35.30
a	10.00	10.00	10.00	10.00	10.00	10.00
T	9.60	9.50	9.40	9.30	8.80	8.40

TABLE 15

Twelve-bladed Impeller, 5-bladed Diffuser
(12 Apr 1960)

T_o = 4.55
Temp. 535°R
P_a = 29.81 inches Hg

		17,000 RPM		
1M	12.90	12.50	12.25	12.15
2M	25.30	19.00	16.00	13.50
01	20.00	27.70	30.60	32.10
a	12.10	12.10	12.10	12.10
T	9.55	9.05	8.85	7.60

18,000 RPM

1M	12.90	12.50	12.25	12.15
2M	25.30	19.00	16.00	13.50
01	22.60	30.40	32.40	34.50
a	12.10	12.10	12.10	12.10
T	9.60	9.30	8.70	7.80

19,000 RPM

1M	12.50	12.25	12.15
2M	19.00	16.00	13.50
01	33.20	35.30	36.20
a	12.10	12.10	12.10
T	9.55	8.90	7.90

TABLE 16

Twelve-bladed Impeller, 7-bladed Diffuser
(18 Apr 1960)

T_o = 4.55
Temp. 538°R
P_a = 27.44 inches Hg

	17,000 RPM				
1M	12.75	12.50	12.40	12.25	12.15
2M	23.00	20.00	18.00	16.00	14.00
O1	20.15	24.50	27.30	29.60	31.50
a	12.10	12.10	12.10	12.10	12.10
T	9.10	8.90	8.65	8.25	7.70

	18,000 RPM				
1M	12.80	12.75	12.50	12.40	12.25
2M	25.00	23.00	20.00	18.00	16.00
O1	20.40	22.75	27.50	29.70	32.00
a	12.10	12.10	12.10	12.10	12.10
T	9.55	9.45	9.30	9.00	8.55

	19,000 RPM				
1M	12.80	12.50	12.35	12.25	12.10
2M	25.00	20.00	28.00	16.00	14.00
O1	22.80	29.70	32.30	34.30	36.50
a	12.10	12.10	12.10	12.10	12.10
T	9.90	9.70	9.40	8.95	8.25

LIST OF REFERENCES

1. Almgren, R.E., "Investigation of the First Stage Diffuser in the Electrolux Vacuum Cleaner". M.E. Thesis. Massachusetts Institute of Technology, Cambridge, 1953.

2. Ellis, G.O., and Stanitz, J.D., "Two-Dimensional Compressible Flow in Centrifugal Compressors with Logarithmic Spiral Blades". NACA Technical Note 2255, Cleveland, 1951.

3. Emmons, H.W., "The Numerical Solution of Compressible Fluid Flow Problems". NACA Technical Note 932, Washington, D.C., 1944.

4. Faulders, C.R., "An Aerodynamic Investigation of Vaned Diffusers for Centrifugal Compressors". Massachusetts Institute of Technology, Gas Turbine Laboratory Report 54-8-T, Cambridge, 1954.

5. Faulders, C.R., "Efficiencies in a Single Stage Centrifugal Compressor". Massachusetts Institute of Technology, Gas Turbine Laboratory Report 54-7, Cambridge, 1954.

6. Hunsaker, J.C., and Rightmire, B.G., "Engineering Applications of Fluid Mechanics". McGraw-Hill Book Company, New York, 1947.

7. Prandtl, L., and Tietjens, O.G., "Fundamentals of Hydro- and Aero-Mechanics". McGraw-Hill Book Company, New York, 1934.

8. Rigney, B.L., "Development of an Improved Interstage Diffuser for the Electrolux Vacuum Cleaner". M.E. Thesis, Massachusetts Institute of Technology, Cambridge, 1953.

9. Shapiro, A.H., "The Dynamics and Thermodynamics of Compressible Fluid Flow". Volume I. The Ronald Press, New York, 1953.

10. "Fluid Meters: Their Theory and Application". Section B. The American Society of Mechanical Engineers, New York, 1959.

11. "ASME Power Test Codes". Supplement, Chapter 4: Fluid
    Measurement. The American Society of Mechanical
    Engineers, New York, 1959.

12. Jansen, W., "Incompressible Fluid Flow in a Radial
    Vaneless Diffuser". Massachusetts Institute of Technology,
    Gas Turbine Laboratory, Report 52-59, Cambridge, 1959.